

Alma Mater Studiorum – Università di Bologna

DOTTORATO DI RICERCA IN
SCIENZE BIOTECNOLOGICHE E FARMACEUTICHE

Ciclo XXX

Settore Concorsuale: 03/D1

Settore Scientifico Disciplinare: CHIM/08

DESIGN AND SYNTHESIS OF SMALL MOLECULES AS TOOLS FOR
DRUG DISCOVERY AND CHEMICAL BIOLOGY:
IDENTIFICATION OF NEW LDH-A INHIBITORS AND
DEVELOPMENT OF FLUORESCENT PROBES TO INVESTIGATE
NEUROGENESIS

Presentata da: Guidotti Laura

Coordinatore Dottorato

Supervisore

Prof. Santi Mario Spampinato

Prof. Marinella Roberti

Esame finale anno 2018

CONTENTS

Abstract.....	1
---------------	---

Part I

IDENTIFICATION OF GALLOFLAVIN ANALOGS AS HUMAN LDH-A INHIBITORS AND THEIR POTENTIAL AS ANTICANCER AGENTS

1. Introduction.....	2
1.1 Project overview.....	2
1.2 Cancer metabolic reprogramming.....	2
1.3 Glucose metabolism in normal and cancer cells.....	4
1.3.1 Oncogenic mechanisms beyond tumor glucose metabolism.....	7
1.4 Targeting glycolytic enzymes as anticancer strategy.....	10
1.5 The enzyme L-lactate dehydrogenase.....	12
1.5.1 Structure and function.....	12
1.5.2 LDH-A in cancer cells.....	14
1.5.3 LDH-A as promising target for anticancer treatment.....	14
1.6 LDH-A inhibitors in the search for antitumor agents: an update.....	16
2. Aim of the work.....	24
3. Biological evaluation and discussion of results.....	42
4. Conclusions.....	47
5. Experimental section.....	48

Part II

TOWARDS THE DEVELOPMENT OF FLUORESCENT AND AFFINITY PROBES TO INVESTIGATE NEUROGENESIS

1. Introduction.....	73
1.1 Project overview.....	73
1.2 Opportunities for neurodegenerative diseases: regenerative medicine.....	73
1.3 NSCs and neurogenesis in the adult mammalian brain.....	76
1.3.1 Adult neurogenesis regulation.....	78
1.4 Therapeutic application of NSCs: from cell therapy to small molecules.....	80
1.4.1 Small molecules promoting neurogenesis	80
2. Aim of the work	82

2.1 Development of OX02672 as fluorescent and affinity probe for chemical proteomics.....	85
2.3 Chemistry.....	86
3. Conclusions	92

Part III (side project)

DESIGN AND SYNTHESIS OF TACRINE-RESVERATROL FUSED HYBRIDS AS MULTI-TARGET-DIRECTED LIGAND AGAINST ALZHEIMER'S DISEASE

1. Introduction.....	93
1.1 Project overview.....	93
1.2 Multi-target drug discovery in Alzheimer's disease.....	93
2. Aim of the work	95
3. Biological evaluation and discussion of results.....	98
4. Conclusions.....	101
5. Experimental section.....	102
Concluding remarks.....	108
Appendix A.....	110
Appendix B.....	112
Abbreviations and acronyms.....	114
References.....	116
Acknowledgements	

ABSTRACT

The present work includes distinct research projects having as common platform the design and synthesis of biologically active small molecules, useful as tools both for drug discovery and chemical biology studies.

The main project (Part I) focused on the identification of LDH-A inhibitors as *hit* candidates in the discovery of new anticancer agents. My work aimed to explore the chemical space around galloflavin (GF) by synthesizing a small library of analogs to perform structure-activity relationships (SAR) studies. GF, LDH-A inhibitor previously identified and synthesized by our group, was not investigated in terms of SAR because of its poor chemical tractability. In the present work, a natural urolithin M6 (UM6) has been selected as a simplified structural analog of GF. It is endowed with improved physicochemical properties and it showed to reproduce GF's biological behaviour on the enzyme and in cancer cells. An efficient fast and modular synthetic strategy has been developed to obtain UM6, which synthesis was not previously reported. This route gave an easy access to a series of structural analogs for SAR investigation, which allowed us to acquire a deeper knowledge about the key pharmacophore of UM6 and GF.

The second project (Part II), carried out at Oxford University under the supervision of Professor Angela Russell, aimed to use a chemical biology approach to develop a proneurogenic small molecule recently identified by the group (OX02672), into a fluorescent probe to assess its molecular interactions and localization in neural stem cells (NSCs). My work focused on the design and synthesis of alkyne-tagged derivatives of OX02672 for subsequent development into probes by "click" conjugation with azide-containing fluorophores.

The third part includes a side-project (Part III), carried out in collaboration with group of Professor Maria Laura Bolognesi. It focused on the design and synthesis of a series of multi-target-directed ligands (MTDLs) useful as potential *hit* candidates in the search for new drugs against Alzheimer's disease (AD). Tacrine-resveratrol hybrid compounds, in which the structural features of the cholinesterase inhibitor drug tacrine are combined with the antioxidant anti-neuroinflammatory properties of resveratrol, have been designed and synthesized by using a *fusing* strategy. They showed interesting multi-target profile against target proteins involved in AD pathogenesis.

Part I

IDENTIFICATION OF GALLOFLAVIN ANALOGS AS HUMAN LDH-A INHIBITORS AND THEIR POTENTIAL AS ANTICANCER AGENTS

1. Introduction

1.1 Project overview

Part I includes the main project of my PhD program, carried out under the supervision of Professor Marinella Roberti at the Department of Pharmacy and Biotechnology (UniBO), in collaboration with the group of Professor Giuseppina di Stefano (DIMES, UniBO). The present project focused on the design and synthesis of small molecules as inhibitors of LDH-A, currently under active investigation in the search for innovative anticancer combination therapies.

1.2 Cancer metabolic reprogramming

Reprogramming of energy metabolism has been recognized as one of the hallmarks of cancer.¹

The most relevant metabolic changes include enhanced glycolysis, increase in glutaminolytic flux, upregulation of amino acid and lipid metabolism, enhancement of mitochondrial biogenesis, induction of pentose phosphate pathway and macromolecule biosynthesis (**Figure 1**).² These pathways are altered in order to provide cancer cells energy and precursors to support and enable rapid proliferation, continuous growth, survival, tissue invasion, metastasis and resistance to anti-cancer treatments.

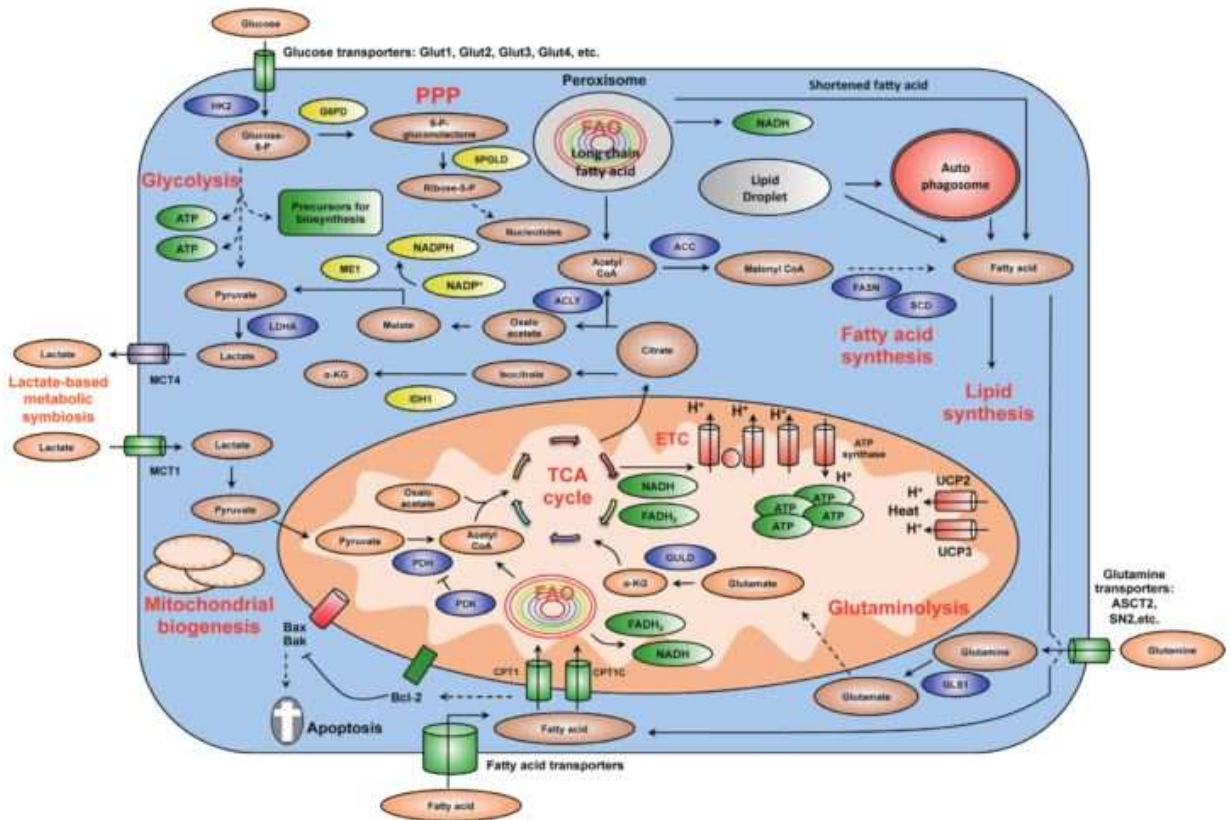


Figure 1. Principal key metabolic changes in cancer.²

In 1920's it was recognised that energy metabolism is one of the first affected processes during neoplastic transformation³ but over the time, interest in metabolic properties of cancer began to decline with the view of cancer as a genetic disease.

The metabolic reprogramming of cancer cells regained great attention in cancer research only in the last decade, when it was established that it is a direct result of alterations in oncogenes and oncosuppressors.⁴⁻⁶

Thus many studies have recently focused on cancer cells altered metabolism with the aim to find new ways for effectively killing tumor cells.^{2,7,8}

1.3 Glucose metabolism in normal and cancer cells

One of the best characterized metabolic hallmark exhibited by tumor cells is the alteration in glucose utilization, with increased glycolysis and lactate production.^{9–11}

In all cells, glycolysis starts with the conversion of glucose in two molecules of pyruvate, the fate of which can be different, as it can be completely oxidized to CO₂ in the mitochondrion or can be converted to lactate in the cytosol (**Figure 2**).¹²

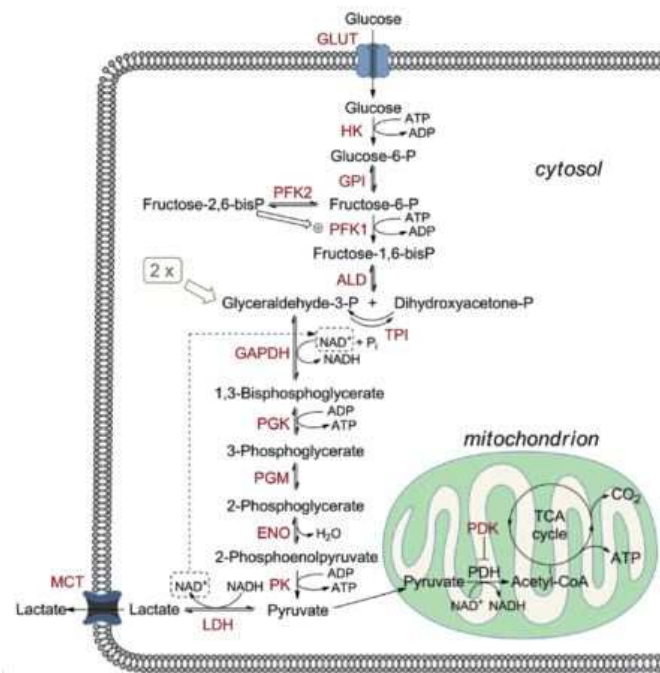


Figure 2. Glucose metabolism through glycolytic flux.

In normal cells (differentiated tissues), glycolysis is mainly coupled with oxidative phosphorylation (OXPHOS), thus pyruvate is completely oxidized to CO₂ in the mitochondria via tricarboxylic acid cycle (TCA) and OXPHOS. Only under oxygen deprivation, OXPHOS cannot take place, thus pyruvate is converted into lactate (anaerobic glycolysis) in the cytosol (**Figure 3A**).¹⁰

In contrast, cancer cells metabolize glucose mainly through glycolysis with a minor use of the mitochondrial OXPHOS, regardless of the availability of oxygen (**Figure 3B**). This alteration is known as “Warburg effect”, from the name of the scientist who first observed this phenomenon.^{3,5,10,13–15}

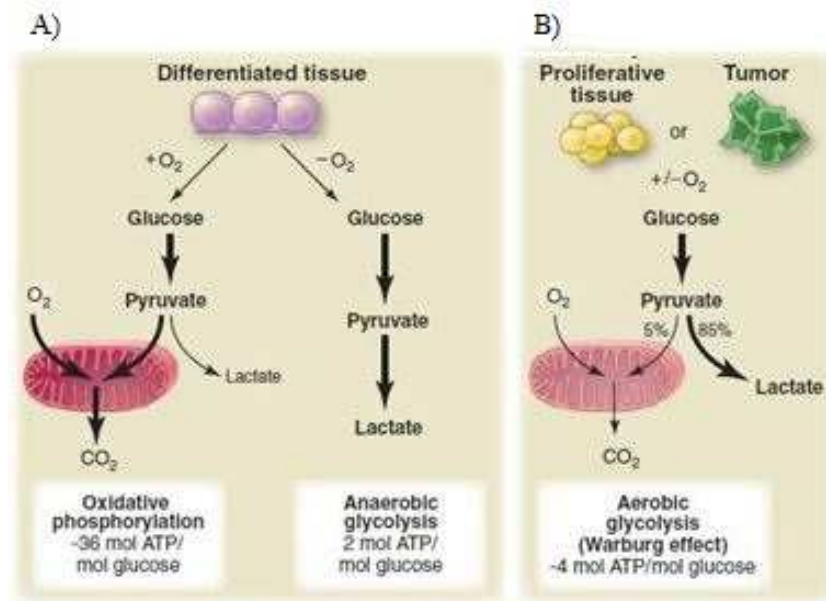


Figure 3. Schematic representation of glucose metabolism in differentiated tissues (A) and tumor/proliferative tissues (B).¹⁰

An increased glycolytic flux, which is uncoupled from OXPHOS, is commonly observed in cancer cells and most of pyruvate is converted to lactate through lactate dehydrogenase (LDH). LDH is a key enzyme for cancer cells glycolysis because it reduces pyruvate to lactate with the coupled oxidation of NADH to NAD⁺, the regeneration of which is necessary for the continuation of glycolysis (See **Figure 2**).

Importantly, while LDH plays a crucial role in tumor metabolism, it is not fundamental and not active in healthy cells, where glycolysis is normally coupled with OXPHOS.

Glycolysis only makes 2 ATP per glucose while mitochondrial respiration can produce up to 36 ATP for each glucose molecule catabolized; this raises the question why cancer cells select a less efficient metabolism in term of ATP production.

The principal explanation is that enhanced glycolysis allows them the rapid production of many intermediates which can be used to generate building blocks (nucleotides, lipids, amino acids, and NADPH) for macromolecules biosynthesis required during cellular proliferation.¹⁶ Thus, contrary to normal cells, that aim to maximize ATP production converting all the glucose to CO₂ via OXPHOS, cancer cells adopt an anabolic-type metabolism aimed at biomass construction.¹⁰ This metabolism is not exclusive of cancer cells, but is also observed in normal proliferative tissues and in many rapidly dividing embryonic tissues, confirming its role in supporting the large-scale biosynthetic programs that are required for cell proliferation.¹⁷

Moreover, conversion of pyruvate to lactate could reduce reactive oxygen species' (ROS) levels, avoiding generation of oxidative stress and promoting tumors' survival.^{18,19}

To compensate for the lower efficacy glycolytic ATP production and to sustain the greater demand for biomass, cancer cells increase the uptake of glucose through transmembrane glucose transporters (GLUTs).^{15,20,21} The increase in glucose uptake is a feature distinguishing tumor cells from normal cells and has been exploited in Positron Emission Tomography (PET) with the use of radiolabeled glucose analog, such as ¹⁸F-deoxyglucose, as a tracer to visualize tumors.²²

It is worth noting that, even if glycolysis is enhanced and OXPHOS is reduced, mitochondria remain functional and some OXPHOS occurs in a large part of cancer cells, which use glycolysis to generate macromolecules but still derive a significant fraction of ATP from OXPHOS.²³ However glycolysis becomes the primary source of ATP when the hypoxic microenvironment obstacles OXPHOS, such as in the hypovascularized tumor regions.

Lactate generated by LDH, secreted through monocarboxylate transporters, contributes to the development of extracellular acidosis that facilitates tumor invasiveness^{24,25} and it is also involved in the energy production. Indeed, lactate released as end product of glycolysis can fuel the oxidative metabolism of cancer cells growing in oxygenated microenvironment.^{7,26}

The reprogramming in glucose metabolism is mainly driven by the oncogenic signals that trigger cell proliferation, as it will be described in the next paragraph.

1.3.1 Oncogenic mechanisms beyond tumor glucose metabolism

The glycolytic phenotype exhibited from cancer cells has been shown to be associated with activation of oncogenes, signaling pathways and transcription factors, as well as the inactivation of tumor suppressors.^{15,21,27,28}

The elevated oncogenic activation, together with insufficient tumor suppressor control induce a transcriptional program that enables cancer cells to maintain a high glycolytic flux.

The main oncogenes reported to induce increased glucose uptake and glycolysis are Ras, AKT, HIF-1, Myc, PIK3 (**Figure 4**).^{4,19}

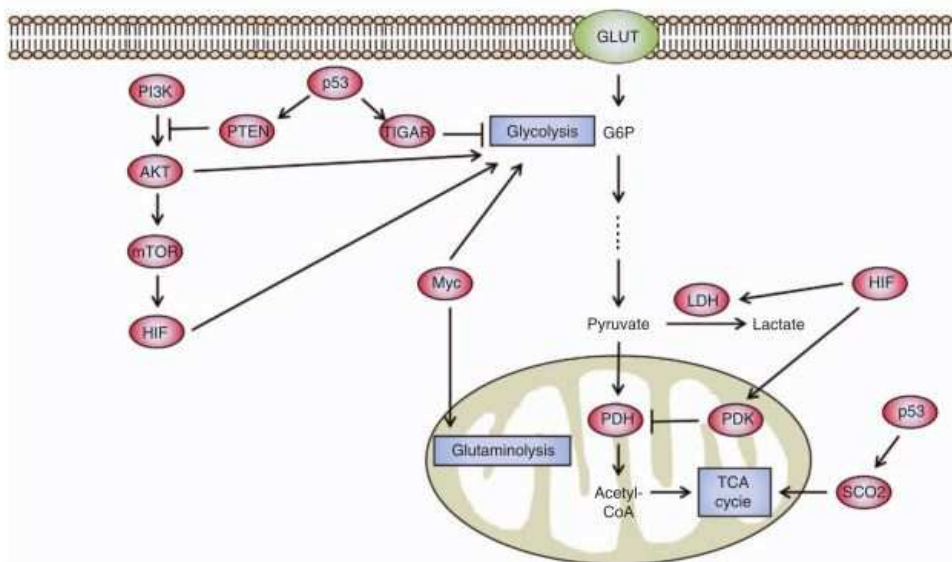


Figure 4. Oncogenes and oncosuppressor implicating in glucose metabolic reprogramming.²⁹

Oncogene mutation of Ras activates mTOR via the PI3K-Akt-mTOR signaling pathway, and mTOR promotes glycolysis through inducing HIFs, particularly HIF-1.³⁰⁻³²

HIF-1 is involved in the promotion of the glycolytic flux through overexpression of glucose transporters (GLUT1, GLUT3), hexokinases (HK1, HK2), phosphofructokinases 1(PFKFB3), aldolases (ALDA, ALDC), phosphoglycerate kinase (PGK1), enolase (ENO1), pyruvate kinase M2 (PKM2), pyruvate dehydrogenase kinases (PDK1, PDK2), lactate dehydrogenase A (LDH-A), and monocarboxylate transporter (MCT4).^{31,33}

Myc directly activates glucose transporters and glycolytic enzymes, among which LDH-A and PDK1.³⁴

Among tumor suppressors, p53 shows an inhibitory effect on glycolysis through different mechanisms, among which upregulation of TIGAR (TP53-inducible glycolysis and apoptosis regulator), that results in a decreased glycolytic flux³⁵ and stimulation of oxidative phosphorylation through upregulation of cytochrome c oxidase 2 (SCO2) (**Figure 4**).³⁶ Thus, loss or deregulation of p53 shifts metabolism from mitochondrial respiration towards glycolysis.

The upregulation of the majority of the glycolytic enzymes allows cancer cells to continuously drive glycolysis for supporting their rapid proliferation and accelerated biosynthesis (**Figure 5**).

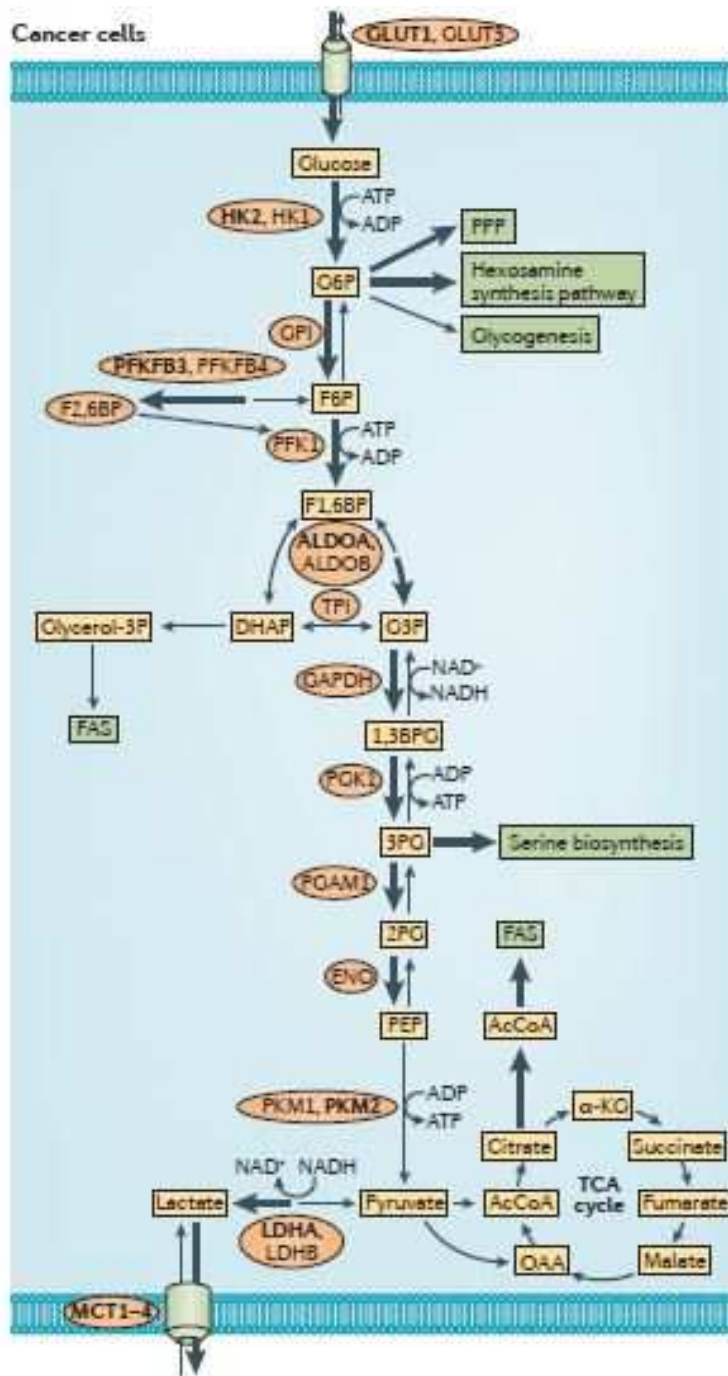


Figure 5. Upregulated enzymes (in bold) in glycolysis of cancer cells.³⁷

1.4 Targeting glycolytic enzymes as anticancer strategy

The reprogrammed glucose metabolism can be exploited for therapeutic approaches to selectively target cancer cells.³⁷

Since the overexpression of most glycolytic enzymes is a common hallmark of tumors, inhibiting their altered activity may provide an effective mechanism by which to kill cancer cells.³⁸⁻⁴⁰

The development of “antiglycolytic” anticancer agents in the search of new antitumor agents has been actively pursued and several small molecule inhibitors of many of the steps of the glycolytic pathway have been identified.⁴¹

Currently, a number of drugs that target glucose transporter 1 (GLUT1)^{42,43}, hexokinases (HK)⁴⁴⁻⁴⁸, phosphofruktokinase 2 (isoform PFKFB3)⁴⁹, pyruvate kinase isoform M2 (PKM2)^{50,51} and lactate dehydrogenase A (LDH-A)⁵² are under active investigation in preclinical or clinical studies, and representative examples are reported in **Table 1**.⁷

Table 1. Glycolytic enzymes targeted in the development of new anticancer drugs.

Target	Agent/s	Development stage	References
GLUT1	WZB117, silibinin	Preclinical studies	42,43
Hexokinases	2-deoxyglucose, lonidamine, 3-bromopyruvic acid, methyl jasmonate	Preclinical and clinical studies	44-48
Phospho- fructokinase 2 (PFKFB3)	PFK158	Preclinical studies	49
Pyruvate kinase M2 (PKM2)	TLN-232	Preclinical studies	50-51
Lactate dehydrogenase (LDH-A)	GNE-140, FX11, galloflavin	Preclinical studies	52

However, it should be recognised that there are potential obstacles in using glycolytic inhibitors for cancer treatments; indeed glycolytic enzymes are also necessary for glucose metabolism of healthy cells and their inhibition may be toxic especially for tissues that use glucose as main energy source.

On the other hand, the enzyme LDH-A is poorly active in normal cells under sufficient oxygen supply.

Therefore, among the glycolytic targets, LDH-A is considered the most promising and safe target to hinder cancer cell metabolism and growth without causing damage to normal tissues.⁵³

1.5 The enzyme L-lactate dehydrogenase

1.5.1 Structure and function

As we stated above, LDH catalyzes the reversible transformation of pyruvate to lactate, with the simultaneous interconversion of NADH to NAD⁺, (**Figure 6**) in the last step of glycolysis (See **Figure 2**).

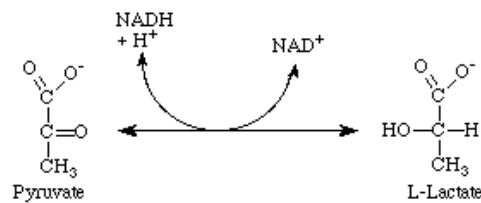


Figure 6. LDH enzymatic reaction.

This enzymatic activity is conserved in organisms of the three domains of life⁵⁴ because it can be an important source of ATP and NAD⁺ for living organisms during periods of anaerobiosis.

Human LDH, mainly found in the cytosol, is a 140 kDa tetrameric enzyme (**Figure 7A**) composed of two major subunits, A (or M, predominately found in muscle) and B (or H, predominately found in heart) that are encoded by *ldh-a* and *ldh-b* genes, respectively. An additional isoform LDH-C was identified in human testis and sperm.⁵⁵

The association of A and B subunits gives rise to five isoforms (**Figure 7B**): the homotetramer LDH-A, (or LDH-5) assembled from four A subunits, the homotetramer LDH-B, (or LDH-1) assembled from four B subunits, and three heterotetramers A3B1, A2B2 and B3A1.⁵³

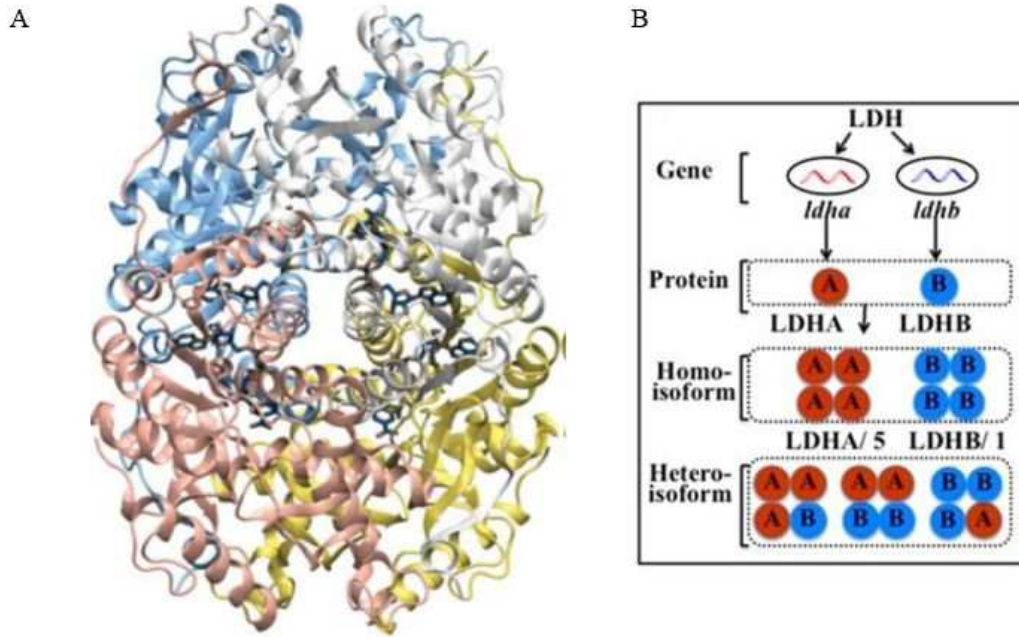


Figure 7. A) Tetrameric LDH structure (each subunit contains a NADH molecule;⁵³ B) Schematic representation of LDH isoforms.⁵²

Crystal structures of the major isoforms in human, LDH-A and LDH-B, are reported;⁵⁶ LDH-A is found mainly in anaerobic tissues such as skeletal muscle and liver while LDH-B in aerobic tissues such as cardiac muscle.

Since the A and B subunits show high amino acid sequence similarity (75%), the active sites is strictly preserved in the two isoforms LDH-A and LDH-B, whereas they differ in the kinetic properties.⁵⁶

The isoform mainly involved in tumorigenesis is LDH-A, as it will be described in the next paragraph, whereas the role and the implication of LDH-B in cancer cells have not yet been elucidated.^{57,58}

In normal cells under sufficient oxygen supply LDH-A is poorly active. It exerts its activity principally in anaerobic conditions: during intense work, for example in the overworking of skeletal muscle, glucose uptake and glycolytic flux massively increase and oxygen is in short supply. In this situation LDH-A reduces pyruvate to lactate regenerating NAD^+ ensuring the maintenance of glycolysis and the resulting ATP production (lactic fermentation).⁵³

1.5.2 LDH-A in cancer cells

LDH-A is fundamental to sustain the high glycolytic flux, thus allowing energy production in tumor cells which largely depend on glycolysis for their growth and survival.

LDH-A-expression is constantly up-regulated in tumors and was found to correlate with tumor size and poor prognosis.^{4-6,59}

The overexpression of LDH-A, mainly driven by Myc and HIF-1, has been reported in highly glycolytic human cancers,⁶⁰⁻⁶⁵ and analysis of several tumors confirmed the higher concentration of LDH-A subunits compared to adjacent normal tissues.⁶⁶

Importantly, the high amount of lactic acid due to increased activity of LDH-A induces extracellular acidosis, that destroys the adjacent normal cell populations and promotes angiogenesis, facilitating tumor invasion and metastasis.^{24,67}

Collectively, these data provided proof of concept that LDH-A is strictly involved in tumorigenesis and encouraged lots of studies on the benefic effects derived from its inhibition.

1.5.3 LDH-A as promising target for anticancer treatment

The inhibition of LDH-A, by knockdown or small molecules, has demonstrated promising effects in preclinical investigations, which have confirmed the critical role of LDH-A in cancer cells and validated its inhibition as effective antitumor strategy, especially in combination with other therapeutic modalities.

Silencing LDH-A expression was found to inhibit cancer cell proliferation and *in vivo* tumorigenesis in different tumor models⁶⁸⁻⁷³ and stimulate mitochondrial respiration with consequent ROS production that facilitates cell death.⁷¹

As we previously stated, it is poorly active in normal cells, therefore its inhibition is considered a valid approach to selectively affect cancer cell metabolism.

Moreover, evidences suggest LDH-A inhibition should be well tolerated by normal cells, since individuals with A or B subunit deficiency don't accuse significant clinical symptoms⁷⁴⁻⁷⁸, in particular individual lacking A subunits complain muscle rigidity and myoglobinuria only after strenuous exercise.^{74,78}

Benefic effects derived from inhibition of LDH-A by small molecules are known for a long time with the LDH inhibitor oxamate, a structural isostere of pyruvate, which inhibits glycolysis of cancer cells cultured *in vitro*, even if only at high concentration.⁷⁹ Furthermore, inhibition of LDH-A with oxamate was found to be a way to overcome the resistance of breast cancer cells to taxol⁸⁰ and trastuzumab.⁸¹ In these works, resistant cells were shown to be more dependent on glycolysis for their survival, as consequence a combination treatment with the chemotherapeutic and LDH inhibitor resulted in a more pronounced therapeutic effect.

Overall, inhibition of LDH-A activity is considered a valid, selective and safe approach to damage cancer cells. Therefore many pharmaceutical industries and academia have recently focused their attention in the search of small molecule inhibitors of LDH-A, reported in several reviews.^{52,53,82}

1.6 LDH-A inhibitors in the search for antitumor agents: an update

Numerous strategies have been adopted in the discovery of LDH-A inhibitors: structure-based virtual screening; high-throughput enzymatic screening of compound libraries; fragment-based approach; modification/optimisation of known inhibitors.

These approaches allowed the development of many inhibitors, some of which showed high selectivity and potency in the nanomolar range against LDH-A; however very few of them resulted sufficient active in cell-based assays to progress toward clinical studies.⁸³

Most of them share the presence of a carboxylic acid moiety, sometimes replaced with a bioisostere or masked as prodrug, that appears to be highly relevant in the binding with the active site of LDH-A together with a high number of hydrogen bond donors, which play a key role in the ligand-LDH binding.

Indeed, the LDH-A reference inhibitor oxamic acid **1** establishes hydrogen-bonds with key catalytic residues in the active site (Arg-105, Arg-168, His-192 and Asp-165) and interacts with the side chain of Arg-168 through its carboxylate group as it is indicated through the analysis of the complex LDH-NADH-oxamate (**Figure 8**).

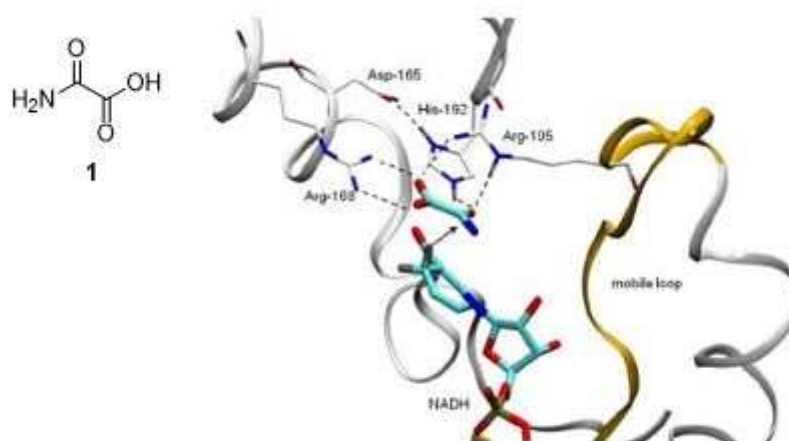


Figure 8. Structure of LDH-A inhibitor oxamic acid **1** and its interaction with LDH-A.

An overview of the main classes of LDH-A inhibitor identified so far is illustrated in **Figure 9**, and the most promising of them will be briefly described.

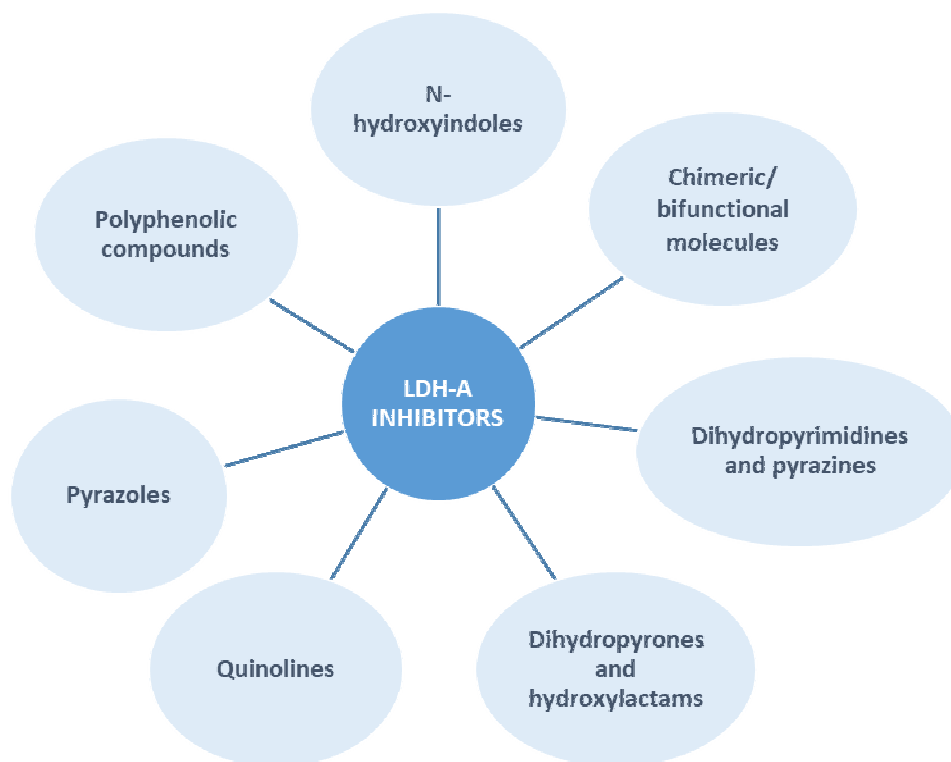
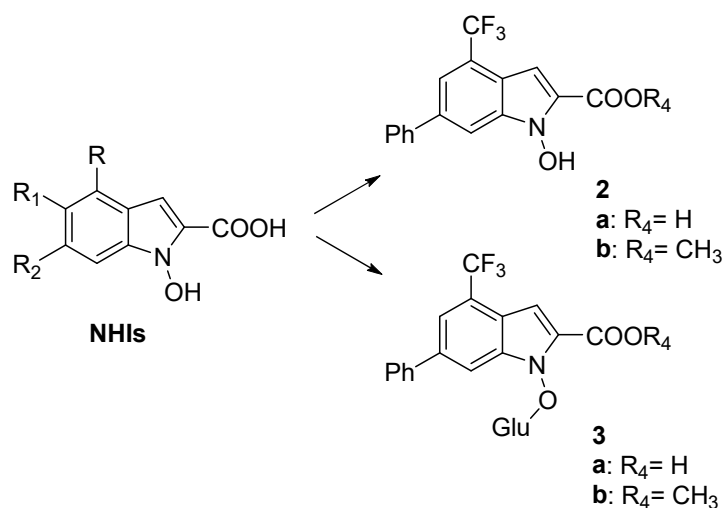


Figure 9. Overview of chemical classes of LDH-A inhibitors.

- **N-hydroxyindole scaffold-based inhibitors**

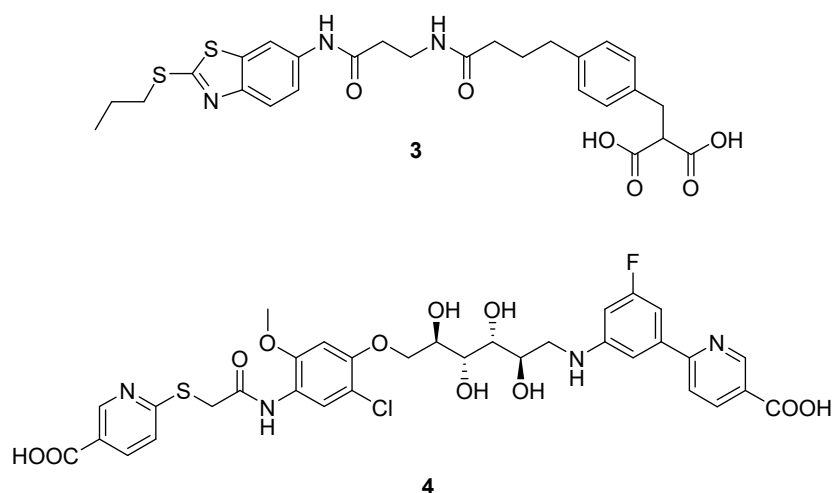
N-hydroxyindoles (NHIs) showed inhibitory activity in competition with both the cofactor NADH and the substrate pyruvate with IC_{50} in the low micromolar range against LDH-A.⁸⁴⁻⁸⁶

SAR studies indicated on the “OH-COOH” motif the pharmacophore of this class, that partially resembles the structure of the natural substrates of LDH, i.e. an α -ketoacid (pyruvate) or α -hydroxyacid (lactate). The most active compounds, **2a-b**, displayed a synergistic cytotoxic effect in combination with gemcitabine under hypoxic conditions and inhibited cell migration and invasion in pancreatic cancer cells.⁸⁷ Glucose derivatives **3a-b** displayed weaker inhibitory activity against LDH-A but they exhibited more efficacy in cell-based assays.⁸⁵



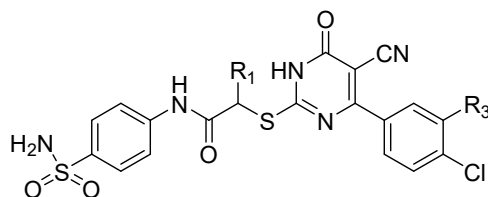
- **Chimeric (bifunctional)-type inhibitors**

Chimeric LDH-A inhibitors are bifunctional molecules in which two portions, one a substrate mimic and the other a cofactor mimic, are conjugated by a linker. Representative examples of this class are compounds **3**⁸⁸ and **4**⁸⁹, discovered through a fragment-based approach by AstraZeneca and ARIAD Pharmaceuticals, respectively. They both showed high potency in enzymatic assays with inhibitory activity in the nanomolar range against LDH-A, but not optimal physicochemical properties, thus they require further optimization.



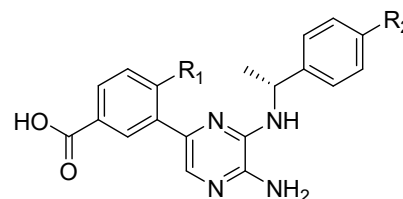
- **Dihydropyrimidine- and pyrazine-based inhibitors**

By following a high-throughput screening approach, Genentech identified dihydropyrimidines **5a-e**⁹⁰ and pyrazines **6a-d**⁹¹ as LDH-A inhibitors active in the micromolar range. Some of these derivatives exhibited potency in the high nanomolar range, but they require further optimization to improve cell membrane permeability and to obtain analogs with improved cellular activity.



5

- a: R₁= R₂= H
- b: R₁= Me, R₂= H
- c: R₁= Et, R₂= H
- d: R₁=Me, R₂= Cl
- e: R₁=Me, R₂= F



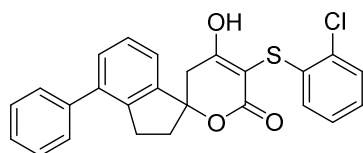
6

- a: R₁= H; R₂= H
- b: R₁= Cl; R₂= H
- c: R₁= CH₃; R₂= H
- d: R₁= CH₃; R₂= Cl

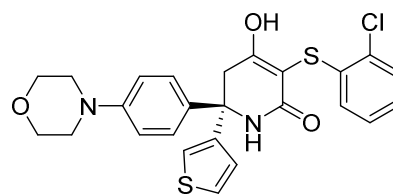
- **Dihydropyrone- and hydroxylactam-based inhibitors**

Dihydropyrone-based derivatives⁹² were identified by Genentech through high throughput screening (HTS), and after *hit to lead* optimisation, **7** resulted the most active compound against LDH-A (in the nanomolar range), but it showed weak activity in cell-based assays.

In order to further investigate this class of compounds the dihydropyrone core was replaced with a hydroxylactam. Among the new hydroxylactam-based derivatives, **8 (GNE-140)** was identified as potent enzymatic inhibitor of both LDH-A and LDH-B, possessing adequate pharmacokinetic properties that make it suitable for its use as an *in vivo* tool compound.⁹³ Results on potency in cells, mechanism of action and tumor growth inhibitor have been recently reported.⁹⁴



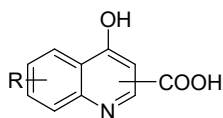
7



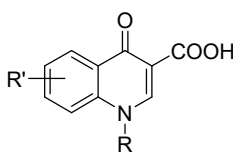
8 (GNE-140)

- **Quinoline scaffold-based inhibitors**

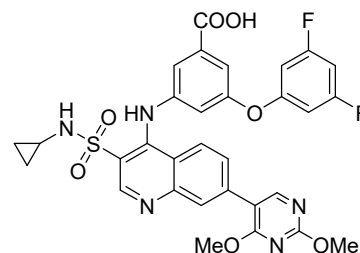
Quinoline and quinolone derivatives (general structure **9** and **10**, respectively) were identified as potential scaffold in the search for new LDH-A several decades ago.^{95,96} Recently, GSK reported potent quinoline-based LDH-A inhibitors, moderately selective for LDH-A over LDH-B.⁹⁷ These molecules, particularly the most active compound **11**, showed LDH-A inhibitory activity also in cultured cancer cells. However, their pharmacokinetic properties need to be improved for further *in vivo* studies.^{97,98}



9



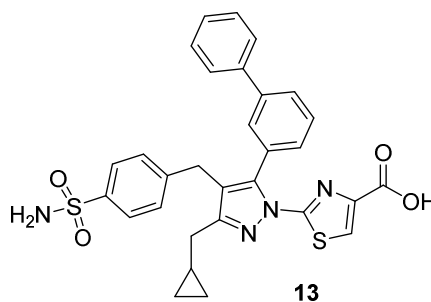
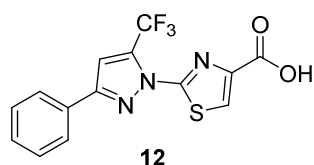
10



11

- **Pyrazole-based inhibitors**

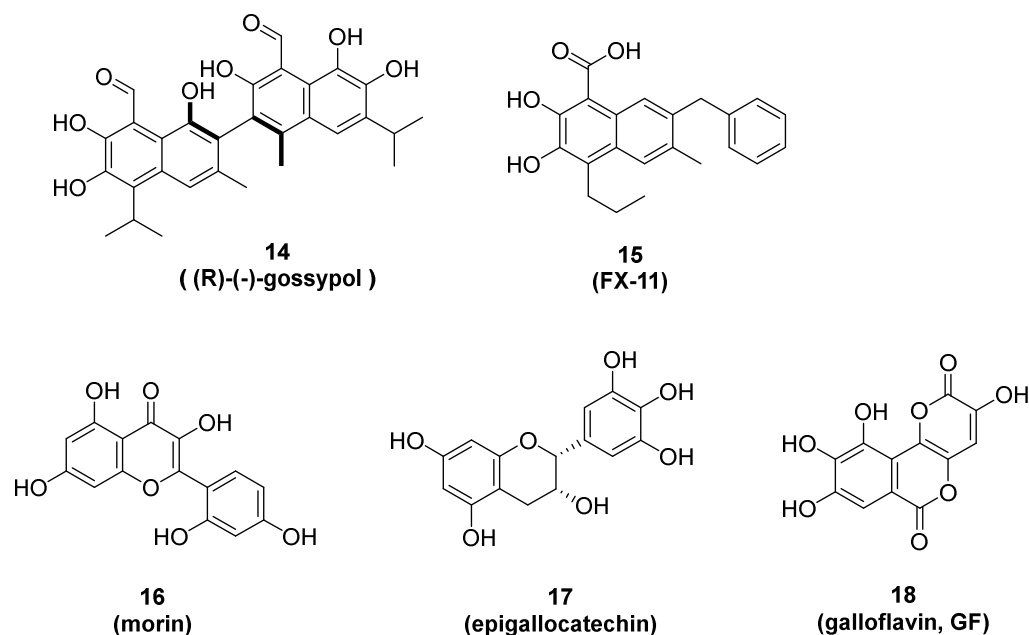
Very recently, Ganesha et al.⁹⁹ reported the discovery and medicinal chemistry optimization of a novel series of pyrazole-based inhibitors of LDH-A. By using a quantitative HTS they identified the hit candidate **12**; by structure-based design and optimization they developed compounds with more potent enzymatic activity. Compound **13** resulted one of the most active, exhibiting low nM inhibition of both LDH-A and LDH-B and inhibition of lactate production and glycolysis in MiaPaCa2 pancreatic cancer and A673 sarcoma cells at submicromolar concentration.⁹⁹



- **Polyphenolic-based inhibitors**

A representative compound of this class is gossypol, a natural polyphenol derived from the cotton plant. The most active enantiomer form, (R)-(-)-gossypol **14**, inhibits both LDH-A and LDH-B in micromolar range by competition with NADH, but it is not specific for this enzyme. It exhibits a broad spectrum of biological activities, such as antitumor, antioxidant, antiviral and antiparasitic,^{100,101} and it also causes unspecific toxicity mainly due to the presence of aldehyde and catechol groups which generate toxic metabolites.^{102–104} Nevertheless, (R)-(-)-gossypol entered clinical trials in combination with antitumor agents for the treatment of different tumors, with some studies terminated because of unacceptable toxicity and other are still ongoing. (clinicaltrials.gov)

In an attempt to develop less toxic and more selective inhibitor, several molecules structurally close to gossypol were synthesized, particularly 2,3-dihydroxynaphthoic acid derivatives,^{105,106} initially designed as antimalarian agents.¹⁰⁶ Among them, compound **15 (FX-11)** resulted the most potent inhibitor and displayed also good selectivity for LDH-A isoform.⁶⁴ It showed to reduce ATP and lactate production, induce oxidative stress and cell death in cultured cancer cells.⁶⁴ However, further studies gave rise to suspicion that its effects could be not ascribed to LDH-A inhibition but to the reactive catechol group^{88,89} and it was never tested in clinical trials.



Other polyphenolic compounds based on flavon structure were found to be potential anticancer agents due to their inhibitory activity against LDH-A such as the flavone morin **16**¹⁰⁷ and the flavon-like derivatives, epigallocatechin **17** and galloflavin **18**.

Epigallocatechin (**17**), naturally found in *Spatholobus suberectus*, inhibited both LDH-A activity and HIF-1 expression, showing significant inhibition of breast cancer growth; it is considered a *lead* compound for further investigation.¹⁰⁸

Finally, galloflavin (GF, **18**) is a derivative of gallic acid recently identified through a virtual screening campaign as LDH-A inhibitor by our group.¹⁰⁹ GF was found to inhibit the enzymatic activity of purified LDH, by occupying the NADH site, and the lactate production in cultured cancer cells in the micromolar range. Many investigations on GF activity in different cancer cell lines and its mechanism of action were carried out.^{110–114} These studies confirmed GF antitumor effects and showed it is not harmful for mitochondrial respiration, suggesting tolerability for normal cell metabolism and thus encouraging the further exploration of this compound.

Hence, the development of promising GF analogs is the aim of the present work, and is directly addressed in the next chapter (2. Aim of the work).

It is evident that very few LDH inhibitors have progressed to the preclinical stage and into clinical trials to date,⁸³ often because of poor pharmacokinetic profile, particularly poor penetration inside cells with consequent lack of cellular activity. The improvement of drug-like properties is fundamental for their use as *in vivo* tool compounds and their further development.

It is worth noting that the discovery of selective LDH-A inhibitors proved to be very difficult because of the high structural homology in the active sites of A and B subunits. However, some of the most potent and cell-active compounds, such as **8** (GNE-140), **13** and **18** (GF), are non-selective for LDH-A over LDH-B.

Therefore, current efforts aim to the discovery of potent LDH inhibitors with good drug-like properties, not necessarily pursuing selectivity towards isoform LDH-A (“pan-LDH inhibitors”).⁹³

2. Aim of the work

Within a research project that aims to the development of new innovative anticancer agent targeting tumor metabolism, our group has been involved in the search for new LDH-A inhibitors, through a collaboration with Professor Recanatini's and Professor Di Stefano's groups.

In these context, we recently discovered LDH-A inhibitor galloflavin (GF, **18**)¹⁰⁹ (**Figure 10a**), which is now produced and sold by several suppliers. GF is considered as a reference compound among the anticancer glycolytic inhibitors since its antitumor effect has been well-established in several studies.^{110,112,114,115} Notably, some of them have suggested that inhibition of LDH is not the only bioactivity of GF. A 2D in-cell NMR metabolomics study recently revealed that GF affects other metabolic pathways, influencing pyruvate dehydrogenase kinase (PDK), alanine aminotransferase 1 (ALT1) and pyruvate dehydrogenase (PDH), and suggesting that GF anticancer effects could be due to its multi-target effect rather than to specific inhibition of LDH.¹¹¹ Fiume *et al.*¹¹³ reported that GF hinders the interaction of LDH-A with ssDNA and inhibits RNA synthesis in cultured cancer cells, suggesting its antiproliferative activity can derive not only by blocking tumor glycolysis but also by RNA synthesis inhibition; furthermore, GF can be a useful tool to study the biological role of LDH-A binding to ssDNA.

GF and oxamate were found to reverse the inflammation-induced effects in cancer cells in a recent study by Manerba *et al.*¹¹⁶ The same group reported that LDH-A inhibition by GF and oxamate led to decreased level and function of the major heat shock proteins involved in tumorigenesis suggesting a connection between LDH and heat shock response.¹¹⁷ These data confirmed the hypothesis that GF possess multiple biochemical properties and suggest that the polyphenolic structure could be an appropriate molecular scaffold to design compounds joining LDH inhibitory activity with other anticancer effects.¹¹⁷

Therefore, the anticancer potential of GF is of great interest as well as its employment as tool to investigate the effects of LDH inhibition.

Galloflavin (GF, **18**) is synthesized from gallic acid (GA) in a one-step dimerization/oxidation process mediated by NaOH^{109,118} (**Figure 10a**). It is a polyhydroxylated tricyclic compound, based on fusion of a isocoumarin and a pyrone core (**Figure 10b**).

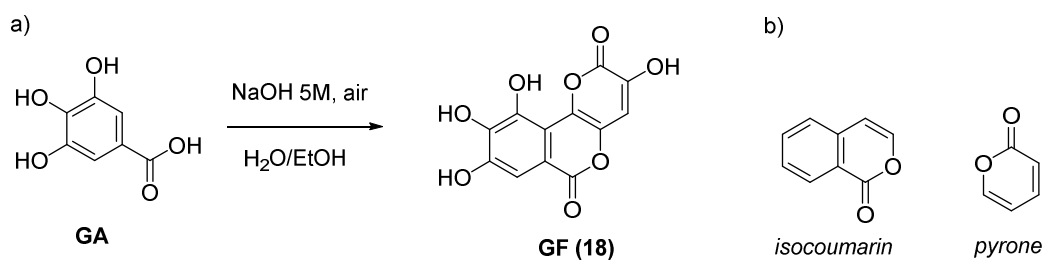


Figure 10. a) Synthesis of GF; b) Molecular structure of isocoumarin and pyrone cores

The calculated binding pose postulated in the initial study, as reported in **Figure 11**, suggested GF binds mainly to the enzyme by hydrogen bonds.¹⁰⁹

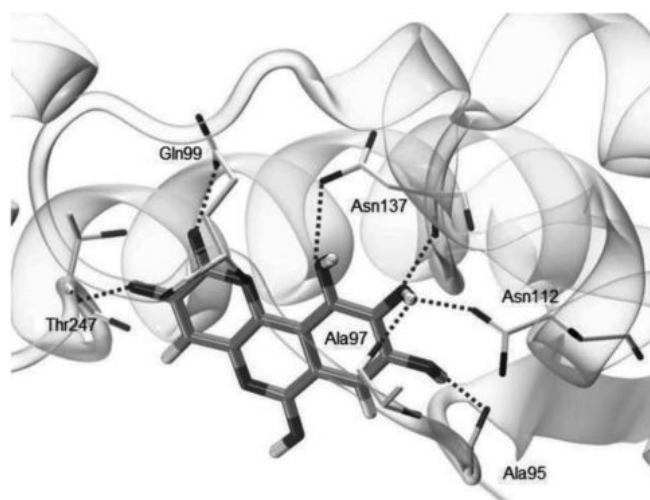


Figure 11. Galloflavin docking pose with human LDH-A, obtained by the VS procedure.¹⁰⁹

However, GF still requires an investigation in terms of Structure Activity Relationships (SAR). The SAR assessment is crucial for candidate *hits*, together with the improvement of the pharmacokinetic profile, to progress towards the *hit to lead* optimization phase in the drug discovery process.

The present work aims to the disclosure of GF SAR, through the synthesis of a series of structural analogs, in order to gain a deeper knowledge on the effective key interactions involved in its binding to LDH.

GF SAR assessment proved to be very challenging for two main reasons: first, its synthesis is not versatile and did not allow access to structural analogs; second, GF did not prove to be a practical starting point for the synthesis of analogs because of its poor solubility in common organic solvents and its fast degradation under both basic and acidic conditions.

Therefore, we undertook a rational design aimed to reproduce GF pharmacophore on simpler and synthetic accessible scaffold, with improved physicochemical properties, which could allow us the synthesis of a series of derivatives, without having to deal with the poor chemical manipulability of the original molecule.

We carried out a structural simplification of GF, taking into account three main aspects: 1) elimination of the double pyrone system (B and C rings, **Figure 12a**) that brings complexity and pose significant synthetic challenges; 2) keeping the same position and distance of the four hydroxyl groups, to best reproduce the H-bond fingerprint of GF, that is likely a key factor in GF binding to LDH; 3) retaining tricyclic skeleton, useful to mimic the original structure. This process led to the identification of compound **19**, known as urolithin M6 (**UM6**), by simply substituting the pyron ring C with a benzene ring. (**Figure 12a**). The overlap of GF and UM6 structures is illustrated in **Figure 12b**.

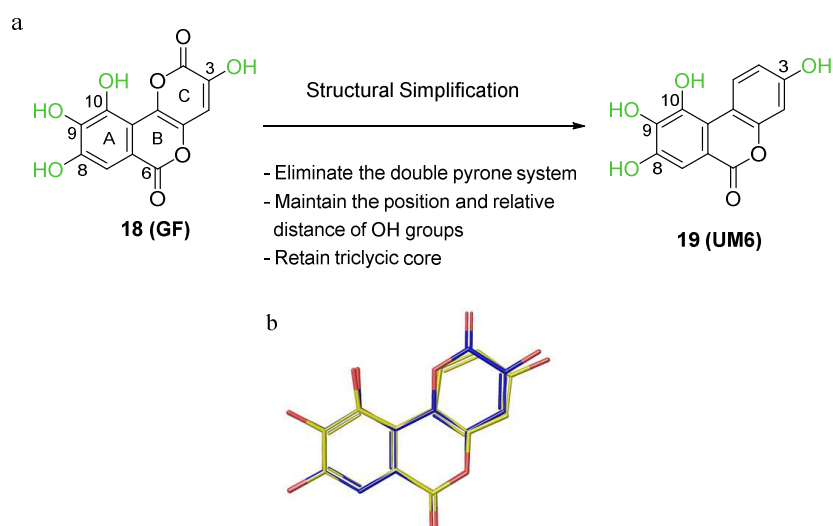


Figure 12. a) Structural simplification of GF toward UM6; b) overlap of GF (blu) and UM6 (yellow).

Particularly, UM6 core is based on the same GF isocoumarin ring (blu, **Figure 13**), fused with a benzene (pink) in place of the pyrone (red), thus resulting in a benzo[c]chromenone core (**Figure 13**).

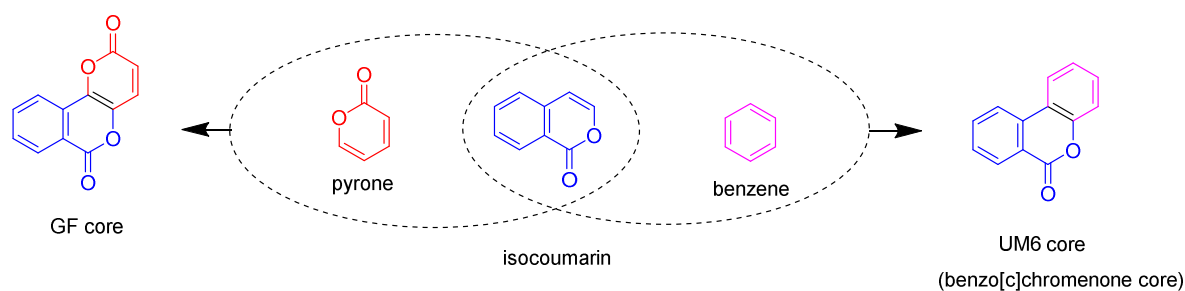


Figure 13. GF and UM6: core structure comparison.

The benzo[c]chromenone scaffold (also called dibenzopyranone or benzocoumarin) is found in many natural products and biologically active molecules, and is considered as a privileged structure, since it is of great importance as intermediate for the synthesis of various pharmaceutically interesting compounds.^{119–122}

In particular, **UM6** is a tetrahydroxylated dibenzopyranone derivative that belongs to the urolithin family, a class of recurrent metabolites after the assumption of aliments rich in ellagitannins, such as pomegranates, berries, walnuts, almonds (**Figure 14**).^{123,124} Their natural origin and common presence in gut microbiota suggested a promising safety profile for this class of compounds. Moreover, a number of beneficial properties and biological activities have been recently attributed to urolithins, such as antioxidant,^{125,126} anti-inflammatory,^{126–129} anticancer^{130–133} and antiglycation¹³³ activities.

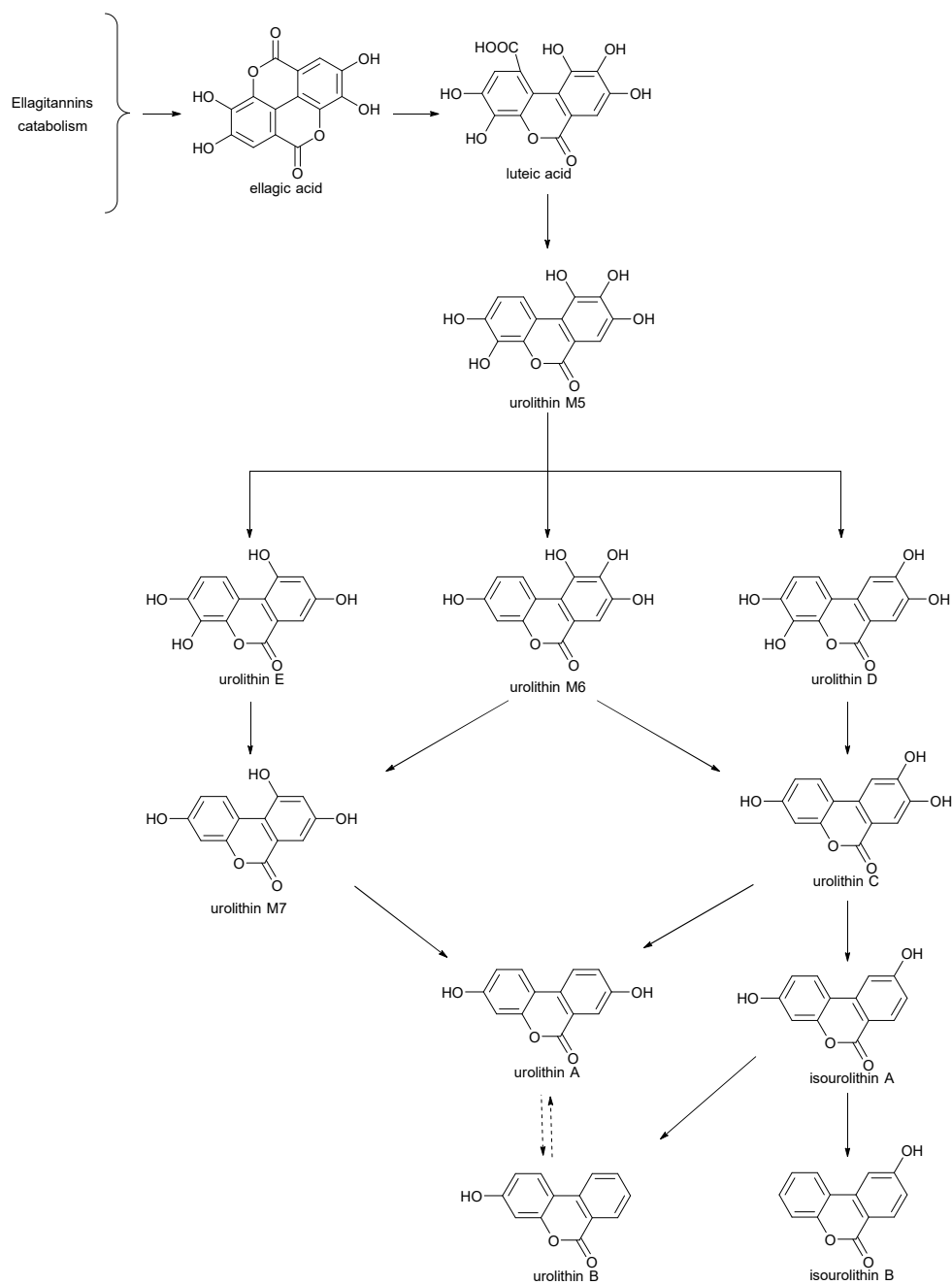


Figure 14. Gut microbiota metabolism of ellagitannins and ellagic acid.

Since both its scaffold and OH substitution pattern is high similar to GF, we assumed that UM6 could maintain GF pharmacophore and mimic its LDH-A inhibitor activity and thus be useful as starting point for our investigations.

It was characterised as an ellagitannin metabolite by Ito et al.¹³⁴ and its production via biotechnological methods has been reported,¹³⁵ while neither a biological study, nor chemical synthesis have been reported.

Therefore, the first step of the present project was the development of a synthesis for UM6 and a preliminary biological evaluation to assess if UM6 could be a GF biomimetic.¹³⁶

Some strategies were reported in the literature for the synthesis of other urolithins, as it is illustrated in **Figure 15** and summarized below:

- 1) copper catalyzed Hurtley reaction, that is described for synthesis of urolithins that possess one or two hydroxyl groups, such as Uro-A, Uro-B;¹²⁵ however it presents issues of very low yields and it doesn't seem much versatile;
- 2) basic decarboxylative hydrolysis of ellagic acid (EA) permits to achieve urolithin M5 according to literature, but no other urolithins have been obtained through this route;¹³⁷
- 3) inverse electron demand Diels–Alder reaction is reported for total synthesis of UM7; however it is highly substrate-dependent and expensive in terms of both starting materials and number of steps;¹³⁸
- 4) Esterification of 2-bromobenzoic acids followed by ring closure through Heck coupling is reported for Uro-D;¹³⁹ however yields are usually poor and reaction times very long.

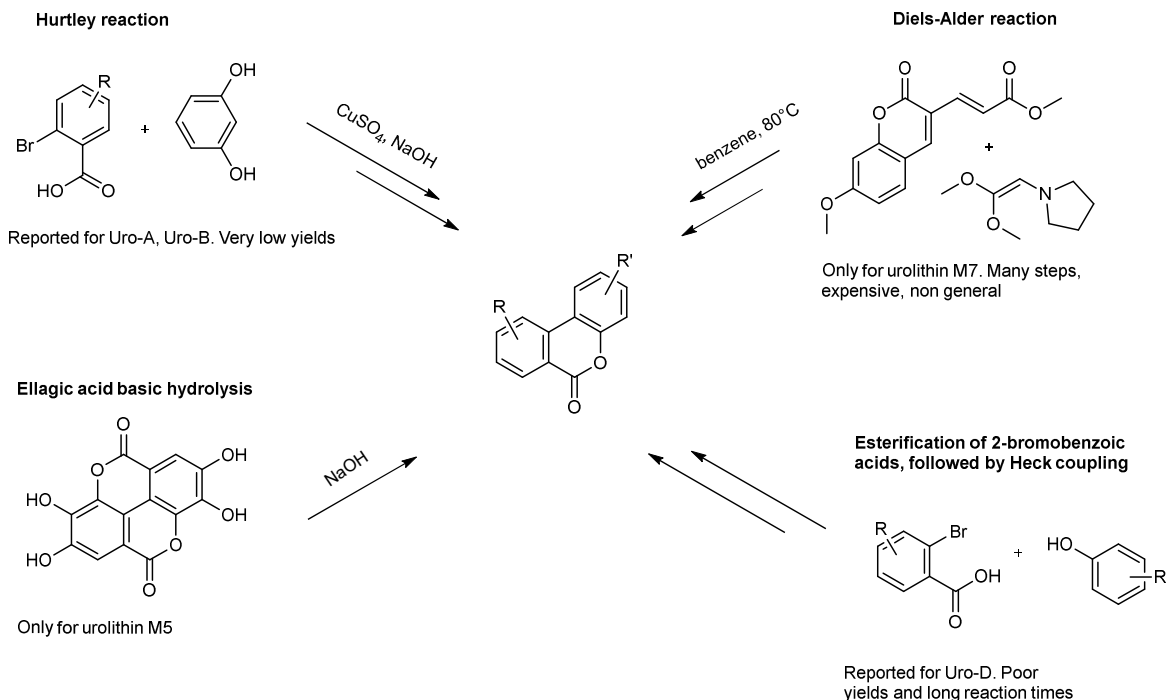
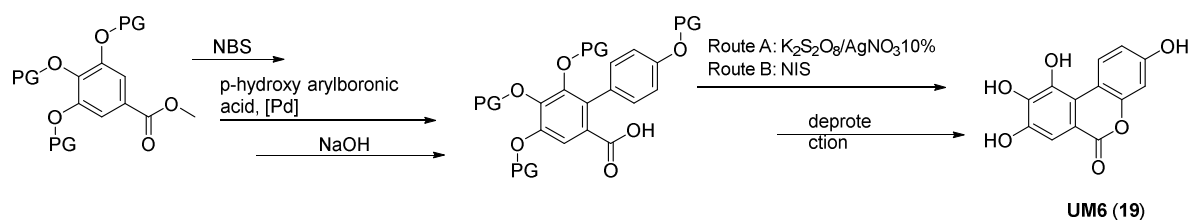


Figure 15. Current methods for urolithins synthesis.

All these methods have some major drawbacks and above all, none of them seemed particularly attractive, since our purpose was to develop an efficient and versatile synthetic procedure that could allow a facile access not only to UM6 but also to the synthesis of future structural analogs for SAR investigations.

Therefore we planned a new synthetic strategy, illustrated in **Scheme 1**, taking into account the use of protecting groups (PG) for the presence of four OH functionalities. The planned synthesis features the use of a methyl ester GA derivative, which is brominated, coupled with the opportune protected boronic acid and then hydrolyzed to give the 2-arylbenzoic acid. This intermediate is then transformed into lactone through $K_2S_2O_8$ - (Route A) or NIS-mediated (Route B) C-H oxygenation and finally deprotected to achieve the desired UM6 (**19**).

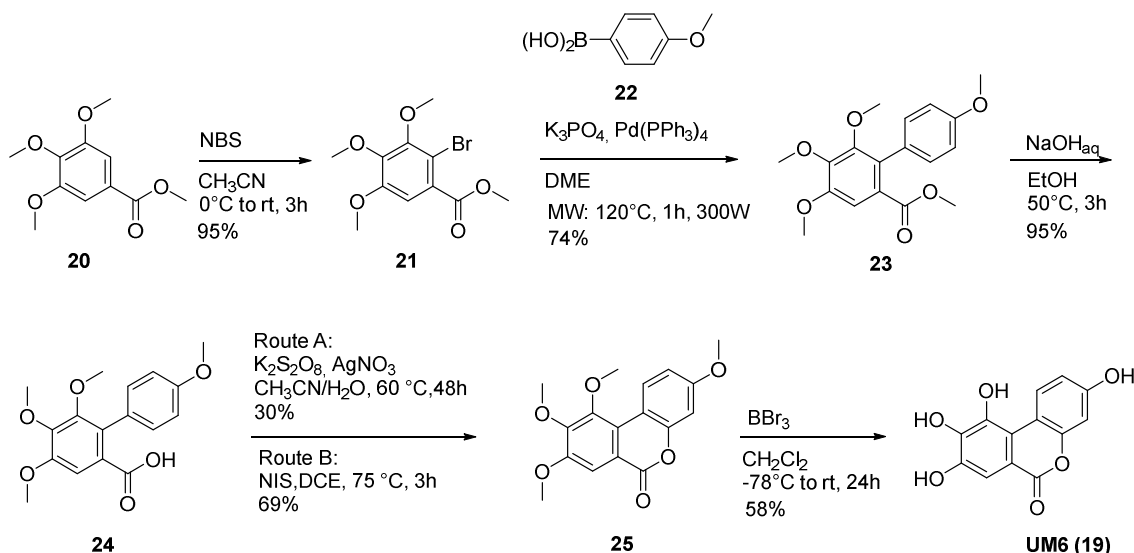
Scheme 1. Planned synthesis of UM6



Different protecting groups were screened, and the methyl ether was selected as the best option as it resulted stable under the synthetic conditions. The optimized synthesis, shown in **Scheme 2**, started with initial NBS-mediated bromination of the commercially available methyl-3,4,5-trimethoxybenzoate **20** to obtain the corresponding methyl-2-bromo-3,4,5-trimethoxybenzoate **21**. The subsequent Suzuki coupling with 4-methoxyphenylboronic acid **22** with $Pd(PPh_3)_4$ and K_3PO_4 in DME in microwave heating for 1 hour (or in conventional heating 24h in a pressure tube) led to methyltetramethoxybiphenyl-2-carboxylate **23**, which was subsequently hydrolyzed with NaOH to generate the free tetramethoxybiphenyl-2-carboxylic acid **24**. Successive ring closure through C–H oxygenation was initially performed using $K_2S_2O_8/AgNO_3$ 10% in 1/1 H_2O/CH_3CN for 48 h at 60 °C, which led to the desired cyclized product **25** with a non-optimal yield of 30% (Route A). To obtain a better yield, 2-arylbenzoic acid intermediate **24** was subjected to a radical oxidative lactonization mediated by N-iodosuccinimide (NIS) (Route B).¹⁴⁰ The reaction was carried out in 1,2-dichloroethane at 75 °C for 3 hours and afforded the desired cyclized compound **25** in a satisfactory

69% yield. The final deprotection in BBr_3 led to the desired **19** in 58% yield, after purification by C18 flash silica gel. This synthetic route provided UM6 in 5 steps and 27% overall yield.¹³⁶

Scheme 2. Optimized UM6 synthesis

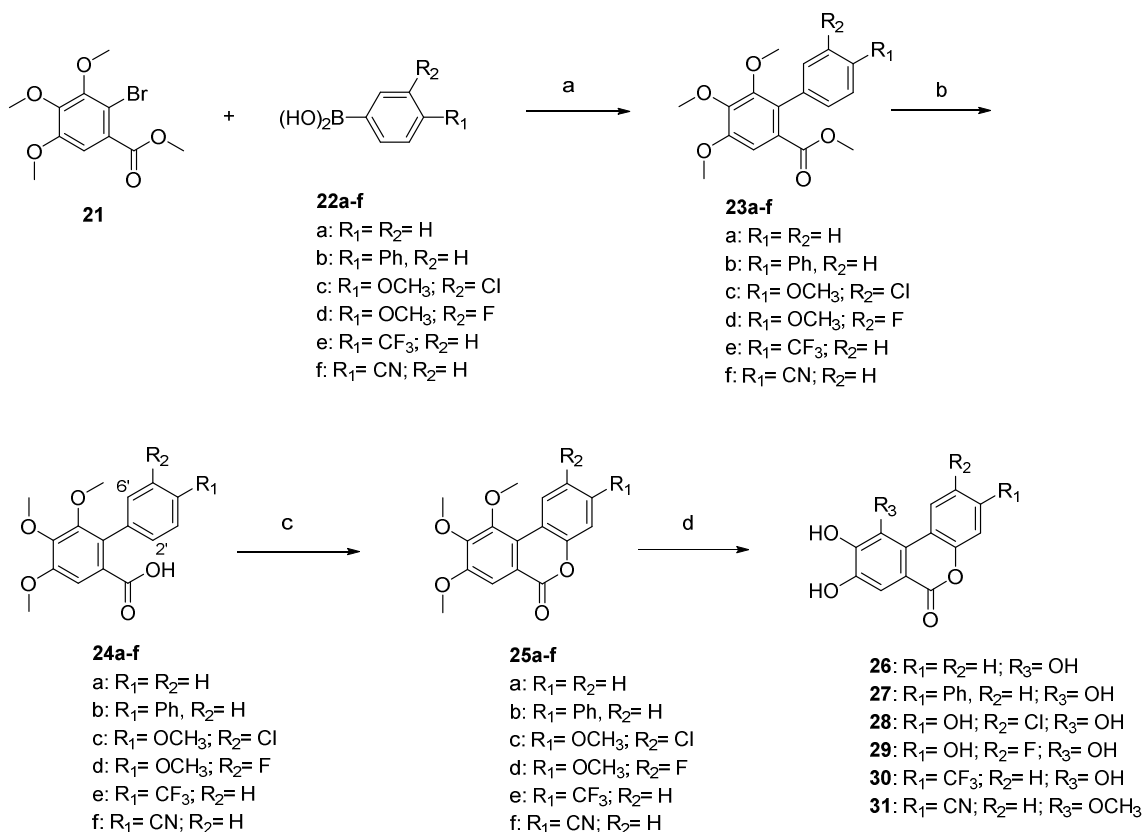


Preliminary biological evaluation revealed UM6 inhibited both the enzymatic activity of LDH-A and lactate production in cultured cancer cells at comparable levels to GF, confirming it can be considered a GF biomimetic and that it could be a suitable *hit* structure in the field of LDH-A inhibitors.¹³⁶

In view of this encouraging result, new UM6 analogs were designed to explore the SAR of this class of compounds and synthesized applying the efficient newly developed synthetic strategy. Indeed, a structural variability of analogs can easily be achieved with this procedure simply by using of different boronic acids as building blocks for the key Suzuki step.

Initially, with the aim to evaluate the role of the hydroxyl group in the C ring and the influence of changes in the lipophilicity of the molecules we designed and synthesized the UM6 analogs **26-31** (**Scheme 3**).

Scheme 3. Synthesis of UM6 analogs 26-31



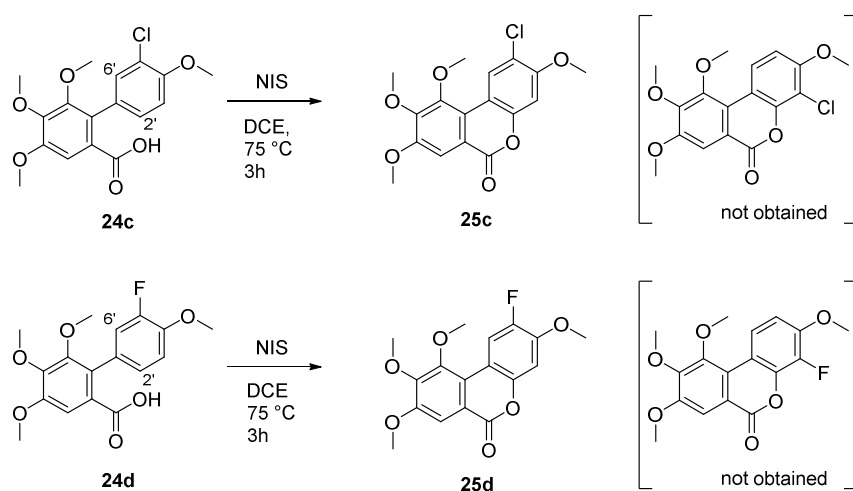
Reagents and conditions: a) K₃PO₄, Pd(PPh₃)₄, DME, 120°C, 24h; b) NaOH_{aq}, EtOH, 50°C, 3h; c) NIS, DCE, 75 °C, 3h; d) BBr₃, CH₂Cl₂, -78°C to rt, 24h.

Starting from methyl-2-bromo-3,4,5-trimethoxybenzoate **21**, Suzuki coupling was performed with the differently substituted boronic acids **22a-f** to give tetramethoxybiphenyl-2-carboxylate derivatives **23a-f**. Suzuki couplings were performed in conventional heating in pressure tube instead of microwave heating conditions, because it allowed to scale up the reaction to ~1 gram. Biphenyl-2-carboxylates **23a-f** then hydrolysed to the corresponding biphenyl-2-carboxylic acids **24a-f**. Successive ring closure were performed using the more efficient procedure of NIS-mediated lactonisation to obtain the benzocoumarin derivatives **25a-f**, which upon deprotection of the methoxyl groups gave the desired OH-free final compounds **26-30** with yields comparable to UM6. Only in the case of benzocoumarin **25f** the final demethylation didn't proceed completely, giving the methoxyderivative **31** instead of the expected trihydroxylated derivative. Characterisation by ¹H-NMR, ¹³C-NMR,

DEPT, HSQC, HMBC and NOESY experiments was performed in order to confirm the position of the methoxy function on the A ring.

Notably, as it is illustrated in **Scheme 4**, cyclisation of the non-symmetrical biphenyl-2-carboxylic acids **24c**, **24d**, could occur in 2' or 6' position leading to different products. In both cases we obtained only the compound derived from cyclisation in 2' position (**25c** and **25d**), as we confirmed by $^1\text{H-NMR}$ spectra.

Scheme 4. NIS-lactonization of non-symmetrical biphenyl-2-carboxylic acids **24c-24d**



After investigating the importance of the substituents on the C ring of *hit* compound UM6, we directed our attention on the lacton moiety and designed compound **32** (**Figure 16**), which differs from UM6 in the reverse position of lacton function in the B pyron ring. Notably, it can be also considered as a UM6 differently OH-substituted analog, as it could be appreciate by drawing the molecules in two different ways (**Figure 16**).

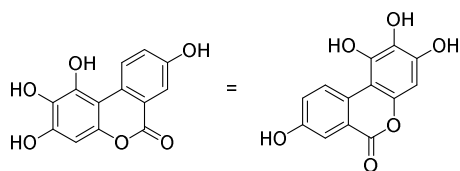
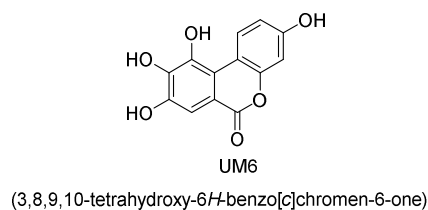
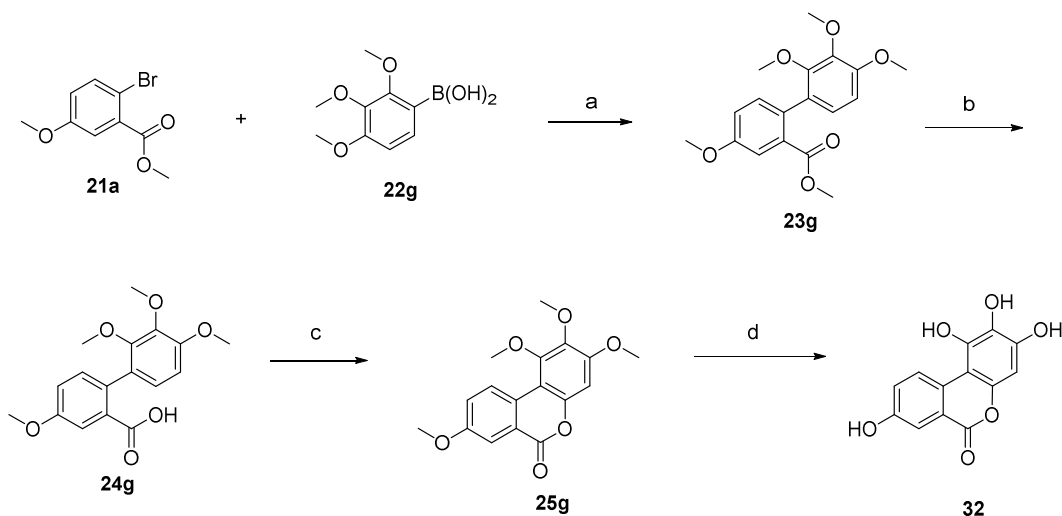


Figure 16. Derivative **32** (different way to representation) in comparison with UM6.

The synthesis of compound **32** (**Scheme 5**) was performed starting from Suzuki coupling between the commercially available methyl 2-bromo-5-methoxybenzoate **21a** and (2,3,4-trimethoxyphenyl)boronic acid **22g**, and proceeded through the same steps previously described for the synthesis of UM6 and its analogs.

Scheme 5. Synthesis of analog **32**



Reagents and conditions: a) K_3PO_4 , $Pd(PPh_3)_4$, DME, $120^\circ C$, 24h; b) $NaOH_{aq}$, EtOH, $50^\circ C$, 3h; c) NIS, DCE, $75^\circ C$, 3h; d) BBr_3 , CH_2Cl_2 , $-78^\circ C$ to rt, 24h.

Additionally, we designed and synthesized three UM6 analogs **33-35** (**Figure 17**) that share the same trihydroxylated ring A and the hydroxybenzene ring C, while they differ in the B portion as follow: i) lacking of B ring gives the lacton ring-opened analog **33**; ii) carbonyl reduction of lactone ring gives analog **34**; iii) substitution of B ring with benzene results in the phenanthrene derivative **35**.

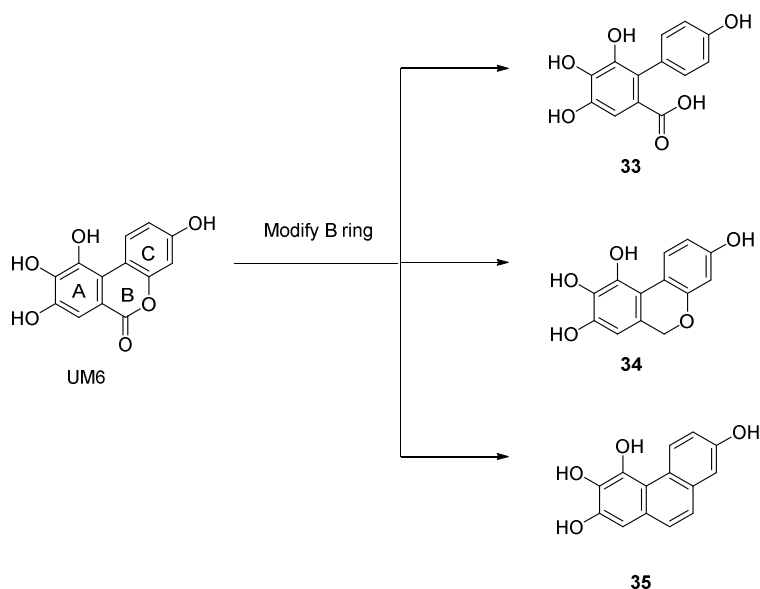
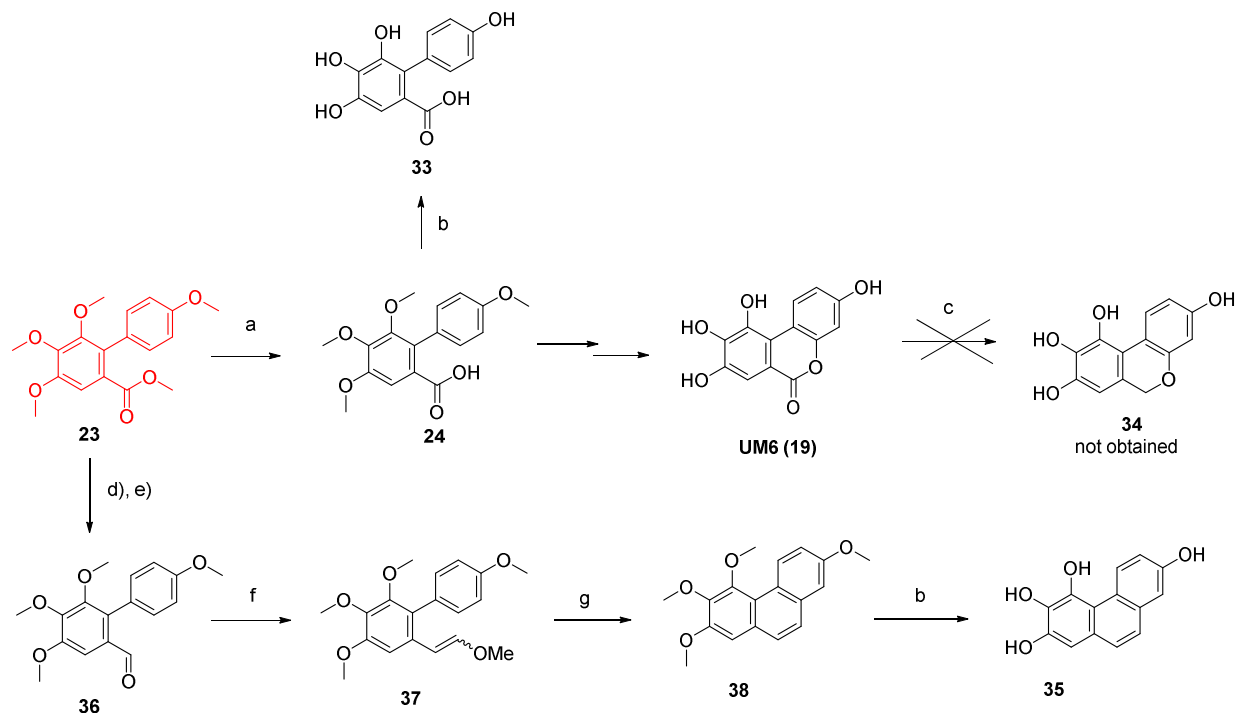


Figure 17. Structural modification of UM6 towards other scaffolds.

The synthesis of **33-35** has been planned starting from the intermediate **23** of UM6 synthesis, which assumes a central role in the intersection between three different synthetic routes, as it is showed in **Scheme 6**. Derivative **33** was obtained through hydrolysis followed by demethylation. Analog **34** was planned through the route that led **23** to UM6 and reduction of the latter with $\text{NaBH}_4/\text{BF}_3 \cdot \text{Et}_2\text{O}$; unfortunately this reaction didn't work as expected and the compound was not obtained. Phenanthrene analog **35** was synthesized starting from conversion of **23** to aldehydes **36** (42% yield over two steps), which reacted in a Wittig fashion with (methoxymethyl)triphenylphosphonium chloride to afford the corresponding arylvinyl methyl ether **37** (56%). Bismuth-catalyzed cyclization-aromatization led to the protected phenanthrene **38** (65%), which was deprotected to obtain the final tetrahydroxyphenanthrene analog **35** (86%) (**Scheme 6**).

Scheme 6. UM6 analogs with different scaffold

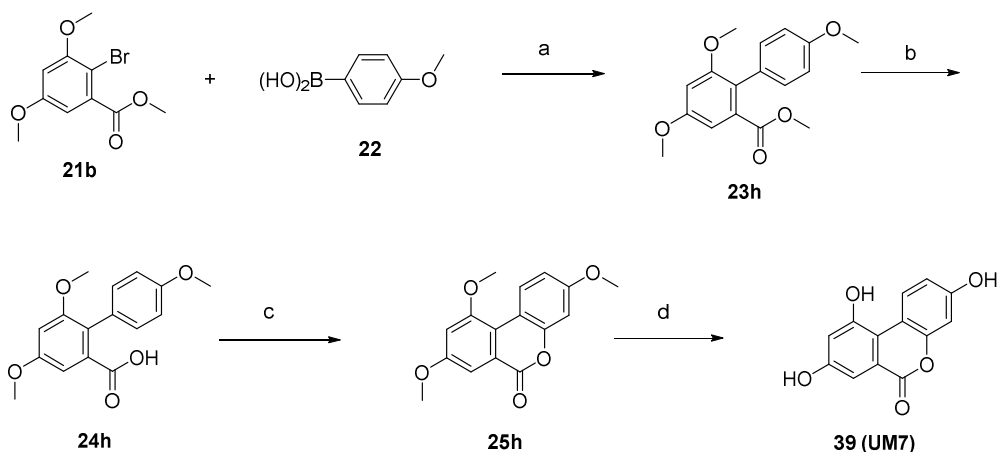


Reagents and conditions: a) NaOH_{aq} , EtOH, 50°C , 3h; b) BBr_3 , CH_2Cl_2 , -78°C to rt, 24h; c) NaBH_4 , $\text{BF}_3\text{Et}_2\text{O}$, THF, 0°C to reflux, 3h; d) DIBAL, CH_2Cl_2 , 0°C to rt, 3h; e) PCC, CH_2Cl_2 , rt, 2h; f) (methoxymethyl)triphenylphosphonium chloride, LiHMDS, THF, rt, 2h; g) $\text{Bi}(\text{OTf})_3$, DCE rt, 30 min.

To further extend the applicability of our synthetic plan and to investigate the role of the trihydroxy-moiety in UM6 A ring, we then synthesized urolithin M7 (UM7), in which the 8,9,10-trihydroxy moiety is substituted with 8,10-dihydroxy moiety. (See **Figure 14**)

Therefore the synthesis of UM7 (**39**, **Scheme 7**) started from methyl 2-bromo-3,5-dimethoxybenzoate **21b** and (4-methoxyphenyl)boronic acid **22** and followed the optimised procedure previously used for UM6 and analogs, leading to the product with a 20% overall yield.

Scheme 7. Synthesis of UM7

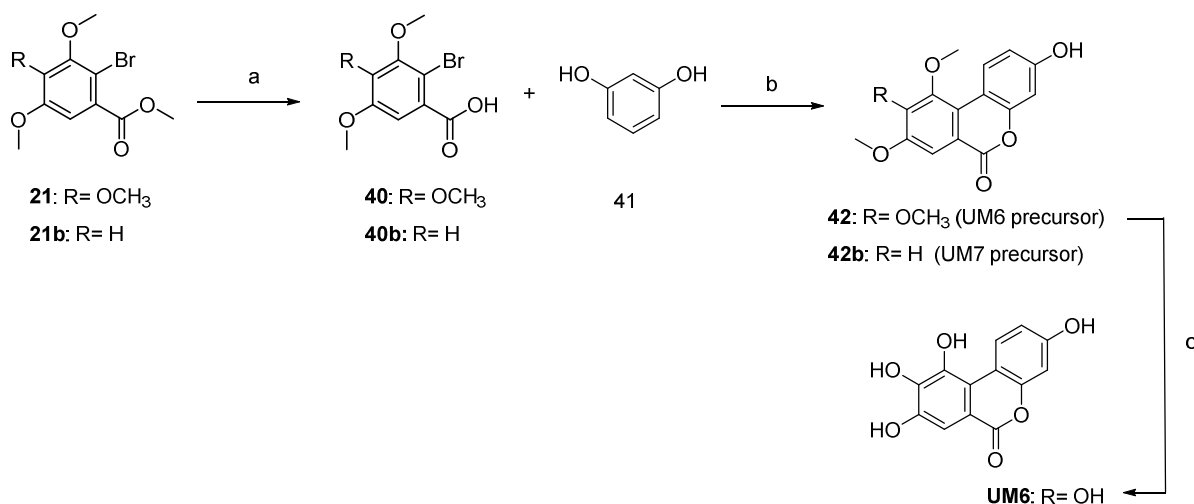


Reagents and conditions: a) K_3PO_4 , $Pd(PPh_3)_4$, DME, $120^\circ C$, 24h; b) $NaOH_{aq}$, EtOH, $50^\circ C$, 3h; c) NIS, DCE, $75^\circ C$, 3h; d) BBr_3 , CH_2Cl_2 , $-78^\circ C$ to rt, 24h.

UM7 synthesis has been previously reported in 2011 by Pottie *et al.*,¹³⁸ however our strategy proved to be a faster and simpler alternative. Indeed, Reddy, M. D. *et al.*¹⁴¹ recently reported a new UM7 synthesis taking into account our synthetic plan.

Additionally, to validate our synthetic strategy, and to compare it with the known methods for urolithins' synthesis, we decided to explore the preparation of UM6 and UM7 through the Hurtley reaction (**Scheme 8**), which is reported to be a fast and effective method for dibenzopyranones synthesis.¹⁴² Thus, methyl ester derivatives **21**, **21b** were hydrolysed to the correspondent acids **40**, **40b**, which were condensed with resorcinol **41** in a 4M NaOH solution with $CuSO_4$ as catalyst to give the methylated benzocoumarins derivatives **42**, **42b** (14% and 3% of yield, respectively). Finally, demethylation of **42** led finally to UM6 (40%). Demethylation of **42b** was not performed because of the too low amount of material obtained, but we can reasonably affirm that the reaction would give UM7 (**Scheme 8**).

Scheme 8. UM6 and UM7 synthesis through Hurtlely reaction



Reagents and conditions: a) NaOH_{aq}, EtOH, 50°C, 3h; b) i. NaOH_{aq}, 60 °C 30 min; ii. CuSO₄ 10%, 95 °C, 3h; c) BBr₃, -78 °C to rt, 24h.

The major drawback of this synthesis is the very poor yield in the key step of benzocoumarin ring formation. However, since it is a very short procedure and the Hurtlely reaction has been recently re-explored for the synthesis of some substituted benzocoumarins,¹⁴² we exploited it to obtain UM7-inspired analogs.

In particular, we designed and synthesized compound **43**, that is the UM7 analog with the reverse lacton function (**Figure 18**) together with dibenzopyranone (**46a-b**, **43**) and dibenzopyrane (**47-49**) derivatives as illustrated in **Scheme 9**.

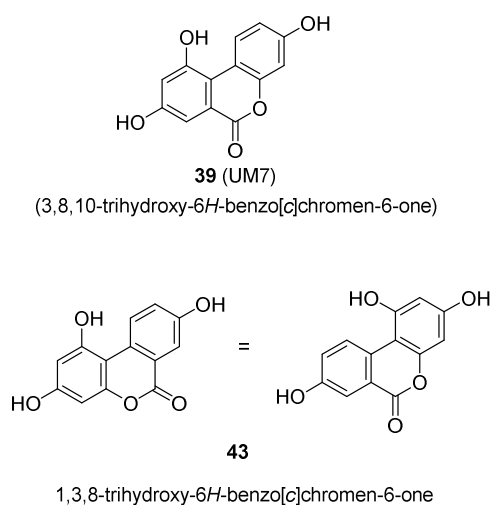
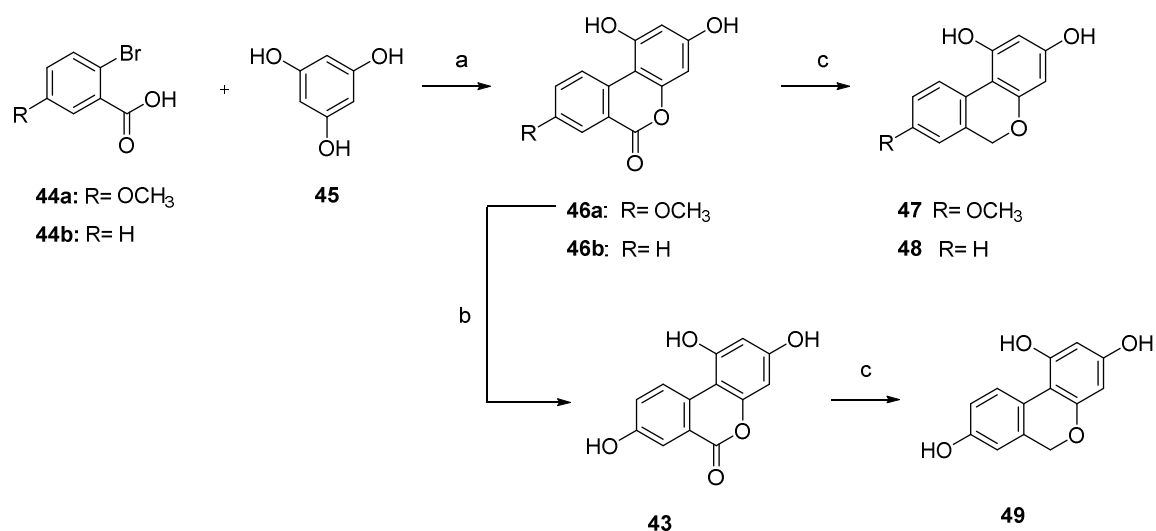


Figure 18. Derivative **43** (different way to representation) in comparison with UM7.

Commercially available 2-bromo-5-methoxybenzoic acid **44a**, and 2-bromobenzoic acid **44b** were condensed with phloroglucinol **45** in a 4M NaOH solution and CuSO₄ as catalyst to give dibenzopyranones **46a**, **46b**¹⁴² (68% and 83%, respectively). Methylated derivative **46a** was subsequent deprotected to obtain compound **43** (34%). The dibenzopyranone compounds **46a**, **46b** and **43** were reduced with NaBH₄/BF₃·Et₂O to the corresponding dibenzopyrane analogs **47**, **48** and **49** (62%, 23% and 17 %, respectively) (**Scheme 9**).

Scheme 9. Synthesis of UM7-inspired analogs by using Hurtley reaction



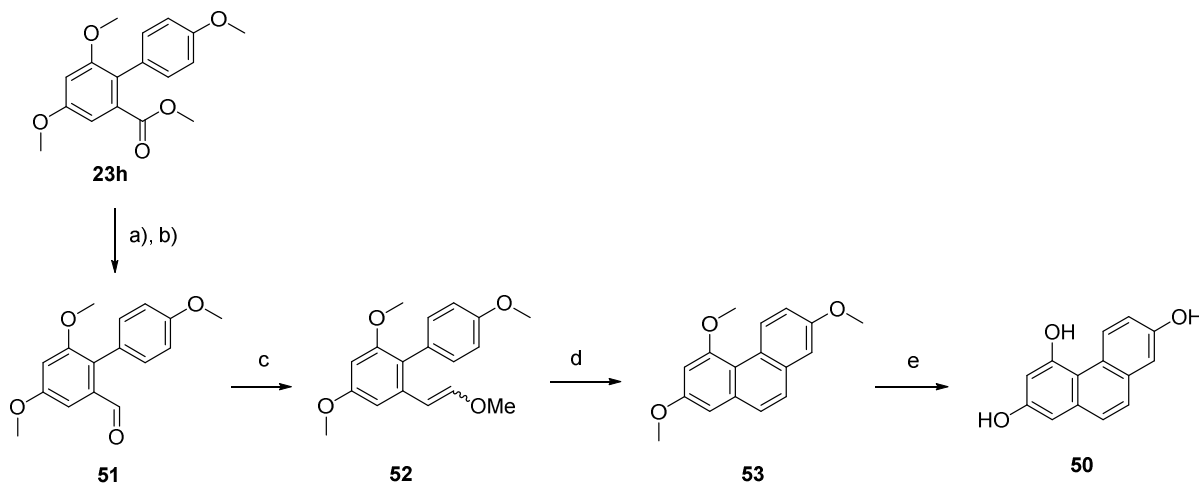
Reagents and conditions: a) i. NaOH_{aq}, 60 °C 30 min; ii. CuSO₄ 10%, 95 °C, 3h; b) BBr₃, CH₂Cl₂, -78 °C to rt, 24h; c) BF₃ Et₂O, NaBH₄, THF dry, 0 °C to reflux, 3h.

Notably, the sodium borohydride-boron trifluoride combination for the reduction of the lactone carbonyl¹⁴³ was previously investigated for the reduction of UM6 (See **Scheme 6**) but it didn't led to the desired product; on the contrary, it was successful with these compounds (**46a**, **46b**, **43**, **Scheme 9**) suggesting that the OH substitution pattern plays an important role for the outcome of this reaction.

Additionally, as we did for the synthesis of UM6 phenanthrene analog **35**, we prepared the UM7 phenanthrene analog **50** (**Scheme 10**), starting from biphenyl-2-carboxylate **23h**, which was converted to the aldehydes **51** (69% of yield over two steps). Wittig reaction with (methoxymethyl)triphenylphosphonium chloride afforded the arylvinyl methyl ether **52** (86%), which through bismuth-catalyzed cyclization-

aromatization was converted to the methylated phenanthrene **53** (78%) that was deprotected to obtain the trihydroxy- analog **50** (15%).

Scheme 10. Synthesis of UM7 phenanthrene analog **50**

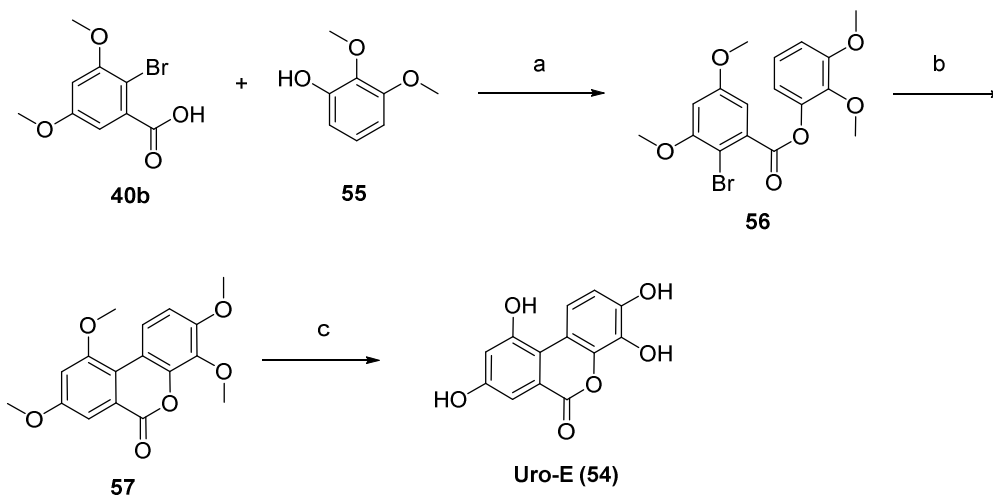


Reagents and conditions: a) DIBAL, CH₂Cl₂, 0°C to rt, 3h; b) PCC, CH₂Cl₂, rt, 2h; c) (methoxymethyl)triphenylphosphonium chloride, LiHMDS, THF, rt, 2h; d) Bi(OTf)₃, DCE rt, 30 min; e) BBr₃, CH₂Cl₂, -78°C to rt, 24h;

Finally, as last UM7-inspired analog, we planned the synthesis of urolithin E (Uro-E, **54**, **Figure 14**), which presents an additional hydroxyl group in the 4 position of C ring and, to the best of our knowledge, its preparation has not been reported.

We reasoned that both the previously adopted strategies to obtain the dibenzopyranone derivatives were not suitable to prepare Uro-E. For this reason, the synthesis of Uro-E was performed through the approach that is reported for the high similar urolithin D (**Figure 14**).¹³⁹ It started with esterification of 2-bromo-3,5-dimethoxybenzoic acid **40b** with 2,3-dimethoxyphenol **55** to obtain **56** (75%), which through intramolecular Heck coupling gave the dibenzopyranone derivative **57** (10%), that was demethylated to obtain the desired product **54** with 68% of yield (**Scheme 11**).

Scheme 11. Synthesis of Uro-E (54)



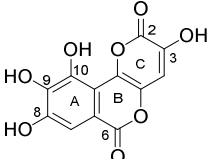
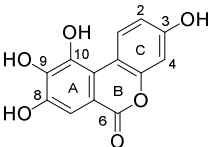
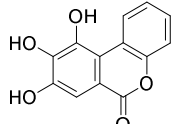
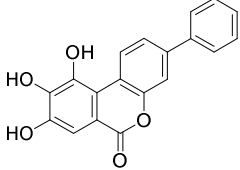
Reagents and conditions: a) i. (COCl)₂, DMF, DCM, 0 °C to rt, 16h; ii. Et₃N, DCM, 0 °C to rt, 16h; b) Pd(OAc)₂, S-Phos, NaOAc, DMA, 130 °C, 72h; c) BBr₃, CH₂Cl₂, -78 °C to rt, 24h.

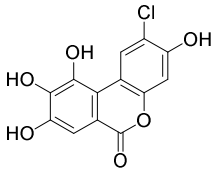
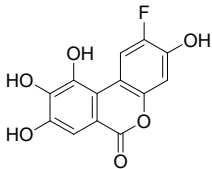
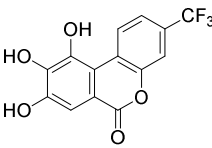
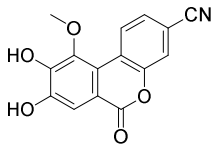
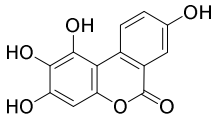
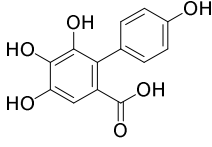
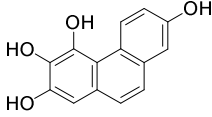
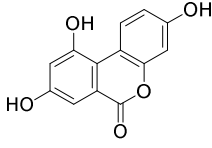
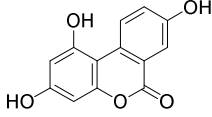
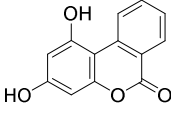
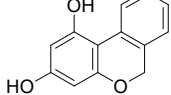
In summary, we developed a synthetic strategy for UM6 and structural analogs, which demonstrated to be very convenient in term of high yields, short reaction times and versatility, as it has been confirmed by its broad application in the synthesis of many UM6 structural analogs (26-33, 35, 39, 50). We also explored some of the reported procedures for urolithins synthesis (Hurtley reaction and esterification/Heck reaction) for a small number of analogs (43, 46a-b, 47-49, 54), confirming the limited versatility and the disadvantages of these methods.

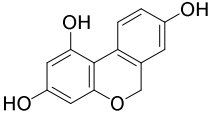
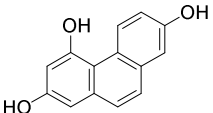
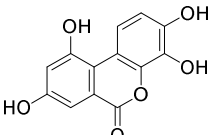
3. Biological evaluation and discussion of results

All new compounds and also some intermediates were evaluated for their inhibitory activity on purified human LDH-A. The compounds able to cause enzyme inhibition at micromolar level were investigated for their activity on lactic acid production and cell proliferation on Raji cell line; these cells are derived from a Burkitt's lymphoma and are characterized by overexpression of the MYC protein. This alteration, which drives the neoplastic change leading to Burkitt's lymphoma, directly alters cell metabolism and causes increased LDH-A levels, rendering cells very responsive to LDH-A inhibition.¹¹² Most interesting results are reported in **Table 2**. Compounds were tested at scalar concentration of 25, 50, 100, 200 μM (detailed biological protocol is reported in **Appendix A**).

Table 2. Activity of GF/UM6 analogs on purified human LDH-A and on lactic acid production and cell proliferation on Raji cells.

Compound	Structure	hLDH-A IC ₅₀ (μM) ^a	In cell lactate production IC ₅₀ (μM) ^a	Cell growth IC ₅₀ (μM) ^a
GF (18)		70 \pm 10	62 \pm 5	33 \pm 4
UM6 (19)		77 \pm 10	36 \pm 3	25 \pm 2
26		83 \pm 5	175 \pm 30	62 \pm 10
27		n.d. Inhibition at 50 μM : 73%	n.d. Increase in lactate production	n.d. Inhibition at 50 μM : 44%

28		36 ± 3	54 ± 11	17 ± 2
29		28 ± 3	87 ± 10	21 ± 4
30		n.a.	n.d.	n.d.
31		32 ± 3	Increase in lactate production	<12
32		n.a.	n.d.	n.d.
33		n.d. Inhibition at 200μM: 36%	n.d.	n.d.
35		62 ± 2	72 ± 15	< 25
UM7 (39)		n.a.	n.a.	n.a.
43		n.a.	n.d.	n.d.
46b		~ 200	128 ± 4	81 ± 5
48		n.a.	n.d.	n.d.

49		n.a.	n.d.	n.d.
50		n.d. Inhibition at 100µM: 30%	n.d. Inhibition at 100µM: 50%	n.d. Inhibition at 100µM <50%
Uro-E (54)		n.a.	n.d.	n.d.

^aAll points were tested in triplicate with error bars indicating the standard deviations; n.a.= not active at 200 µM; n.d.= not determined

The data obtained allowed to establish a SAR assessment for this series of derivatives. Compounds that showed a comparable activity to UM6 and GF, both on the purified enzyme and in cellular assays, present the tricyclic scaffold and the 8,9,10-trimethoxybenzene moiety on A ring (**26**, **28**, **29**, **35**).

Compounds **28** and **29**, which maintain all the four hydroxyl groups (as UM6 and GF) and present a small lipophilic group (chlorine and fluorine, respectively) in 2-position, showed the best activity on the enzyme (36µM and 28µM, respectively) retaining good activity in cells.

Modification of hydroxyl in 3 position affects the activity: particularly, its removal preserves the activity on the enzyme but induces loss of activity in cellular assays (**26**). Compound **30**, in which it is substituted with a trifluoromethyl group resulted in an inactive compound. Its substitution with a phenyl ring gives compound **27**, for which, even if it showed good enzymatic inhibition (73%) and cell growth inhibition (44%) at 50 µM, no IC₅₀ was determined because of its not optimal solubility and precipitation at 100 µM; however, it showed to increase lactate production suggesting different cellular mechanisms of action.

Compound **31**, which presents a nitrile group in 3-position and a methoxyl group in place of the hydroxyl group in position 10, showed good enzyme inhibition, suggesting that hydroxyl in position 3 could be substituted with a hydrogen bond acceptor group (such as a nitrile) and hydroxyl in position 10 could be not necessary for activity. However it increased lactate production and inhibited cell growth of 100% at 12 µM, suggesting an action based on different mechanisms.

Compound **32**, which presents the reverse lactone function compared to UM6, did not show enzymatic activity, revealing the importance of lactone position in the tetrahydroxylated ring.

The lactone ring-opened analog **33** showed a minimal activity on the enzyme, and has not been evaluated for its cellular effects.

Importantly, UM7 (**35**) and Uro-E (**54**), with the same UM6 scaffold in which the 8,9,10-trihydroxybenzene moiety is substituted with 8,10-dihydroxybenzene moiety, resulted inactive. Even if it didn't show enzymatic activity, UM7 was also tested in cell assays as negative control, resulting inactive in both inhibition of lactate production and cell growth.

Compound **43**, UM7 analog with the reverse lactone moiety, resulting also inactive on the enzyme, while its analog **46b**, which lacks a hydroxyl group, showed a minimal activity on the enzymatic assay and poor activity in cellular assays.

The reduced analogs **48**, **49** did not show any activity, suggesting the importance of the lactone function for this class of compounds.

Compound **35** (phenanthrene analog of UM6) showed good inhibition activity (62 μ M) on the enzyme and in lactate production (75 μ M), however at concentration of 25 μ M inhibited completely cell proliferation (100%), therefore suggesting an action based on different mechanisms involving not only LDH-A as a target. Derivative **50**, (phenanthrene analog of UM7) was less soluble and IC₅₀ was not determined, however it resulted very poorly active on the enzyme (at 100 μ M LDH-A inhibition was 30%) and also in cells, thus suggesting the relevance of the trihydroxybenzene moiety compared to the dihydroxy one, for the LDH-A inhibition.

Overall, SAR suggest the following considerations for this class of inhibitors:

- UM6 benzopyranone scaffold has been confirmed as good structure able to mimic GF activity;
- key interactions of this class of inhibitor with LDH-A probably involve 8,9,10 and 3 hydroxyl groups, together with lactone function in 6 position;
- substitutions in position 2 with small lipophilic groups are allowed.

Some aspects remains to be established, particularly, if the hydroxyl group in position 10 is necessary for the bioactivity, since it lacks in derivative **31** that is active on the enzyme, and if position 3 can be substituted with other hydrogen bond acceptor groups.

Docking studies are ongoing on the active molecules by Computational chemistry group to find the interactions with LDH-A and compare their putative binding mode

with that of GF and other reference inhibitors. These studies will allow a further optimization of the active compounds toward more potent inhibitors.

Furthermore, cell uptake studies were performed by groups of Professors Giuseppina Di Stefano and Laura Mercolini on the reference compounds GF and UM6, and on the inactive compound UM7, to evaluate the ability of this class of molecules to penetrate cancer cells. Intracellular concentration of GF, UM6 and UM7 were determined in Raji cells by treating cells (100 μ M) for 1h and 4h, after which cell lysates were subjected to LC-MS/MS analysis.

Significant amount of each compound were detected in the intracellular fraction, proving they exhibit good cell penetration. (Details of this study will be published elsewhere.)

4. Conclusions

The main project of the present thesis focused on the synthesis of a series of structural analogs of LDH-A inhibitor galloflavin GF, recently discovered by our group, with the aim to assess its SAR and gain a deeper knowledge on the key interactions involved in its binding to the target. Since the poor chemical manipulability of GF did not allow an easy access to synthesis of analogs, a structural simplification was performed which led to the identification of a natural dibenzopyranone, urolithin M6 (UM6). An efficient and versatile synthetic procedure to obtain UM6 has been developed and preliminary biological test showed it reproduced GF's behaviour, making it a new *hit* suitable for our investigations.

Initially, the synthetic route developed for UM6 has been exploited for the synthesis of a small library of UM6 structural analogs (**26-33**, **35**, **39**, **50**) bearing the same dibenzopyranone scaffold or phenanthrene and biphenyl scaffolds, proving to be a convenient strategy in term of high yields, short reaction times and versatility. Then a small number of dibenzopyranone and dibenzopyrane derivatives (**43**, **46a-b**, **47-49**, **54**), were obtained through some of the previously reported procedures for urolithins synthesis (Hurtley reaction and esterification/Heck reaction), confirming the limited versatility and the disadvantages of these previously described methods.

Biological evaluation of the new derivatives allowed us to assess SAR for this class of compounds. We found that compounds that showed a comparable activity to GF and UM6, both on the purified enzyme and in cellular assays, present the tricyclic scaffold and the 8,9,10-trimethoxybenzene moiety on A ring (**26**, **28**, **29**, **35**). UM6 scaffold has been confirmed as the best structure able to mimic GF activity, since dibenzopyranone analogs resulted the most active compounds, while analogs carrying different scaffolds all showed low or no activity. Key interactions of this class of inhibitor with LDH-A probably involve 8,9,10 and 3 hydroxyl groups, together with lactone function in 6 position.

Moreover UM6 exhibited good cell penetration in preliminary cell uptake studies, as well as GF, predicting a desirable pharmacokinetic profile for this class of compounds. UM6 and the new active compounds are currently under further investigations to a deeper understanding of their pharmacokinetic properties and their evaluation as glycolytic inhibitors.

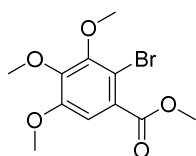
5. Experimental section

General methods

Reaction progress was monitored by TLC on pre-coated silica gel plates (Kieselgel 60 F₂₅₄, Merck) and visualized by UV254 light. Flash column chromatography was performed on silica gel (particle size 40-63 μM , Merck) or C18-reversed phase fully endcapped silica gel (particle size 40-63 μM , Sigma-Aldrich). If required, solvents were distilled prior to use. All reagents were obtained from commercial sources and used without further purification. When stated, reactions were carried out under an inert atmosphere. Reactions involving microwave irradiation were performed using a microwave synthesis system (CEM Discover[®] SP, 2.45 GHz, maximum power 300 W), equipped with infrared temperature measurement. Compounds were named relying on the naming algorithm developed by CambridgeSoft Corporation and used in Chem-BioDraw Ultra 15.0. ¹H-NMR and ¹³C-NMR spectra were recorded on Varian Gemini at 400 MHz and 100 MHz respectively. Chemical shifts (δ_{H}) are reported relative to TMS as internal standard. HPLC analysis (UM6) was performed under reversed-phase conditions on a Phenomenex Jupiter C18 (150x4,6 mm I.D.) column, using a binary mixture of 0.1% formic acid in H₂O/methanol 60/40 (v/v) as mobile phase, UV detection at $\lambda = 365$ nm and a flow-rate of 0.8 mL/min. A loop valve of 20 μL volume was used. The liquid chromatograph was by Jasco Corporation (Tokyo, Japan), model PU-1585 UV.

Experimental procedures

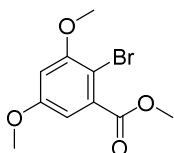
Methyl 2-bromo-3,4,5-trimethoxybenzoate **21**



Commercially available methyl 3,4,5-trimethoxybenzoate **20** (10.2 g, 45.1 mmol, 1 eq) was dissolved in CH₃CN (0.1 M). The mixture was cooled to 0°C and N-bromosuccinimide (8.8 g, 49.6 mmol, 1.1 eq) was added portionwise. The reaction was let warm up to room temperature and then stirred at rt for 3h. After TLC showed completion, Na₂S₂O₃ 2M was added and the reaction mixture was stirred for 5 minutes. CH₃CN was evaporated in vacuum and the mixture extracted 3 times with EtOAc. The combined organic phases were dried over anhydrous

Na₂SO₄, and the solvent evaporated in vacuum. The crude product was purified via silica gel column chromatography (Petroleum ether/EtOAc 95/5 ratio) to obtain the pure product **21** as a colourless viscous liquid which solidifies after standing overnight (13.1 g, 42.8 mmol). Y= 95%. ¹H NMR (400MHz, CDCl₃) δ 7.13 (s, 1H), 3.90 (s, 3H), 3.89 (s, 3H), 3.86 (s, 6H) ppm.

Methyl 2-bromo-3,5-dimethoxybenzoate **21b**

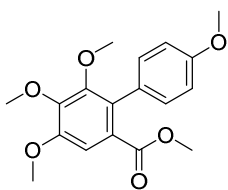


Commercially available methyl 3,5-dimethoxybenzoate (5.0 g, 25.5 mmol, 1 eq), was dissolved in CH₃CN (0.1 M). The mixture was cooled to 0°C and N-bromosuccinimide (5.0 g, 28.1 mmol, 1.1 eq) was added portionwise. The reaction was let warm up to room temperature and then stirred at rt for 3h. After TLC showed completion, Na₂S₂O₃ 2M was added and the reaction mixture was stirred for 5 minutes. CH₃CN was evaporated in vacuum and the mixture extracted 3 times with EtOAc. The combined organic phases were dried over anhydrous Na₂SO₄, and the solvent evaporated in vacuum. The crude product was purified via silica gel column chromatography (Petroleum ether/EtOAc 95/5 ratio) to obtain the pure product **21b** as a colourless viscous liquid which solidifies after standing overnight (5.6 g, 20.4 mmol). Y= 88%. ¹H NMR (400MHz, CDCl₃) δ 6.76 (d, *J* = 2.7 Hz, 1H), 6.54 (d, *J* = 2.4 Hz, 1H), 3.89 (s, 3H), 3.84 (s, 3H), 3.78 (s, 3H) ppm.

General Suzuki coupling procedure to obtain biphenyl-2-carboxylate derivatives (**23**, **23a-h**) (performed in pressure tube)

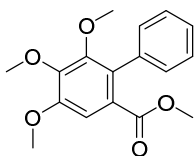
Methyl 2-bromobenzoate derivatives (**21**, **21a**, **21b**) (1.0 eq) were dissolved in 1,2-dimethoxyethane (0.03 M), inside a pressure tube. Commercially available phenylboronic acid derivatives (**22**, **22a-g**) (1.5 eq), K₃PO₄ (2.0 eq) and tetrakis(triphenylphosphine)palladium (0.1 eq) were added. The tubes were sealed, the reactions were heated to 120 °C and stirred for 24h. The reaction mixtures was transferred to round bottom flask and the solvent removed in vacuum. The crude products were purified via silica gel column chromatography to obtain the pure compounds **23**, **23a-h**.

Methyl 4,4',5,6-tetramethoxybiphenyl-2-carboxylate **23**



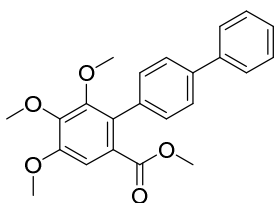
The compound was obtained according to the general Suzuki coupling procedure starting from methyl 2-bromo-3,4,5-trimethoxybenzoate **21** (800 mg, 2.62 mmol, 1.0 eq) and 4-methoxyphenylboronic acid **22** (598 mg, 3.93 mmol, 1.5 eq). The crude product was purified via silica gel column chromatography (Petroleum ether/EtOAc 90/10 ratio) to obtain the pure product as a colourless viscous liquid (714 mg, 2.15 mmol). Y= 82%. ¹H NMR (400 MHz, CDCl₃) δ 7.18 (s, 1H), 7.16 (d, J= 8.7 Hz, 2H), 6.91 (d, J= 8.7 Hz, 2H), 3.94 (s, 3H), 3.91 (s, 3H), 3.82 (s, 3H), 3.56 (s, 3H), 3.55 (s, 3H) ppm. ¹³C NMR (100 MHz, CDCl₃) δ 168.42, 158.61, 152.20, 151.72, 145.34, 130.51, 130.23, 128.84, 126.67, 116.02, 114.75, 113.19, 108.88, 61.01, 60.93, 56.16, 55.17, 52.00 ppm.

Methyl 4,5,6-trimethoxybiphenyl-2-carboxylate **23a**



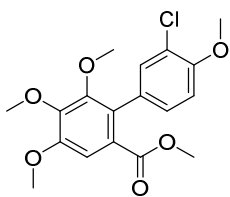
The compound was obtained according to the general Suzuki coupling procedure starting from methyl 2-bromo-3,4,5-trimethoxybenzoate **21** (600 mg, 1.97 mmol, 1.0 eq) and phenylboronic acid **22a** (360 mg, 2.95 mmol, 1.5 eq). The crude product was purified via flash silica gel column chromatography (Petroleum ether/EtOAc 90/10 ratio) to obtain the pure product as a colourless viscous liquid which solidified after standing overnight (488 mg, 1.62 mmol). Y= 82%. ¹H NMR (400 MHz, CDCl₃) δ 7.40 – 7.30 (m, 3H), 7.24-7.22 (m, 3H), 3.95 (s, 3H), 3.93 (s, 3H), 3.57 (s, 3H), 3.53 (s, 3H) ppm.

Methyl 4,5,6-trimethoxy-[1,1':4',1''-terphenyl]-2-carboxylate **23b**



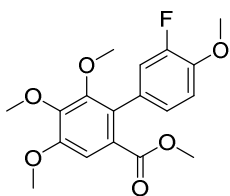
The compound was obtained according to the general Suzuki coupling procedure starting from methyl 2-bromo-3,4,5-trimethoxybenzoate **21** (800 mg, 2.62 mmol, 1.0 eq) and biphenyl-4-ylboronic acid **22b** (778 mg, 3.93 mmol, 1.5 eq). The crude product was purified via flash silica gel column chromatography (Petroleum ether/EtOAc 90/10 ratio) to obtain the pure product as a yellow viscous liquid (694 mg, 1.83 mmol). Y= 70%. ¹H NMR (400 MHz, CDCl₃) δ 7.69-7.63 (m, 4H), 7.46 (t, J = 7.5 Hz, 2H), 7.36 (d, J = 7.4 Hz, 1H), 7.32 (d, J = 8.1 Hz, 2H), 7.25 (s, 1H), 3.98 (s, 3H), 3.95 (s, 3H), 3.62 (s, 3H), 3.57 (s, 3H) ppm.

Methyl 3'-chloro-4,4',5,6-tetramethoxybiphenyl-2-carboxylate **23c**



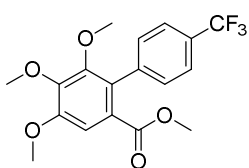
The compound was obtained according to the general Suzuki coupling procedure starting from methyl 2-bromo-3,4,5-trimethoxybenzoate **21** (1.0 eq) and 3-chloro-4-methoxyphenylboronic acid **22c** (733 mg, 3.93 mmol, 1.5 eq). The crude product was purified via flash silica gel column chromatography (Petroleum ether/EtOAc 95/5 ratio) to obtain the pure product as a white solid (692 mg, 1.89 mmol). Y= 72%. ¹H NMR (400 MHz, CDCl₃) δ 7.26 (s, 1H), 7.20 (s, 1H), 7.09 (dd, J = 8.4, 1.9 Hz, 1H), 6.94 (d, J = 8.4 Hz, 1H), 3.94 (s, 3H), 3.93 (s, 3H), 3.92 (s, 3H), 3.60 (s, 3H), 3.58 (s, 3H) ppm.

Methyl 3'-fluoro-4,4',5,6-tetramethoxybiphenyl-2-carboxylate **23d**



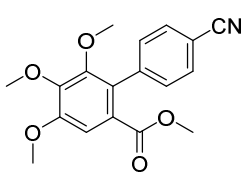
The compound was obtained according to the general Suzuki coupling procedure starting from methyl 2-bromo-3,4,5-trimethoxybenzoate **21** (800 mg, 2.62 mmol, 1.0 eq) and 3-fluoro-4-methoxyphenylboronic acid **22d** (668 mg, 3.93 mmol, 1.5 eq). The crude product was purified via flash silica gel column chromatography (Petroleum ether/EtOAc 95/5 ratio) to obtain the pure product as a yellow oil (799 mg, 2.27 mmol). Y= 87%. ¹H NMR (400 MHz, CDCl₃) δ 7.19 (s, 1H), 7.02 – 6.91 (m, 3H), 3.94 (s, 3H), 3.92 (d, 6H), 3.60 (s, 3H), 3.58 (s, 3H) ppm.

Methyl 4,5,6-trimethoxy-4'-(trifluoromethyl)biphenyl-2-carboxylate **23e**



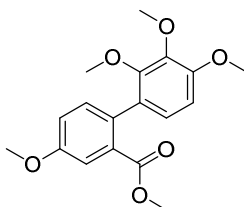
The compound was obtained according to the general Suzuki coupling procedure starting from methyl 2-bromo-3,4,5-trimethoxybenzoate **21** (800 mg, 2.62 mmol, 1.0 eq) and 4-(trifluoromethyl)phenylboronic acid **22e** (746 mg, 3.93 mmol, 1.5 eq). The crude product was purified via flash silica gel column chromatography (Petroleum ether/EtOAc 95/5 ratio) to obtain the pure product as a white solid (922 mg, 2.49 mmol). Y= 95%. ¹H NMR (400 MHz, CDCl₃) δ 7.64 (d, J = 8.0 Hz, 2H), 7.35 (d, J = 8.0 Hz, 2H), 7.28 (s, 1H), 3.96 (s, 3H), 3.95 (s, 3H), 3.58 (s, 3H), 3.56 (s, 3H) ppm.

Methyl 4'-cyano-4,5,6-trimethoxybiphenyl-2-carboxylate **23f**



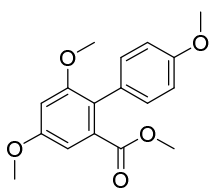
The compound was obtained according to the general Suzuki coupling procedure starting from methyl 2-bromo-3,4,5-trimethoxybenzoate **21** (800 mg, 2.62 mmol, 1.0 eq) and 4-cyanophenylboronic acid **22f** (578 mg, 3.93 mmol, 1.5 eq). The crude product was purified via flash silica gel column chromatography (Petroleum ether/EtOAc 95/5 ratio) to obtain the pure product as a white solid (849 mg, 2.59 mmol). Y= 99%. ¹H NMR (400 MHz, CDCl₃) δ 7.67 (d, J = 8.4 Hz, 2H), 7.33 (d, J = 8.4 Hz, 2H), 7.30 (s, 1H), 3.96 (s, 3H), 3.95 (s, 3H) 3.58 (s, 3H), 3.57 (s, 3H) ppm.

Methyl 2',3',4,4'-tetramethoxy-[1,1'-biphenyl]-2-carboxylate **23g**



The compound was obtained according to the general Suzuki coupling procedure starting from commercially available methyl 2-bromo-3,4,5-trimethoxybenzoate **21a** (250 mg, 1.02 mmol, 1.0 eq) and 2,3,4-trimethoxyphenylboronic acid **22g** (320 mg, 1.53 mmol, 1.5 eq). The crude product was purified via flash silica gel column chromatography (Petroleum ether/EtOAc 95/5 ratio) to obtain the pure product as a white solid (340 mg, 1.02 mmol). Y= 100%. ¹H NMR (400 MHz, CDCl₃) δ 7.40 (d, J = 2.8 Hz, 1H), 7.24 (d, J = 8.5 Hz, 1H), 7.06 (dd, J = 8.5, 2.8 Hz, 1H), 6.91 (d, J = 8.5 Hz, 1H), 6.70 (d, J = 8.5 Hz, 1H), 3.89 (d, J = 2.0 Hz, 6H), 3.87 (s, 3H), 3.67 (s, 3H), 3.53 (s, 3H) ppm.

Methyl 4,4',6-trimethoxybiphenyl-2-carboxylate **23h**

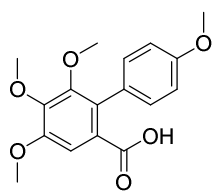


The compound was obtained according to the general Suzuki coupling procedure starting from methyl 2-bromo-3,5-dimethoxybenzoate **21b** (800 mg, 2.91 mmol, 1.0 eq) and 4-methoxyphenylboronic acid **22** (663 mg, 4.36 mmol, 1.5 eq). The crude product was purified via silica gel column chromatography (Petroleum ether/EtOAc 95/5 ratio) to obtain the pure product as a colourless viscous liquid (748 mg, 2.47 mmol). Y= 85%. ¹H NMR (400 MHz, CDCl₃) δ 7.16 (d, J = 8.6 Hz, 2H), 6.91 (d, J = 8.6 Hz, 2H), 6.86 (d, J = 2.3 Hz, 1H), 6.64 (d, J = 2.3 Hz, 1H), 3.87 (s, 3H), 3.83 (s, 3H), 3.73 (s, 3H), 3.56 (s, 3H) ppm.

General procedure for ester hydrolysis: biphenyl-2-carboxylate derivatives (23, 23a-h) to free biphenyl-2-carboxylic acid derivatives (24, 24a-h) and methyl-2-bromobenzoates 21, 21b to free acids 40, 40b.

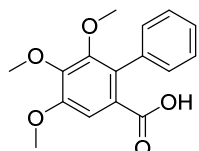
Esters **23**, **23a-h**, **21**, **21b** were treated with a 1/1 mixture of 4M NaOH (10 eq) and EtOH at 60 °C for 1-2h. After TLC showed absence of starting material the reaction mixtures were treated with 37% HCl until acidic pH, brine was added and the mixtures were extracted 3 times with EtOAc. The combined organic phases were dried over anhydrous Na₂SO₄, and the solvent evaporated in vacuum to obtain free carboxylic acids which were used in the next step without further purification.

4,4',5,6-tetramethoxybiphenyl-2-carboxylic acid 24



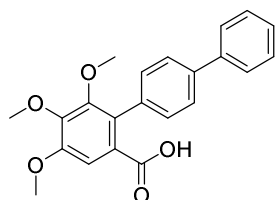
Methyl 4,4',5,6-tetramethoxybiphenyl-2-carboxylate **23** (1590 mg, 4.78 mmol) was treated following the general procedure for ester hydrolysis and gave free acid **24** as a white solid (1445 mg, 4.54 mmol). Y= 95% (crude). ¹H NMR (400 MHz, DMSO-d₆) δ 12.48 (s, 1H), 7.12 (s, 1H), 7.10 (d, *J* = 8.6 Hz, 2H), 6.91 (d, *J* = 8.6 Hz, 2H), 3.85 (s, 3H), 3.82 (s, 3H), 3.78 (s, 3H), 3.46 (s, 3H) ppm.

4,5,6-trimethoxybiphenyl-2-carboxylic acid 24a



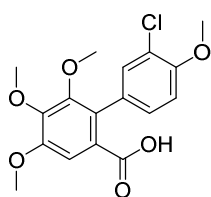
Methyl 4,5,6-trimethoxybiphenyl-2-carboxylate **23a** (340 mg, 1.12 mmol) was treated following the general procedure for ester hydrolysis and gave **24a** as a white solid (320 mg, 1.11 mmol). Y= 99% (crude). ¹H NMR (400 MHz, DMSO-d₆) δ 12.53 (br, OH), 7.36-7.29 (m, 3H), 7.19-7.17 (m, 3H), 3.87 (s, 3H), 3.82 (s, 3H), 3.47 (s, 3H) ppm.

4,5,6-trimethoxy-[1,1':4',1''-terphenyl]-2-carboxylic acid 24b



Methyl 4,5,6-trimethoxy-[1,1':4',1''-terphenyl]-2-carboxylate **23b** (610 mg, 1.61 mmol) was treated following the general procedure for ester hydrolysis and gave **24b** as a light yellow solid (590 mg, 1.59 mmol). Y= 99% (crude). ¹H NMR(400 MHz, DMSO-d₆) δ 12.59 (br, OH), 7.73 – 7.71 (m, 2H), 7.66 (d, *J* = 8.4 Hz, 2H), 7.48 (t, *J* = 7.6 Hz, 2H), 7.37 (t, *J* = 7.4 Hz, 1H), 7.27 (d, *J* = 8.4 Hz, 2H), 7.19 (s, 1H), 3.88 (s, 3H), 3.84 (s, 3H), 3.52 (s, 3H) ppm.

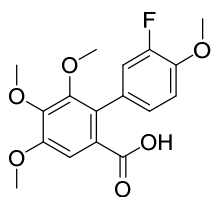
3'-chloro-4,4',5,6-tetramethoxybiphenyl-2-carboxylic acid **24c**



Methyl 3'-chloro-4,4',5,6-tetramethoxybiphenyl-2-carboxylate **23c** (870 mg, 2.37 mmol) was treated following the general procedure for ester hydrolysis and gave **24c** as a white solid (830mg, 2.35 mmol). Y= 99% (crude). ¹H NMR (400 MHz, DMSO-d₆) δ 12.64 (br, OH),

7.20 (d, *J* = 1.7 Hz, 1H), 7.18 (s, 1H), 7.12 – 7.11 (m, 2H), 3.88 (s, 3H), 3.87 (s, 3H), 3.83 (s, 3H), 3.50 (s, 3H) ppm.

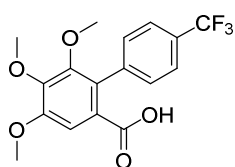
3'-fluoro-4,4',5,6-tetramethoxybiphenyl-2-carboxylic acid **24d**



Methyl 3'-fluoro-4,4',5,6-tetramethoxybiphenyl-2-carboxylate **23d** (800 mg, 2.28 mmol) was treated following the general procedure for ester hydrolysis and gave **24d** as a white solid (720 mg, 2.14 mmol). Y= 93% (crude). ¹H NMR (400 MHz, DMSO-d₆) δ 12.61 (br, OH),

7.17 (s, 1H), 7.13 (t, *J* = 8.8 Hz, 1H), 7.02 (dd, *J* = 12.4, 2.0 Hz, 1H), 6.93-6.91 (m, 1H), 3.86 (s, 6H), 3.82 (s, 3H), 3.50 (s, 3H) ppm.

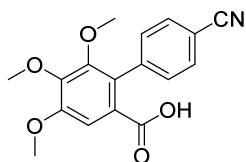
4,5,6-trimethoxy-4'-(trifluoromethyl)biphenyl-2-carboxylic acid **24e**



Methyl 4,5,6-trimethoxy-4'-(trifluoromethyl)biphenyl-2-carboxylate **23e** (1.15 g, 3.11 mmol) was treated following the general procedure for ester hydrolysis and gave **24e** as a white solid (1.11 g, 3.11 mmol). Y= 100% (crude). ¹H NMR (400 MHz,

DMSO-d₆) δ 12.68 (br, OH), 7.71 (d, *J* = 8.0 Hz, 2H), 7.41 (d, *J* = 8.0 Hz, 2H), 7.27 (s, 1H), 3.89 (s, 3H), 3.84 (s, 3H), 3.51 (s, 3H) ppm.

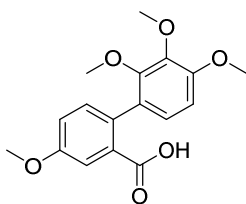
4'-cyano-4,5,6-trimethoxybiphenyl-2-carboxylic acid **24f**



Methyl 4'-cyano-4,5,6-trimethoxybiphenyl-2-carboxylate **23f** (940 mg, 2.87 mmol) was treated following the general procedure for ester hydrolysis and gave **24f** as a white solid (910 mg, 2.90 mmol). Y= 101% (crude). ¹H NMR (400 MHz, DMSO-d₆) δ 12.62

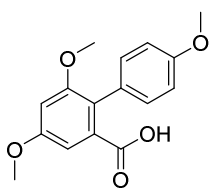
(br, OH), 7.97 (s, 1H), 7.85-7.80 (m, 2H), 7.25 – 7.22 (m, 2H), 3.88 (s, 3H), 3.84 (s, 3H), 3.50 (s, 3H) ppm.

2',3',4,4'-tetramethoxy-[1,1'-biphenyl]-2-carboxylic acid **24g**



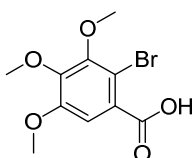
Methyl 2',3',4,4'-tetramethoxy-[1,1'-biphenyl]-2-carboxylate **23g** (350 mg, 1.05 mmol) was treated following the general procedure for ester hydrolysis and gave **24g** as a white solid (300 mg, 0.94 mmol). Y= 90% (crude). ¹H NMR (401 MHz, Methanol-*d*₄) δ 7.39 (d, *J* = 2.7 Hz, 1H), 7.23 (d, *J* = 8.5, 1H), 7.11 (dd, *J* = 8.5, 2.8 Hz, 1H), 6.90 (d, *J* = 8.5 Hz, 1H), 6.79 (d, *J* = 8.6 Hz, 1H), 3.87 (s, 6H), 3.83 (s, 3H), 3.52 (s, 3H) ppm.

4,4',6-trimethoxybiphenyl-2-carboxylic acid **24h**



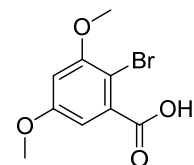
Methyl 4,4',6-trimethoxybiphenyl-2-carboxylate **23h** (600 mg, 1.81 mmol) was treated following the general procedure for ester hydrolysis and gave **24h** as a white solid (548 mg, 1.72 mmol). Y= 95% (crude). ¹H NMR (400 MHz, DMSO-*d*₆) δ 12.54 (br, OH), 7.06 (d, *J* = 8.8 Hz, 2H), 6.87 (d, *J* = 8.8 Hz, 2H), 6.74-6.73 (m, 2H), 3.81 (s, 3H), 3.76 (s, 3H), 3.67 (s, 3H) ppm.

2-bromo-3,4,5-trimethoxybenzoic acid **40**



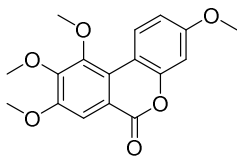
The compound was obtained starting from methyl 2-bromo-3,4,5-trimethoxybenzoate **21** following the general procedure for ester hydrolysis as a white solid. Y= 95%. ¹H NMR (400 MHz, DMSO-*d*₆) δ 13.39 (s, OH), 7.17 (s, 1H), 3.83 (s, 3H), 3.81 (s, 3H), 3.78 (s, 3H) ppm.

2-bromo-3,5-dimethoxybenzoic acid **40b**



The compound was obtained starting from methyl 2-bromo-3,5-dimethoxybenzoate **21b** following the general procedure for ester hydrolysis as a white solid. Y= 97 %. ¹H NMR (400 MHz, DMSO-*d*₆) δ 13.37 (s, OH), 6.77 (d, *J* = 2.5 Hz, 2H), 3.87 (s, 3H), 3.81 (s, 3H) ppm.

3,8,9,10-tetramethoxy-6H-benzo[c]chromen-6-one 25



Route A. 4,4',5,6-tetramethoxybiphenyl-2-carboxylic acid **24** was added 50 mL of a 1/1 H₂O/CH₃CN mixture. K₂S₂O₈ (3880 mg, 14.353 mmol, 3.0 equiv) and AgNO₃ (81 mg, 0.478 mmol, 0.1 equiv) were added and the reaction was stirred at 60°C for 48h.

CH₃CN was evaporated in vacuum and the mixture extracted 3 times with EtOAc. The combined organic phases were dried over anhydrous Na₂SO₄, and the solvent evaporated in vacuum. The crude product was purified via silica gel column chromatography (Petroleum ether/EtOAc 85/15 ratio) to obtain the pure product as an off white solid (yield 30%).

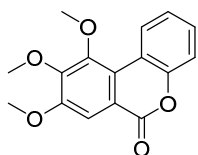
Route B. To a solution of 4,4',5,6-tetramethoxybiphenyl-2-carboxylic acid **24** (540 mg, 1.70 mmol) in ClCH₂CH₂Cl (18 mL) was added N-iodosuccinimide (950 mg, 4.24 mmol, 2.5 eq) in one portion and the mixture was heated to 75 °C for 3 h. After completion of the reaction, EtOAc (35 mL) was added and the mixture was washed with sat. Na₂S₂O₃ (20 mL), then with H₂O (2 × 20 mL). The organic layer was dried over anhydrous Na₂SO₄ and concentrated in vacuo. The crude product was purified via silica gel column chromatography (Petroleum ether/EtOAc, 92:8) to obtain the pure product as an off white solid (yield 69%).

¹H NMR: (400MHz, CDCl₃) δ 8.74 (d, J = 8.0, 1H), 7.72 (s, 1H), 6.91-6.86 (m, 2H), 4.04 (s, 3H), 3.99 (s, 3H), 3.96 (s, 3H), 3.88 (s, 3H) ppm; ¹³C NMR (100 MHz, CDCl₃) δ 161.50, 160.44, 153.10, 151.96, 150.62, 127.77, 123.49, 116.26, 112.26, 110.81, 110.18, 108.29, 101.67, 61.33, 60.61, 56.41, 55.72 ppm.

General procedure (*Route B*) to obtain 6H-benzo[c]chromen-6-one derivatives (**25a-h**)

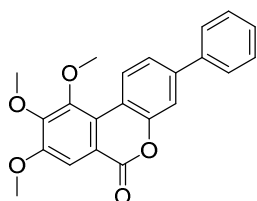
To a solution of biphenyl-2-carboxylic acid (**24a-h**) in ClCH₂CH₂Cl (0.1 M) was added N-iodosuccinimide (2.5 eq) in one portion and the mixture was heated to 75 °C for 3 h. After completion of the reaction, EtOAc was added and the mixture was washed with sat. Na₂S₂O₃ then with H₂O. The organic layer was dried over anhydrous Na₂SO₄ and concentrated in vacuo. The crude products was purified via silica gel column chromatography to obtain pure 6H-benzo[c]chromen-6-ones (**25a-h**).

8,9,10-trimethoxy-6H-benzo[c]chromen-6-one 25a



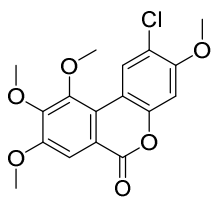
The compound was obtained according to the general procedure (*Route B*) starting from 4,5,6-trimethoxybiphenyl-2-carboxylic acid **24a** (240 mg, 0.83 mmol, 1 eq). The crude product was purified via flash silica gel column chromatography (Petroleum ether/EtOAc 90/10 ratio) to obtain the pure product as a white solid (190 mg, 0.66 mmol). Y= 80% ¹H NMR (400 MHz, CDCl₃) δ 8.85 (d, *J* = 8.2 Hz, 1H), 7.77 (s, 1H), 7.44 (t, *J* = 7.7 Hz, 1H), 7.39 – 7.28 (m, 2H), 4.04 (s, 3H), 4.00 (s, 3H), 3.99 (s, 3H) ppm.

8,9,10-trimethoxy-3-phenyl-6H-benzo[c]chromen-6-one 25b



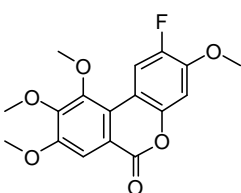
The compound was obtained according to the general procedure (*Route B*) starting from 4,5,6-trimethoxy-[1,1':4',1''-terphenyl]-2-carboxylic acid **24b** (560mg, 1.48 mmol, 1 eq). The crude product was purified via flash silica gel column chromatography (Petroleum ether/EtOAc 90/10 ratio) to obtain the pure product as a light yellow solid (510 mg, 1.41 mmol). Y= 95%. ¹H NMR (400 MHz, CDCl₃) δ 8.89 (d, *J* = 8.7 Hz, 1H), 7.78 (s, 1H), 7.70 – 7.64 (m, 2H), 7.62 – 7.55 (m, 2H), 7.49 (t, *J* = 7.5 Hz, 2H), 7.41 (t, *J* = 7.5 Hz, 1H), 4.06 (s, 3H), 4.02 (s, 6H) ppm.

2-chloro-3,8,9,10-tetramethoxy-6H-benzo[c]chromen-6-one 25c



The compound was obtained according to the general procedure (*Route B*) starting from 3'-chloro-4,4',5,6-tetramethoxybiphenyl-2-carboxylic acid **24c** (830 mg, 2.35 mmol, 1 eq). The crude product was purified via flash silica gel column chromatography (Petroleum ether/EtOAc 90/10 ratio) to obtain the pure product as an off white solid (520 mg, 1.48 mmol). Y= 63%. ¹H NMR (400 MHz, CDCl₃) δ 8.85 (s, 1H), 7.71 (s, 1H), 6.90 (s, 1H), 4.04 (s, 3H), 3.99 (s, 6H), 3.96 (s, 3H) ppm.

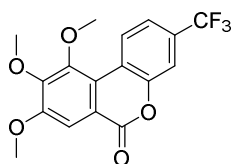
2-fluoro-3,8,9,10-tetramethoxy-6H-benzo[c]chromen-6-one 25d



The compound was obtained according to the general procedure (*Route B*) starting from 3'-fluoro-4,4',5,6-tetramethoxybiphenyl-2-carboxylic acid **24d** (705 mg, 2.10 mmol, 1 eq). The crude product

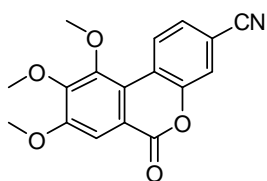
was purified via flash silica gel column chromatography (Petroleum ether/EtOAc 90/10 ratio) to obtain the pure product as an off white solid (351 mg, 1.05 mmol). Y= 50%. ^1H NMR (400 MHz, CDCl_3) δ 8.56 (d, $J = 13.8$ Hz, 1H), 7.72 (s, 1H), 6.93 (d, $J = 7.7$ Hz, 1H), 4.03 (s, 3H), 3.99 (s, 6H), 3.96 (s, 3H) ppm.

8,9,10-trimethoxy-3-(trifluoromethyl)-6H-benzo[c]chromen-6-one 25e



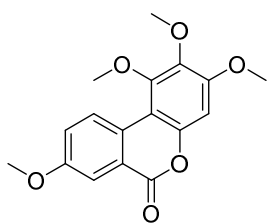
The compound was obtained according to the general procedure (*Route B*) starting from 4,5,6-trimethoxy-4'-(trifluoromethyl)biphenyl-2-carboxylic acid **24e** (670 mg, 1.88 mmol, 1 eq). The crude product was purified via flash silica gel column chromatography (Petroleum ether/EtOAc 90/10 ratio) to obtain the pure product as a light yellow solid (460 mg, 1.30 mmol). Y= 69%. ^1H NMR (400 MHz, CDCl_3) δ 8.99 (d, $J = 8.6$ Hz, 1H), 7.78 (s, 1H), 7.60 (s, 1H), 7.56 (d, $J = 8.6$ Hz, 1H), 4.05 (s, 3H), 4.02 (s, 3H), 4.01 (s, 3H) ppm.

8,9,10-trimethoxy-6-oxo-6H-benzo[c]chromene-3-carbonitrile 25f



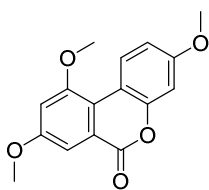
The compound was obtained according to the general procedure (*Route B*) starting from 4'-cyano-4,5,6-trimethoxybiphenyl-2-carboxylic acid **24f** (300 mg, 0.96 mmol, 1 eq). The crude product was purified via flash silica gel column chromatography (Petroleum ether/EtOAc 85/15 ratio) to obtain the pure product as a white solid (100 mg, 0.32 mmol). Y= 33%. ^1H NMR (400 MHz, CDCl_3) δ 8.97 (d, $J = 8.5$ Hz, 1H), 7.77 (s, 1H), 7.61 (s, 1H), 7.56 (d, $J = 8.5$ Hz, 1H), 4.05 (s, 3H), 4.03 (s, 3H), 4.01 (s, 3H) ppm.

1,2,3,8-tetramethoxy-6H-benzo[c]chromen-6-one 25g



The compound was obtained according to the general procedure (*Route B*) starting from 2',3',4,4'-tetramethoxy-[1,1'-biphenyl]-2-carboxylic acid **24g** (290 mg, 0.91 mmol, 1 eq). The crude product was purified via flash silica gel column chromatography (Petroleum ether/EtOAc 90/10 ratio) to obtain the pure product as a white solid (70 mg, 0.22 mmol). Y= 24%. (impurities detected) ^1H NMR (401 MHz, Chloroform-d) δ 8.78 (d, $J = 9.2$ Hz, 1H), 7.80 (d, $J = 2.9$ Hz, 1H), 7.34 (dd, $J = 9.1, 3.0$ Hz, 1H), 6.70 (s, 1H), 3.90 (m, 9H), 3.88 (s, 3H) ppm.

3,8,10-trimethoxy-6H-benzo[c]chromen-6-one 25h



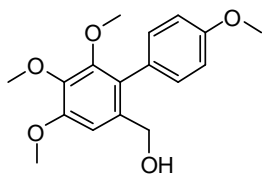
The compound was obtained according to the general procedure (*Route B*) starting from 4,4',6-trimethoxybiphenyl-2-carboxylic acid **24h** (300 mg, 1.04 mmol, 1 eq). The crude product was purified via flash silica gel column chromatography (Petroleum ether/EtOAc 95/5 ratio) to obtain the pure product as a white solid (106 mg, 0.37 mmol). Y= 36 %. ¹H NMR (400 MHz, CDCl₃) δ 8.75 (d, J = 9.9 Hz, 1H), 7.47 (d, J = 2.4 Hz, 1H), 6.89 – 6.79 (m, 3H), 4.01 (s, 3H), 3.92 (s, 3H), 3.87 (s, 3H) ppm.

General procedure to obtain biphenyl-2-carbaldehyde derivatives 36, 51

Step 1) Biphenyl-2-carboxylate derivatives (**23**, **23h**) were dissolved in dry DCM (0.2 M) and the mixtures were cooled to 0 °C. Diisobutylaluminum hydride (DIBAL) 1.0 M in hexane (4.2 eq) was added dropwise. The reaction mixtures were then stirred for 3h at rt. H₂O and DCM were added and the mixtures were filtered to remove the precipitate. The phases were separated and the aqueous phase was extracted with DCM. The combined organic phase was dried over anhydrous Na₂SO₄ and the solvent evaporated in vacuum. The crude products were purified as indicated to obtain the pure biphenyl alcohol intermediate (**23'**, **23h'**).

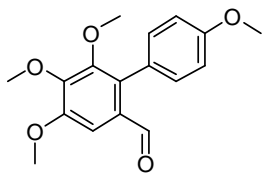
Step 2) Alcohol intermediate **23'**, **23h'** were dissolved in CH₂Cl₂ (0.1 M). PCC (1.5 eq) was added and the reactions were stirred at room temperature for 4 hours. The reaction mixtures were filtered on celite and the solvent evaporated to yield the crude products **36**, **51**, which were purified as indicated.

(4,4',5,6-tetramethoxybiphenyl-2-yl)methanol 23'



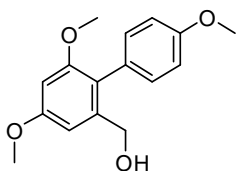
The compound was obtained according to the general procedure (**step 1**) starting from methyl 4,4',5,6-tetramethoxybiphenyl-2-carboxylate **23** (650 mg, 1.96 mmol, 1 eq). The crude product was purified via flash silica gel column chromatography (Petroleum ether/EtOAc 80/20 ratio) to obtain the pure product as a light brown viscous liquid (435 mg, 1.43 mmol, 1 eq). Y= 73%. ¹H NMR (400 MHz, CDCl₃) δ 7.18 (d, J = 8.3 Hz, 2H), 6.96 (d, J = 8.4 Hz, 2H), 6.89 (s, 1H), 4.41 (s, 2H), 3.92 (s, 3H), 3.90 (s, 3H), 3.85 (s, 3H), 3.60 (s, 3H) ppm.

4,4',5,6-tetramethoxybiphenyl-2-carbaldehyde **36**



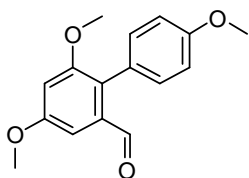
The compound was obtained according to the general procedure (**step 2**) starting from (4,4',5,6-tetramethoxybiphenyl-2-yl)methanol **23'** (359 mg, 1.18 mmol, 1 eq). The crude product was used in the next step without further purification (207 mg, 0.68 mmol). Y= 58%. ¹H NMR (400 MHz, CDCl₃) δ 9.66 (s, 1H), 7.33 (s, 1H), 7.23 (d, J = 8.5 Hz, 2H), 6.99-6.93 (m, 2H), 3.98 (s, 3H), 3.93 (s, 3H), 3.85 (s, 3H), 3.57 (s, 3H) ppm.

(4,4',6-trimethoxybiphenyl-2-yl)methanol **23h'**



The compound was obtained according to the general procedure (**step 1**) starting from methyl 4,4',6-trimethoxybiphenyl-2-carboxylate **23h** (520 mg, 1.71 mmol, 1 eq). The crude product was purified via flash silica gel column chromatography (Petroleum ether/EtOAc 80/20 ratio) to obtain the pure product as a white solid (352 mg, 1.28 mmol). Y= 75%. ¹H NMR (400 MHz, CDCl₃) δ 7.15 (d, J = 8.4 Hz, 2H), 6.95 (d, J = 8.5 Hz, 2H), 6.72 (d, J = 2.3 Hz, 1H), 6.49 (d, J = 2.3 Hz, 1H), 4.42 (d, J = 5.3 Hz, 2H), 3.87 (s, 3H), 3.84 (s, 3H), 3.71 (s, 3H) ppm.

4,4',6-trimethoxybiphenyl-2-carbaldehyde **51**



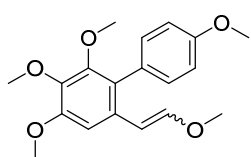
The compound was obtained according to the general procedure (**step 2**) starting from (4,4',6-trimethoxybiphenyl-2-yl)methanol **23h'** (350 mg, 1.28 mmol, 1 eq). The crude product was purified via flash silica gel column chromatography (Petroleum ether/EtOAc 90/10 ratio) to obtain the pure **51** as a white solid (320 mg, 1.17 mmol). Y= 92%. ¹H NMR (400 MHz, CDCl₃) δ 9.73 (s, 1H), 7.22 (d, J = 8.8 Hz, 2H), 7.09 (d, J = 2.5 Hz, 1H), 6.97 (d, J = 8.8 Hz, 2H), 6.75 (d, J = 2.5 Hz, 1H), 3.90 (s, 3H), 3.86 (s, 3H), 3.77 (s, 3H) ppm.

General Wittig procedure to obtain (2-methoxyvinyl)biphenyl derivatives (**37**, **52**)

(Methoxymethyl)triphenylphosphonium chloride (1.5 eq) was dissolved in dry THF (0.3 M) and the mixture was cooled to 0°C under inert atmosphere. LiHMDS 1.0 M in THF

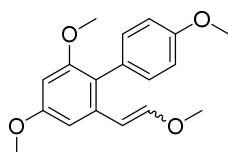
(2 eq) was slowly added and the reaction was stirred for 10 minutes. Biphenyl-2-carbaldehyde derivative (**36**, **51**) (1.0 eq) was dissolved in dry THF (0.2 M) in a separate flask and the solution was added slowly to the reaction mixture. The reaction was warmed to room temperature and stirred for 1 hour. H₂O was added and the mixture was extracted 3 times with EtOAc. The combined organic phases were dried over anhydrous Na₂SO₄, and the solvent evaporated in vacuum. The crude product was purified via silica gel column chromatography to obtain the pure product (**37**, **52**) as a mixture of E/Z isomers.

2,3,4,4'-tetramethoxy-6-(2-methoxyvinyl)biphenyl **37**



The compound was obtained according to the general Wittig procedure starting from 4,4',5,6-tetramethoxybiphenyl-2-carbaldehyde **36** (207 mg, 0.69 mmol, 1 eq). The crude product was purified via silica gel column chromatography (Petroleum ether/EtOAc 90/10 ratio) to obtain the pure product as a colourless viscous liquid (128 mg, 0.39 mmol). Y= 56% (60/40 mixture of E/Z isomers). ¹H NMR (400 MHz, CDCl₃) δ 7.53 (s, 1H), 7.18-7.15 (m, 2H), 6.94 (d, *J* = 8.6 Hz, 2H), 6.80 (d, *J* = 12.9 Hz, 1H, trans), 6.70 (s, 1H), 5.97 (d, *J* = 7.2 Hz, 1H, cis), 5.52 (d, *J* = 12.9 Hz, 1H, trans), 4.92 (d, *J* = 7.2 Hz, 1H, cis), 3.91 (s, 3H), 3.89 (s, 3H), 3.85 (s, 3H), 3.74 (s, 0.40x3H), 3.57 (s, 0.60x3H), 3.56 (s, 0.40x3H), 3.48 (s, 0.60x3H) ppm.

2,4,4'-trimethoxy-6-(2-methoxyvinyl)biphenyl **52**

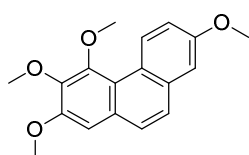


The compound was obtained according to the general Wittig procedure starting from 4,4',6-trimethoxybiphenyl-2-carbaldehyde **51** (210 mg, 0.77 mmol, 1 eq). The crude product was purified via silica gel column chromatography (Petroleum ether/EtOAc 90/10 ratio) to obtain the pure product as a colourless viscous liquid (200 mg, 0.66 mmol). Y= 86% (50 /50 mixture of E/Z isomers). ¹H NMR (400 MHz, CDCl₃) δ 7.40 (d, *J* = 2.3 Hz, 1H), 7.21-7.17 (m, 4H), 6.99-6.91 (m, 4H), 6.93 (d, *J* = 12.9 Hz, 1H, trans), 6.60 (d, *J* = 2.2 Hz, 1H), 6.45-6.43 (m, 2H), 6.02 (d, *J* = 7.3 Hz, 1H, cis), 5.58 (d, *J* = 12.9 Hz, 1H, trans), 4.99 (d, *J* = 7.3 Hz, 1H, cis), 3.88 (s, 3H), 3.87 (s, 3H), 3.86 (d, 6H), 3.75 (s, 3H), 3.72 (s, 3H), 3.71 (s, 3H), 3.50 (s, 3H) ppm.

General Bismuth-cyclisation procedure to obtain methoxy-protected phenanthrene derivatives (38, 53)

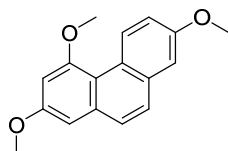
(2-methoxyvinyl)biphenyl derivatives (**37**, **52**) (1 eq) was dissolved in 1,2-dichloroethane (0.1-0.2 M) under nitrogen atmosphere. Bismuth(III) trifluoromethanesulfonate (0.05 eq) was added and the reaction was stirred at room temperature for 30 minutes. After TLC showed full conversion, the solvent was evaporated. The crude product was purified via silica gel column chromatography to obtain the pure products.

2,3,4,7-tetramethoxyphenanthrene **38**



The compound was obtained according to the general Bismuth-cyclization procedure starting from 2,3,4,4'-tetramethoxy-6-(2-methoxyvinyl)-1,1'-biphenyl **37** (127 mg, 0.38 mmol, 1 eq). The crude product was purified via silica gel column chromatography (Petroleum ether/EtOAc 95/5 ratio) to obtain the pure product as a white solid (74 mg, 0.25 mmol). Y= 65%. ¹H NMR (400 MHz, CDCl₃) δ 9.40 (d, J = 9.2 Hz, 1H), 7.57 (s, 2H), 7.27 – 7.19 (m, 2H), 7.06 (s, 1H), 4.02 (s, 3H), 4.00 (s, 1H), 3.99 (s, 3H), 3.94 (s, 3H) ppm.

2,4,7-trimethoxyphenanthrene **53**



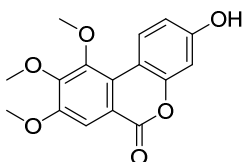
The compound was obtained according to the general Bismuth-cyclization procedure starting from 2,4,4'-trimethoxy-6-(2-methoxyvinyl)biphenyl **52** (200 mg, 0.66 mmol, 1 eq). The crude product was purified via silica gel column chromatography (Petroleum ether/EtOAc 95/5 ratio) to obtain the pure product as a white solid (140 mg, 0.52 mmol). Y= 78%. ¹H NMR (400 MHz, CDCl₃) δ 9.54 – 9.44 (m, 1H), 7.68-7.61 (m, 2H), 7.29-7.26 (m, 2H), 6.90 (d, J = 2.5 Hz, 1H), 6.79 (d, J = 2.5 Hz, 1H), 4.10 (s, 3H), 3.97 (s, 3H), 3.96 (s, 3H) ppm.

General procedure of Hurtley condensation for the synthesis of benzocoumarins **42**, **42b**, **46a**, **46b**.

Commercially available phenol derivatives (resorcinol **41** or phloroglucinol **45**) (2 eq) and 2-bromobenzoic acid derivatives **40**, **40b** (synthesized by us), or commercially available 2-bromo-5-methoxybenzoic acid **44a** and 2-bromobenzoic acid **44b** (1 eq)

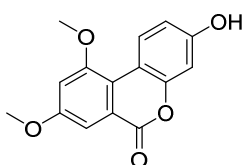
were added to a 4 M NaOH solution (2 eq) and heated at 60 °C for 30 min under N₂ atmosphere. Aq. CuSO₄ 10% (0.1 eq) was added dropwise to the hot reaction and heating was continued at 95 °C for 3 h. The reaction mixture was cooled to room temperature. The precipitate was filtered off, washed with water and dried under vacuum.

3-hydroxy-8,9,10-trimethoxy-6H-benzo[c]chromen-6-one **42**



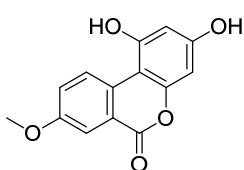
According to the general procedure of Hurltley condensation, 2-bromo-3,4,5-trimethoxybenzoic acid **40** (1 g, 3.44 mmol, 1 eq) and resorcinol **41** (758 mg, 6.88 mmol, 2 eq) afforded **42** (140 mg, 0.47 mmol) as an off-white solid. Y= 14%. ¹H NMR (401 MHz, DMSO-*d*₆) δ 10.28 (s, 1H), 8.58 (d, *J* = 9.0 Hz, 1H), 7.58 (s, 1H), 6.83 (dd, *J* = 9.0, 2.6 Hz, 1H), 6.73 (d, *J* = 2.5 Hz, 1H), 3.93 (s, 5H), 3.89 (s, 3H)ppm.

3-hydroxy-8,10-dimethoxy-6H-benzo[c]chromen-6-one **42b**



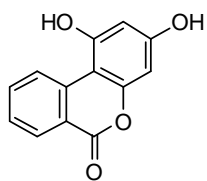
According to the general procedure of Hurltley condensation, 2-bromo-3,5-dimethoxybenzoic acid **40b** (960 mg, 3.52 mmol, 1 eq) and resorcinol **41** (776 mg, 7.05 mmol, 2 eq) afforded **42b** as a yellow-green powder (30 mg, 0.11 mmol). (Y= 3%) ¹H NMR (401 MHz, DMSO-*d*₆) δ 8.66 (d, *J* = 8.6 Hz, 1H), 7.33 (d, *J* = 2.5 Hz, 1H), 7.12 (d, *J* = 2.5 Hz, 1H), 6.74-6.69 (m, 2H), 4.03 (s, 3H), 3.90 (s, 3H) ppm.

1,3-dihydroxy-8-methoxy-6H-benzo[c]chromen-6-one **46a**¹⁴⁴



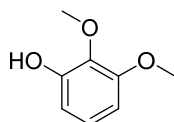
According to the general procedure of Hurltley condensation, 2-bromo-5-methoxybenzoic acid **44a** (1.0 g, 4 mmol, 1 eq) and phloroglucinol **45** (1.09 g, 8.66 mmol, 2 eq) afforded product **46a** as an off-white solid (700mg, mmol).Y= 68%. ¹H NMR (400 MHz, DMSO-*d*₆) δ 10.81 (br, OH), 10.03 (br, OH), 8.90 (d, *J* = 9.2 Hz, 1H), 7.62 (d, *J* = 2.7 Hz, 1H), 7.44 (dd, *J* = 9.2, 2.9 Hz, 1H), 6.39 (d, *J* = 2.1 Hz, 1H), 6.26 (d, *J* = 2.1 Hz, 1H), 3.87 (s, 3H) ppm; ¹³C NMR (100 MHz, DMSO-*d*₆) δ 160.6, 158.3, 157.3, 156.8, 152.4, 128.8, 127.7, 123.2, 119.7, 110.9, 99.8, 98.7, 94.9, 55.40 ppm.

1,3-dihydroxy-6H-benzo[c]chromen-6-one **46b**¹⁴²



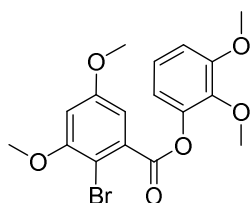
According to the general procedure of Hurtley condensation, 2-bromobenzoic acid **44b** (2.01 g, 10 mmol, 1 eq) and phloroglucinol **45** (2.52 g, 20 mmol, 2 eq) product **46b** as an off-white solid (1.89 g, 8.3 mmol). Y= 83 %. ¹H NMR (400 MHz, DMSO-d₆) δ 10.90 (s, OH), 10.14 (s, OH), 8.96 (d, J = 8.4 Hz, 1H), 8.19 (d, J = 7.9 Hz, 1H), 7.83 (t, J = 7.8 Hz, 1H), 7.49 (t, J = 7.6 Hz, 1H), 6.43 – 6.37 (m, 1H), 6.28 – 6.23 (m, 1H) ppm; ¹³C NMR (100 MHz, DMSO-d₆) δ 160.7, 159.2, 157.6, 153.3, 135.4, 134.9, 129.3, 126.3, 125.8, 118.4, 99.8, 98.6, 95.1 ppm.

2, 3 dimethoxyphenol **55**¹⁴⁶



To a mixture of 30% H₂O₂ (2.02 mL, 19.8 mmol, 2.2 eq) of and boric acid (2.78 g, 45.0 mmol, 5 eq) in 30mL THF was added 0.9 mL of sulfuric acid. The mixture was stirred a t rt for 30 min and a solution of 2,3-dimethoxybenzaldehyde (1.5 g, 9.0 mmol, 1 eq) in 10mL THF was added. The mixture was heated to 50 °C for 24h, quenched with saturated NaHCO₃ and filtered. The filtrate was extracted with Et₂O and the combined organic extracts were dried over Na₂SO₄ and concentrated in vacuo. Purification by column flash chromatography (EtPet 85/EtOAc 15) afforded 1.2g (7.65 mmol) of product, white powder (Y= 85%). ¹H NMR (401 MHz, Chloroform-*d*) δ 6.93 (t, J = 8.3 Hz, 1H), 6.60 (dd, J = 8.2, 1.4 Hz, 1H), 6.48 (dd, J = 8.3, 1.4 Hz, 1H), 5.79 (s, 1H), 3.90 (s, 3H), 3.86 (s, 3H) ppm.

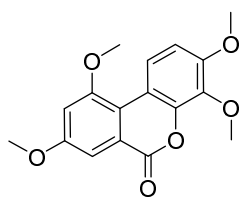
2,3-dimethoxyphenyl 2-bromo-3,5-dimethoxybenzoate **56**



Oxalyl chloride (0.13mL, 1.49mmol, 1.1 eq) and DMF (1 drop, cat) were added to a 0 °C suspension of 2-bromo-3,5-dimethoxybenzoic acid **40b** (355mg, 1.36mmol, 1 eq) in CH₂Cl₂ (2.5mL). The reaction mixture was stirred for 5min at 0 °C and then for 16h at rt. The reaction mixture was concentrated under reduced pression. The resulting oil was solubilized in CH₂Cl₂ (1.20mL) and cooled to 0 °C. 2,3 dimethoxyphenol **55** (230mg, 1.49 mmol, 1.1 eq) and trimethylamine (0.3mL, 2.03 mmol, 1.5 eq) were added and the mixture was stirred for 5min. Acetonitrile (1.20 mL) was finally added and the resulting mixture was stirred at rt for 16h. The reaction was quenched with a saturated solution of ammonium chloride and the layers were separated. The aqueous phase was extracted with CH₂Cl₂ and the combined organic layers were

dried over Na₂SO₄ and concentrated in vacuo. Purification by column flash chromatography (EtPet 92/EtOAc 8) afforded 400mg (1.01 mmol) of product as white powder (Y= 75%). ¹H NMR (401 MHz, Chloroform-*d*) δ 7.12 – 7.04 (m, 2H), 6.87 (d, *J* = 1.2 Hz, 1H), 6.85 (d, *J* = 1.2 Hz, 1H), 6.66 (dd, *J* = 2.8, 1.2 Hz, 1H), 3.92 (s, 3H), 3.90 (s 3H), 3.88 (s, 3H), 3.87 (s, 3H) ppm.

3,4,8,10-tetramethoxy-6H-benzo[*c*]chromen-6-one **57**

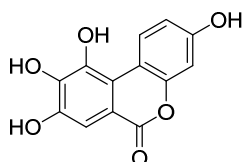


Sodium acetate (180mg, 2.22mmol, 2eq), S-Phos (45mg, 0.11mmol, 0.1 eq) and Pd(OAc)₂ (24mg, 0.11mmol, 0.1 eq) were added to a solution of 2,3-dimethoxyphenyl 2-bromo-3,5-dimethoxybenzoate **56** (440 mg, 1.11mmol, 1eq) in dry dimethylacetamide (DMA) (20mL) under inert atmosphere. The reaction mixture was stirred at 130 °C for 3 days. The reaction was quenched by addition of water and the mixture extracted with CH₂Cl₂ and the combined organic layers were dried over Na₂SO₄ and concentrated under reduced pressure. The remaining DMA was eliminated by distillation under reduced pressure. The crude oil was purified by column flash chromatography (DCM 99.5/MeOH 0.5) afforded 50mg (0.16 mmol) of product as yellow powder (Y= 14%) (Starting material recovered 170 mg). ¹H NMR (401 MHz, Chloroform-*d*) δ 8.55 (d, *J* = 9.3 Hz, 1H), 7.48 (d, *J* = 2.6 Hz, 1H), 6.88 – 6.86 (m, 1H), 6.85 (s, 1H), 4.00 (s, 3H), 4.00 (s, 3H), 3.95 (s, 3H), 3.92 (s, 3H) ppm.

General demethylation procedure to obtain the final deprotected UM6 (**19**), **26-33**, **35**, **39**, **43**, **50**, **54**

O-Methoxy protected compound was dissolved in dry DCM (0.03-0.09 M) in a flame dried flask and the mixture was cooled to -78°C. BBr₃ 1.0M in DCM (2 eq per methoxy group) was slowly added dropwise. The reaction was let warm up to room temperature and stirred for 24-48h. MeOH was added and the solvent was removed in vacuum. The crude products were purified as specified.

3,8,9,10-tetrahydroxy-6H-benzo[*c*]chromen-6-one **19** (UM6)



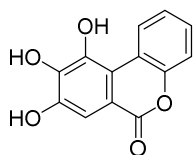
The compound was obtained starting from 3,8,9,10-tetramethoxy-6H-benzo[*c*]chromen-6-one **25** (105 mg, 0.332 mmol, 1.0 equiv),

following the general demethylation procedure. The crude product was purified via C18 silica gel reverse phase column chromatography (H₂O/MeOH/HCOOH elution gradient from a 70/30/0.1 ratio to a 30/70/0.1 ratio) to obtain the product in a mixture with a minor dark impurity not detectable using NMR, which was removed washing the product with small amounts of MeOH, yielding the pure compound as a grey solid (yield 58%).

The product was also obtained starting from 3-hydroxy-8,9,10-trimethoxy-6H-benzo[c]chromen-6-one **42** (130 mg, 0.43 mmol, 1 eq), following the general demethylation procedure. The crude product was purified as previously described, to obtain the pure product with Y= 38%.

¹H NMR (400 MHz, DMSO-d₆) δ 10.21 (s, OH, exchange with D₂O), 9.97 (s, OH, exchange with D₂O), 9.93 (s, OH, exchange with D₂O), 9.51 (s, OH, exchange with D₂O), 8.80 (d, J = 9 Hz, 1 H), 7.28 (s, 1H), 6.75 (dd, J = 2.2, 9.0 Hz, 1 H), 6.67 (d, J = 1.8 Hz, 1 H) ppm; ¹³C NMR (100 MHz, DMSO-d₆) δ 160.74, 157.30, 150.68, 145.27, 142.52, 140.30, 128.02, 116.00, 112.01, 110.63, 110.23, 106.82, 102.57 ppm; MS (ES): m/z 261 [M + H]⁺, 283 [M + Na]⁺. HPLC t_R = 4.76 min, purity ≥ 99.5%.

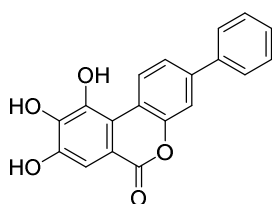
8,9,10-trihydroxy-6H-benzo[c]chromen-6-one **26**



The compound was obtained starting from 8,9,10-trimethoxy-6H-benzo[c]chromen-6-one **25a** (100 mg, 0.35 mmol, 1 eq), following the general demethylation procedure. The crude product was purified via

C18 silica gel reverse phase column chromatography (H₂O/MeOH/HCOOH elution gradient from a 70/30/0.1 ratio to a 30/70/0.1 ratio) to obtain an off white solid (74 mg, 0.30 mmol). Y= 87%. ¹H NMR (400 MHz, DMSO-d₆) δ 10.40 (br, OH), 10.03 (br, OH), 9.74 (br, OH), 9.01 (d, J = 7.7 Hz, 1H), 7.45 – 7.23 (m, 4H) ppm. ¹³C NMR (100 MHz, DMSO-d₆) δ 160.42, 149.28, 146.38, 143.78, 140.25, 127.83, 126.87, 124.02, 118.59, 116.46, 114.78, 112.11, 107.16 ppm; MS (ES): m/z 245 [M + H]⁺, 267 [M + Na]⁺.

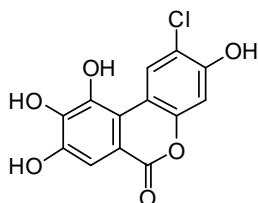
8,9,10-trihydroxy-3-phenyl-6H-benzo[c]chromen-6-one **27**



The compound was obtained starting from 8,9,10-trimethoxy-3-phenyl-6H-benzo[c]chromen-6-one **25b** (100 mg, 0.28 mmol, 1 eq), following the general demethylation procedure. The crude

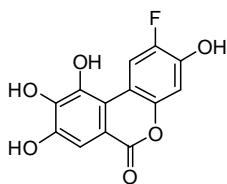
product was purified via C18 silica gel reverse phase column chromatography (H₂O/MeOH/HCOOH elution gradient from a 70/30/0.1 ratio to a 30/70/0.1 ratio) to obtain a beige solid (56 mg, 0.17 mmol, 1 eq). Y= 62%. ¹H NMR (400 MHz, DMSO-d₆) δ 10.43 (s, OH), 10.05 (s, OH), 9.80 (s, OH), 9.06 (d, *J* = 8.5 Hz, 1H), 7.79 (d, *J* = 7.3 Hz, 2H), 7.69 – 7.61 (m, 2H), 7.49 (t, *J* = 7.6 Hz, 2H), 7.41 (d, *J* = 7.2 Hz, 1H), 7.37 (s, 1H) ppm; ¹³C NMR (100 MHz, DMSO-d₆) δ 160.50, 149.84, 146.49, 143.79, 140.28, 139.35, 138.60, 129.02, 127.96, 127.92, 127.38, 126.63, 122.22, 119.50, 117.73, 114.68, 114.02, 112.03, 107.27 ppm; MS (ES): *m/z* 321 [M + H]⁺, 343 [M + Na]⁺.

2-chloro-3,8,9,10-tetrahydroxy-6H-benzo[*c*]chromen-6-one 28



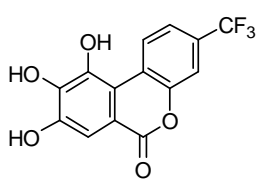
The compound was obtained starting from 2-chloro-3,8,9,10-tetramethoxy-6H-benzo[*c*]chromen-6-one **25c** (250 mg, 0.71 mmol, 1 eq), following the general demethylation procedure. The crude product was purified via C18 silica gel reverse phase column chromatography (H₂O/MeOH/HCOOH elution gradient from a 70/30/0.1 ratio to a 30/70/0.1 ratio) to obtain a white solid (111 mg, 0.38 mmol). Y= 53%. ¹H NMR (400 MHz, DMSO-d₆) δ 10.71 (br, OH), 10.05 (br, 3OH), 8.94 (s, 1H), 7.29 (s, 1H), 6.88 (s, 1H) ppm; ¹³C NMR (100 MHz, DMSO-d₆) δ 160.34, 152.49, 149.08, 145.81, 142.64, 140.55, 127.31, 115.55, 114.61, 111.20, 109.56, 107.03, 103.85 ppm.

2-fluoro-3,8,9,10-tetrahydroxy-6H-benzo[*c*]chromen-6-one 29



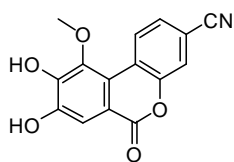
The compound was obtained starting from 4-fluoro-3,8,9,10-tetramethoxy-6H-benzo[*c*]chromen-6-one **25d** (300 mg, 0.89 mmol, 1 eq), following the general demethylation procedure. The crude product was purified via C18 silica gel reverse phase column chromatography (H₂O/MeOH/HCOOH elution gradient from a 70/30/0.1 ratio to a 30/70/0.1 ratio) to obtain an off white solid (80 mg, 0.29 mmol). Y= 32%. ¹H NMR (400 MHz, DMSO-d₆) δ 10.41 (br, 2H), 10.00 (br, 2H), 8.68 (d, ³*J*_{H-F} = 14.0 Hz, 1H), 7.29 (s, 1H), 6.87 (d, ⁴*J*_{H-F} = 8.0 Hz, 1H) ppm; ¹³C NMR (100 MHz, DMSO-d₆) δ 160.53, 148.49, 146.16, 145.84, 144.73 (d, *J*_{C-F} = 14.6 Hz), 142.55, 140.36, 115.1, 113.25 (d, *J*_{C-F} = 23.8 Hz), 110.79, 109.79 (d, *J*_{C-F} = 8.4 Hz), 107.00, 104.95 (d, *J*_{C-F} = 3.4 Hz) ppm.

8,9,10-trihydroxy-3-(trifluoromethyl)-6H-benzo[c]chromen-6-one 30



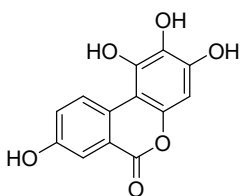
The compound was obtained starting from 8,9,10-trimethoxy-3-(trifluoromethyl)-6H-benzo[c]chromen-6-one **25e** (300 mg, 0.85 mmol, 1 eq), following the general demethylation procedure. The crude product was purified via C18 silica gel reverse phase column chromatography (H₂O/MeOH/HCOOH elution gradient from a 70/30/0.1 ratio to a 30/70/0.1 ratio) to obtain a white solid (256 mg, 0.82 mmol). Y= 97%. ¹H NMR (400 MHz, DMSO-d₆) δ 10.58 (br,OH), 10.15 (br, OH), 10.04 (br, OH), 9.19 (d, *J* = 8.5 Hz, 1H), 7.67 (d, *J* = 8.6 Hz, 2H), 7.39 (s, 1H) ppm. ¹³C NMR (100 MHz, DMSO-d₆) δ 159.81, 149.06, 147.35, 144.49, 140.38, 127.71, 127.44 (d, *J* = 32.7 Hz), 125.07, 122.36, 120.38 (d, *J* = 3.8 Hz), 113.51 (d, *J* = 4.1 Hz), 113.28, 112.52, 107.55.

8,9-dihydroxy-10-methoxy-6-oxo-6H-benzo[c]chromene-3-carbonitrile 31



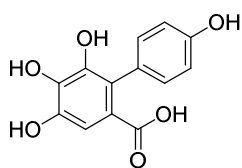
The compound was obtained starting from 8,9,10-trimethoxy-6-oxo-6H-benzo[c]chromene-3-carbonitrile **25f** (140 mg, 0.45 mmol, 1 eq), following the general demethylation procedure. The crude product was purified via silica gel column chromatography (DCM/MeOH 70/30 ratio) to obtain the pure product as white solid (20 mg, 0.07 mmol). Y=16%. ¹H NMR (400 MHz, DMSO-d₆) δ 8.91 (d, *J* = 8.6 Hz, 1H), 7.94 (d, *J* = 1.6 Hz, 1H), 7.77 (dd, *J* = 8.5, 1.7 Hz, 1H), 7.55 (s, 1H), 3.86 (s, 3H) ppm; ¹³C NMR (101 MHz, DMSO-d₆) δ 159.26, 149.38, 149.20, 146.90, 145.62, 127.94, 126.90, 122.31, 120.84, 118.60, 118.12, 112.48, 111.21, 110.25, 59.60 ppm.

1,2,3,8-tetrahydroxy-6H-benzo[c]chromen-6-one 32



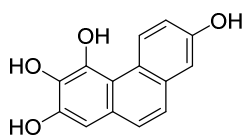
The compound was obtained starting from 1,2,3,8-tetramethoxy-6H-benzo[c]chromen-6-one **25g** (70 mg, 0.22 mmol, 1 eq), following the general demethylation procedure. The crude product was purified via C18 silica gel reverse phase column chromatography (H₂O/MeOH/HCOOH elution gradient from a 70/30/0.1 ratio to a 30/70/0.1 ratio) to obtain a brown solid (20 mg, 0.08 mmol), Y= 35%. ¹H NMR (400 MHz, CD₃OD) δ 8.97 (d, *J* = 9.0 Hz, 1H), 7.64 (d, *J* = 2.8 Hz, 1H), 7.26 (dd, *J* = 9.0, 2.8 Hz, 1H), 6.39 (s, 1H). ¹³C NMR (100 MHz, CD₃OD) δ 164.12, 157.37, 147.87, 146.01, 145.67, 129.70, 129.32, 124.46, 121.53, 114.79, 111.45, 101.29, 95.80 ppm.

4,4',5,6-tetrahydroxybiphenyl-2-carboxylic acid **33**



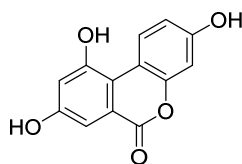
The compound was obtained starting from 4,4',5,6-tetramethoxybiphenyl-2-carboxylic acid **24** (160 mg, 0.50 mmol, 1 eq), following the general demethylation procedure. The crude product was purified via C18 silica gel reverse phase column chromatography (H₂O/MeOH/HCOOH elution gradient from a 70/30/0.1 ratio to a 30/70/0.1 ratio) to obtain a light brown solid (55 mg, 0.21 mmol). Y= 42%. ¹H NMR (400 MHz, DMSO-d₆) δ 11.76 (br, OH), 9.34 (br, OH), 9.15 (br, OH), 8.92 (br, OH), 8.02 (br, OH), 6.91 (d, J = 8.4 Hz, 2H), 6.77 (s, 1H), 6.66 (d, J = 8.4 Hz, 2H) ppm; ¹³C NMR (100 MHz, DMSO-d₆) δ 169.18, 155.55, 143.81, 143.66, 135.77, 130.88, 128.18, 122.81, 121.62, 114.06, 108.21 ppm.

phenanthrene-2,3,4,7-tetraol **35**



The compound was obtained starting from 2,3,4,7-tetramethoxyphenanthrene **38** (63 mg, 0.21 mmol, 1 eq) following the general demethylation procedure. The crude product was purified via C18 silica gel reverse phase column chromatography (H₂O/MeOH/HCOOH elution gradient from a 70/30/0.1 ratio to a 30/70/0.1 ratio) to obtain a grey solid (44 mg, 0.18 mmol). Y= 86%. ¹H NMR (400 MHz, DMSO-d₆) δ 9.65 (br, OH), 9.42 (br, OH) 9.42 (d, J = 9.2 Hz, 1H), 8.94 (br, OH), 8.87 (br, OH), 7.40 (d, J = 8.8 Hz, 1H), 7.33 (d, J = 8.8 Hz, 1H), 7.09 (d, J = 2.3 Hz, 1H), 7.02 (dd, J = 9.2, 2.6 Hz, 1H), 6.79 (s, 1H) ppm; ¹³C NMR (100 MHz, DMSO-d₆) δ 153.99, 144.84, 143.25, 132.77, 132.73, 128.63, 126.86, 125.30, 123.83, 123.52, 115.64, 113.60, 110.92, 103.81 ppm; MS (ES): m/z 243 [M + H]⁺, 265 [M + Na]⁺.

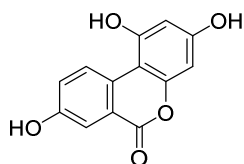
3,8,10-trihydroxy-6H-benzo[c]chromen-6-one **39** (UM7)



The compound was obtained starting from 3,8,10-trimethoxy-6H-benzo[c]chromen-6-one **25h** (145 mg, 0.51 mmol, 1 eq), following the general demethylation procedure. The crude product was purified via C18 silica gel reverse phase column chromatography (H₂O/MeOH/HCOOH elution gradient from a 70/30/0.1 ratio to a 30/70/0.1 ratio) to obtain a light yellow solid (100 mg, 0.41 mmol). Y= 80%. ¹H NMR (400 MHz, DMSO-d₆) δ 10.78 (br, OH), 10.03 (br, OH), 9.99 (br, OH), 8.74 (d, J = 9.0 Hz, 1H), 7.13 (d, J = 2.5 Hz, 1H), 6.86 (d, J = 2.5 Hz, 1H), 6.76 (dd, J = 9.0, 2.5 Hz, 1H), 6.70 (d, J = 2.5

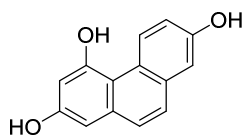
Hz, 1H) ppm; ^{13}C NMR (100 MHz, DMSO- d_6) δ 160.78, 157.28, 156.99, 156.06, 150.23, 128.01, 121.64, 114.78, 112.36, 109.93, 109.63, 106.01, 102.65 ppm.

1,3,8-trihydroxy-6H-benzo[c]chromen-6-one **43**



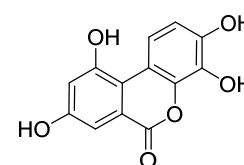
The product was obtained starting from 1,3-dihydroxy-8-methoxy-6H-benzo[c]chromen-6-one **46a** (250 mg, 0.968 mmol), following the demethylation general procedure. The crude product was purified via C18 silica gel reverse phase column chromatography ($\text{H}_2\text{O}/\text{MeOH}/\text{HCOOH}$ elution gradient 60/40/0.1 ratio) to obtain a yellow powder (80 mg, 0.33 mmol). Y= 34%. ^1H NMR (400 MHz, DMSO- d_6) δ 10.71 (br, OH), 10.03 (br, 2OH), 8.82 (d, J = 9.0 Hz, 1H), 7.53 (d, J = 2.8 Hz, 1H), 7.27 (dd, J = 9.0, 2.6 Hz, 1H), 6.37 (d, J = 2.2 Hz, 1H), 6.23 (d, J = 2.1 Hz, 1H) ppm; ^{13}C NMR (100 MHz, DMSO- d_6) δ 160.70, 157.9, 156.6, 155.7, 152.2, 127.8, 127.2, 123.5, 119.8, 113.5, 99.7, 99.0, 94.82 ppm.

phenanthrene-2,4,7-triol **50**



The compound was obtained starting from 2,4,7-trimethoxyphenanthrene **53** (200 mg, 0.75 mmol, 1 eq), following the general demethylation procedure. The crude product was purified via C18 silica gel reverse phase column chromatography ($\text{H}_2\text{O}/\text{MeOH}/\text{HCOOH}$ elution gradient from a 70/30/0.1 ratio to a 30/70/0.1 ratio) to obtain a brown solid (17 mg, 0.08 mmol). Y= 10%. ^1H NMR (400 MHz, DMSO- d_6) δ 10.34 (br, OH), 9.48 (br, 2OH), 9.37 (d, J = 9.2 Hz, 1H), 7.48-7.43 (m, 2H), 7.11 (d, J = 2.4 Hz, 1H), 7.04 (dd, J = 9.2, 2.5 Hz, 1H), 6.68 (s, 2H) ppm; ^{13}C NMR (100 MHz, DMSO- d_6) δ 156.53, 154.88, 153.95, 134.04, 132.43, 128.59, 126.95, 126.78, 123.89, 116.30, 112.86, 111.12, 103.69, 103.08 ppm.

3,4,8,10-tetrahydroxy-6H-benzo[c]chromen-6-one **54 (Uro-E)**



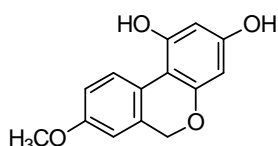
The compound was obtained starting from 3,4,8,10-tetramethoxy-6H-benzo[c]chromen-6-one **57** (50mg, 0.16 mmol, 1 eq), following the general demethylation procedure. The crude product was purified via C18 silica gel reverse phase column chromatography ($\text{H}_2\text{O}/\text{MeOH}/\text{HCOOH}$ elution gradient from a 70/30/0.1 ratio to a 30/70/0.1 ratio) to obtain an off white solid (28 mg, 0.11 mmol). Y= 67%. ^1H NMR

(401 MHz, CD₃OD) δ 8.38 (d, J = 9.0 Hz, 1H), 7.27 (d, J = 2.4 Hz, 1H), 6.80 (d, J = 2.5 Hz, 1H), 6.76 (d, J = 9.0 Hz, 1H); ¹³C NMR (100 MHz, CD₃OD) δ 163.38, 158.42, 157.88, 146.75, 140.65, 133.34, 122.95, 119.12, 117.56, 112.63, 112.53, 111.03, 107.34 ppm.

General procedure for the carbonyl reduction of dibenzopyranones **46a**, **46b**, **43** to dibenzopyranes **47-49**.

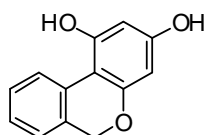
A cooled solution of dibenzopyranones (1 eq), in a mixture of BF₃·Et₂O (25 eq) in dry THF was added over 10 minutes to a suspension of NaBH₄ (3.5 eq) in dry THF under nitrogen atmosphere while maintaining the reaction temperature below 10 °C. The reaction mixture was then raised within 30 min to the reflux temperature for 2h. The solvent was removed in vacuum and the crude product was dried in high vacuum to remove the excess of boron trifluoride etherate. Then water was added and the mixture extracted with diethyl ether. The combined organic phases were dried over Na₂SO₄, and the solvent evaporated in vacuum. The crude product was purified via flash silica gel column chromatography.

8-methoxy-6H-benzo[*c*]chromene-1,3-diol **47**



The compound was obtained starting from 1,3-dihydroxy-8-methoxy-6H-benzo[*c*]chromen-6-one **46a** (800 mg, 3.1 mmol, 1 eq) followed the general procedure for carbonyl reduction. The crude product was purified via flash silica gel column chromatography (DCM/MeOH 99.5/0.5) to obtain a white solid (470 mg, 1.92 mmol). Y= 62%. ¹H NMR (400 MHz, DMSO-*d*₆) δ 9.84 (s, OH), 9.37 (s, OH), 8.17 (d, J = 8.7 Hz, 1H), 6.85 (dd, J = 8.8, 2.8 Hz, 1H), 6.80 (d, J = 2.6 Hz, 1H), 6.08 (d, J = 2.4 Hz, 1H), 5.87 (d, J = 2.4 Hz, 1H), 4.87 (s, 2H), 3.75 (s, 3H) ppm; ¹³C NMR (100 MHz, DMSO-*d*₆) δ 157.4, 156.9, 156.4, 156.1, 131.72, 126.2, 122.5, 113.2, 109.8, 102.8, 97.5, 95.4, 68.0, 55.1 ppm.

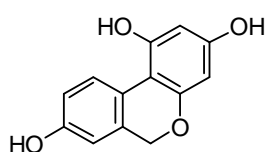
6H-benzo[*c*]chromene-1,3-diol **48**¹⁴⁵



The compound was obtained starting from 1,3-dihydroxy-6H-benzo[*c*]chromen-6-one **46b** (800 mg, 3.51 mmol, 1 eq) followed the general procedure for carbonyl reduction. The crude product was

purified via flash silica gel column chromatography (DCM/MeOH 99/1 ratio) to obtain a white solid (170 mg, 0.79 mmol). Y= 23%. ¹H NMR (400 MHz, DMSO-d₆) δ 9.99 (s, OH), 9.53 (s, OH), 8.25 (d, J = 7.9 Hz, 1H), 7.28 (t, J = 7.5 Hz, 1H), 7.19-7.12 (m, 2H), 6.11 (d, J = 2.3 Hz, 1H), 5.89 (d, J = 2.3 Hz, 1H), 4.90 (s, 2H) ppm; ¹³C NMR (100 MHz, DMSO-d₆) δ 158.3, 157.3, 156.8, 130.0, 129.8, 127.7, 125.1, 124.8, 124.2, 102.8, 97.5, 95.4, 67.9 ppm.

6H-benzo[c]chromene-1,3,8-triol **49**



The compound was obtained starting from 1,3,8-trihydroxy-6H-benzo[c]chromen-6-one **43** (190 mg, 0.78 mmol, 1 eq) following the general procedure for carbonyl reduction. The crude product was purified via flash silica gel column chromatography (DCM/MeOH 99.3/0.7) to obtain a white solid (30 mg, 0.13 mmol). Y= 17%. ¹H NMR (400 MHz, CD₃OD) δ 8.16 (d, J = 8.6 Hz, 1H), 6.71 (dd, J = 8.6, 2.5 Hz, 1H), 6.58 (d, J = 2.5 Hz, 1H), 6.04 (d, J = 2.0 Hz, 1H), 5.94 (d, J = 2.0 Hz, 1H), 4.83 (s, 2H) ppm; ¹³C NMR (100 MHz, CD₃OD) δ 158.2, 158.1, 157.2, 156.3, 133.5, 128.0, 123.1, 115.5, 111.8, 105.4, 98.50, 96.7, 69.8 ppm.

Part II

TOWARDS THE DEVELOPMENT OF FLUORESCENT AND AFFINITY PROBES TO INVESTIGATE NEUROGENESIS

1. Introduction

1.1 Project overview

This part deals with the research activity carried out during the six-month placement under the supervision of Professor Angela Russell at Chemistry Research Laboratory, Department of Chemistry, University of Oxford, part-funded by and in collaboration with the spin-out company OxStem Neuro.

The present project, in collaboration with Professor Francis Szele (Department of Physiology, Anatomy and Genetics, University of Oxford) focused on the development of small molecules as affinity and fluorescent probes to detect new pathways involved in neurogenesis and Neural Stem Cell (NSC) fate.

1.2 Opportunities for neurodegenerative diseases: regenerative medicine

Age related neurological diseases are estimated to affect as many as a billion people worldwide and with the growth of the aging population and increasing life expectancy, are predicted to increase 12% by 2030 (World Health Organization 2006). These disorders include Parkinson and Alzheimer's diseases, less common conditions such as motor neuron disease, multiple sclerosis and rare diseases such as spinal muscular atrophy. There are also numerous psychiatric conditions that may involve neuronal damage.

A common hallmark of neurodegenerative diseases is the progressive loss of neurons and other brain cells.¹⁴⁷ Currently, treatment for these disorders are limited and aims to treat the symptoms, but are not effective to slow or stop the neuronal death process. The development of disease-modifying therapies has been slower and there is a pressing need for improved and novel therapeutic approaches to treat these disorders.^{148,149}

Emerging therapeutic opportunities arise from regenerative medicine that involves methods to replace or regenerate human cells, tissues or organs in order to restore or

establish normal function; it is founded on the possibility to exploit stem and progenitor cells, which have the capacity for self-renewal and differentiation to various cell lineages.^{150,151}

In recent years a number of treatment options have been investigated, including cell therapy and tissue engineering.¹⁵² A diverse and innovative regenerative approach, that led medicinal chemistry to play a pivotal role in this field, is the Endogenous Cell Activation Therapy (ECAT), that is based on the *in situ* modulation of adult stem or precursor cells using small molecules, to induce regeneration or repair of adult tissue.^{153,154} **(Figure 19)**

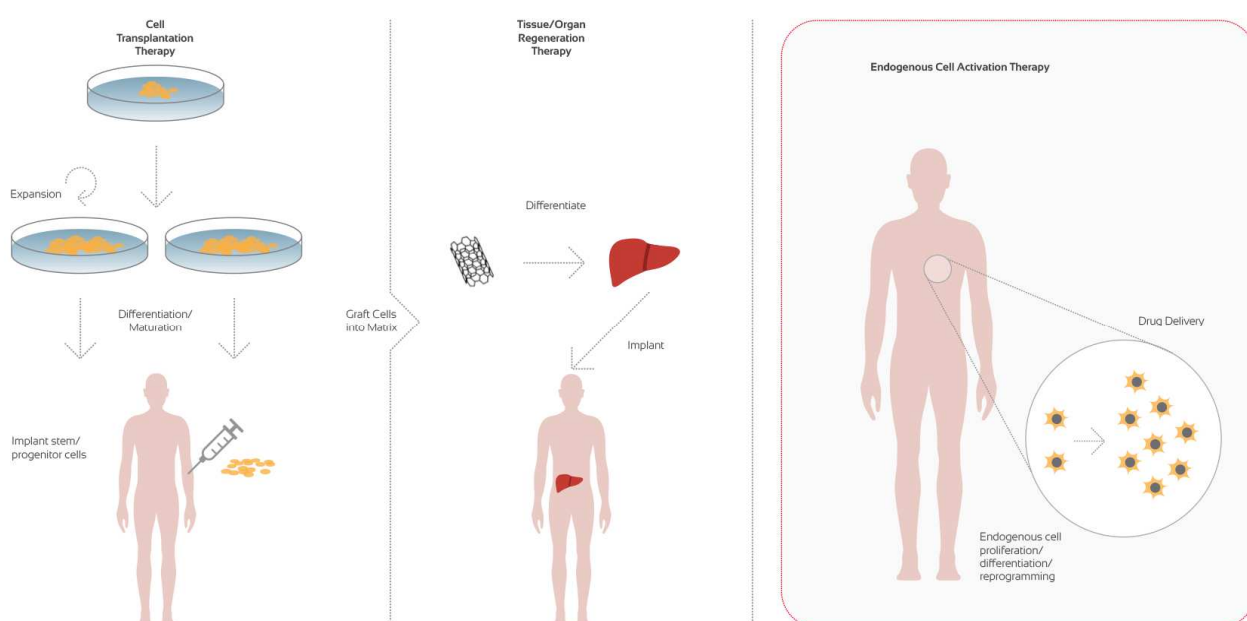


Figure 19. Regenerative medicine approaches: cell transplantation and tissue engineering vs ECAT (Image from <http://www.oxstem.co.uk/stem-cells/oxstem-approach>).

The potential of small molecules to control stem cell fate has been deeply investigated in the literature.^{155–157} ECAT can offer significant advantages over cell therapy, in term of reduced costs and risks, and also for its ability to control cell fate reversibly.^{158,159}

Therefore, the search for drugs that target endogenous stem cell populations *in vivo* to stimulate repair and regeneration processes is actively pursued and represent a powerful application of regenerative medicine, elegantly defined by A. Russell as “regenerative medicinal chemistry”.¹⁵⁸ Recent years have seen the enter in clinical use of the first small molecule regenerative drug acting *in situ* on resident progenitor cells

(eltromboplag, FDA first approved 2008) and many other agents are in preclinical and clinical development, the majority of which targeting the hematopoietic stem cells. Interest in this direction is expanding also for the treatment of other disorders with high unmet medical need, among which neurodegenerative diseases.¹⁵³

In the adult brain, functional neurons and other brain cells are generated from neural stem cells (NSCs) and neural precursor cells (NPCs) in a process called neurogenesis.¹⁶⁰⁻¹⁶²

The discovery of adult neurogenesis has sparked optimism that this endogenous process can be harnessed to repair the injured or diseased brain, offering great promise for treating neurodegenerative diseases.^{163,164}

Over the past five decades, adult neurogenesis and NSCs have been deeply investigated: pioneers works focused on characterizing the process of adult neurogenesis¹⁶⁵⁻¹⁶⁸ were followed by efforts to understand its molecular mechanism and functional significance.^{163,169,170} Current research in the field continues to study NSC regulatory mechanisms in an effort to take advantage of the regenerative capacity of adult NSCs: a deeper understanding of the processes underlying adult neurogenesis and its function in the mammalian brain may lead to new potential therapeutic targets for stimulating neurogenesis and contribute to regenerative approaches for treating neurological diseases.¹⁷¹

1.3 NSCs and neurogenesis in the adult mammalian brain

Adult neurogenesis is the process of generating neurons and glial cells from neural precursors, NSCs and NPCs, and occurs throughout life in restricted brain regions in mammals.^{163,172,173}

NSCs are multipotent stem cells characterized by the properties of self renewal and differentiation. They can generate three cell types: neurons, astrocytes and oligodendrocytes (**Figure 20**).¹⁷⁴

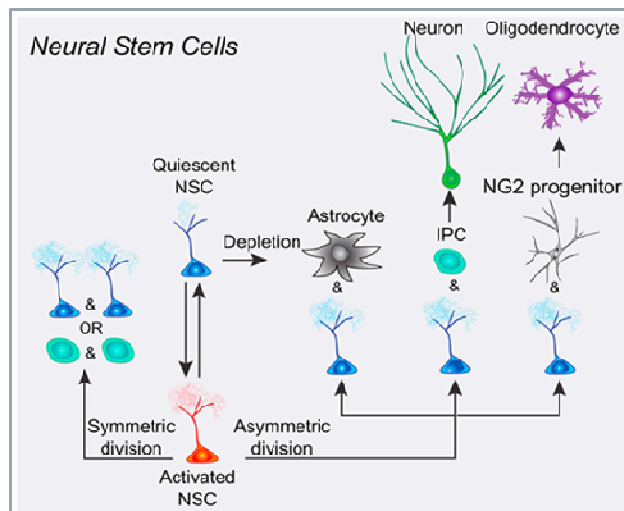


Figure 20. Schematic diagram illustrating potential behavior of adult NSC over its life cycle.

Interestingly, astrocytes release factors that induce neuronal differentiation.¹⁷⁵ NSCs reside within specific environment, or “niche”. The two major niches in the adult mammalian brain are the subventricular zone (SVZ) lining the lateral ventricles and the subgranular zone (SGZ) within the dentate gyrus (DG) of the hippocampus (**Figure 21**).^{163,174}

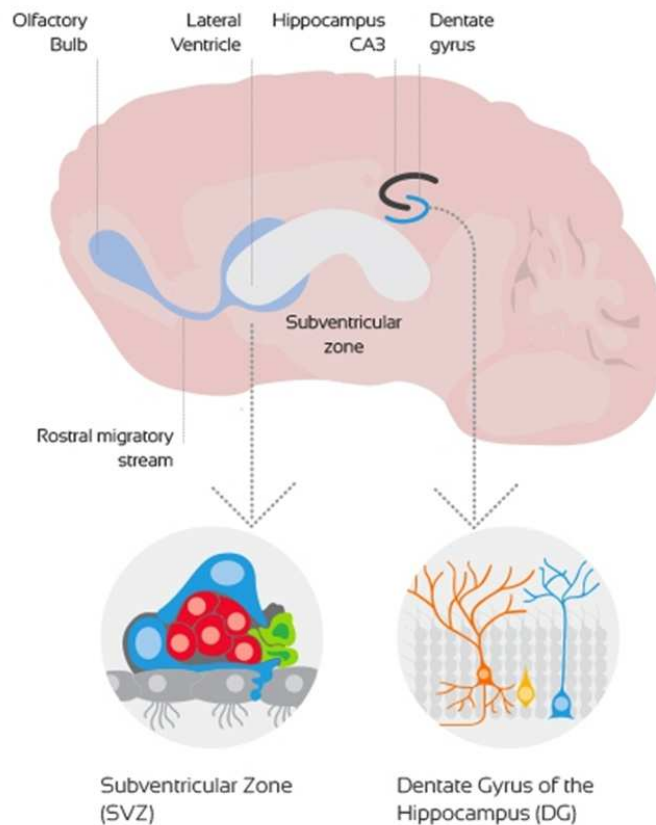


Figure 21. Schematic illustration of the NSCs nests in the brain: SVZ and DG.

Particularly, neurogenesis in the dentate gyrus (DG) of the hippocampus has been robustly demonstrated in adult rodents and has also been observed in sheep, non-human primates, and humans.^{168,176} A comparison study of the two neurogenic niches in humans has been reported.¹⁷⁷

Embryonic stem cell-derived NSCs cultured *in vitro*, in the presence of defined growth factor generate all three brain cell types, however several studies have shown that they are more lineage restricted *in vivo*;¹⁷⁸⁻¹⁸⁰ we can reasonable affirm that adult NSCs are intrinsically tri-potent, but the *in vivo* niche in which they reside may limit the adult NSC potential.

Understand and manipulate the molecular signalling pathways that control NSC features such as activation, fate specification and lineage restriction in the brain is currently under active investigation.

1.3.1 Adult neurogenesis regulation

Adult neurogenesis is a dynamic, finely tuned process regulated by both intrinsic and extrinsic factors (**Figure 22**).^{171,174}

Intrinsic factors are the intracellular regulators: epigenetic modifications, cell cycle regulators, transcription factors. Extrinsic factors are the extracellular component that constitutes the niche microenvironment in which NSCs reside: morphogens (Notch, Sonic Hedgehog, Wnts), hormones, cytokines, neurotrophines, growth factors, neurotransmitters.¹⁶⁹

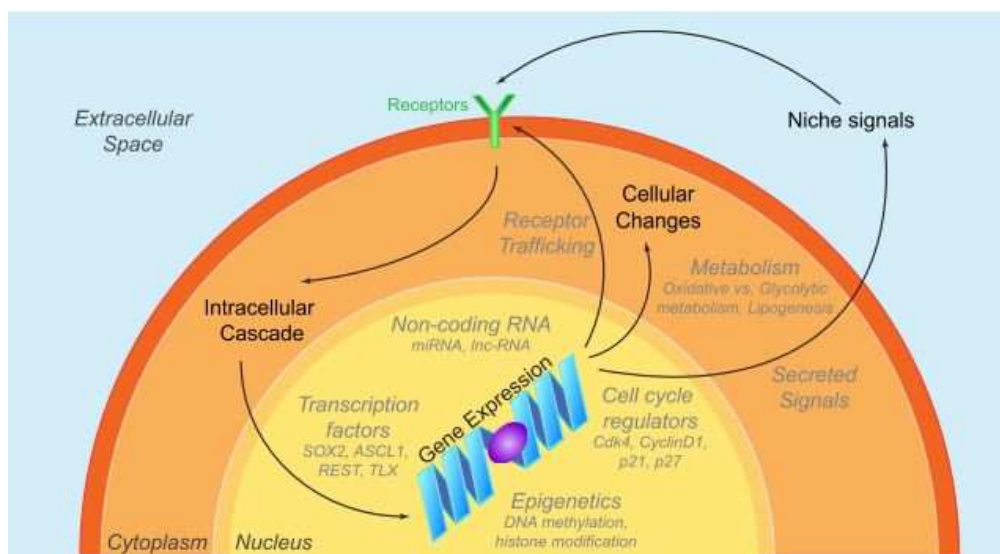


Figure 22. Schematic illustration of intrinsic and extrinsic mechanisms that regulate adult NSCs.¹⁷⁴

Signaling mechanisms, including morphogens, growth and neurotrophic factors, neurotransmitters, transcription factors, epigenetic modulators interact with each other in the regulation of NSCs and adult neurogenesis.¹⁷⁰

Moreover, adult neurogenesis is subject to modulation by various physiological, pathological, and pharmacological stimuli, including exercise, aging, stress and disease.^{169,181}

Finally, it is worth noting that numerous studies have reported alterations in adult neurogenesis that are associated with several neurological and psychiatric disorders, providing a link between adult neurogenesis and human disease.¹⁸²

This provides a further evidence that stimulating neurogenesis represent a promising approach in the search for effective therapies in such diseases.

It is clear that every single phase of adult neurogenesis can be regulated by different stimuli and different stimuli interact with each other, affecting the final outcome of adult neurogenesis. The major challenge is to identify cellular and molecular mechanisms underlying adult neurogenesis regulation.

Importantly, small molecules can stimulate NSC-mediated neurogenesis through one or more mechanisms, including direct targeting stem cells and interference with mediators of the niche.

1.4 Therapeutic application of NSCs: from cell therapy to small molecules

The self-renewing and multipotent properties of NSCs in the adult brain can be exploited to replace damaged neurons with functioning, normal ones according to the principles of regenerative medicine.

Manipulation of NSCs and NPCs *in vitro* for stem cell therapy approaches, involving *ex vivo* stimulation and differentiation followed by transplantation into the patient, have been explored. Clinical trials using NSCs are under investigation for spinal cord injury, macular degeneration and amyotrophic lateral sclerosis (US National Institute of Health clinical trials database). However, clinical applications of NSCs based on cell therapy has shown limited success due to several unsolved problems such as increased risks of tumorigenicity and immune rejection.¹⁸³

On the contrary, the *in situ* modulation of NSCs by small molecules, (ECAT, endogenous cell activation therapy), is considered more clinically acceptable; indeed it would be without immunogenicity problems, and also evades the need for invasive surgery.

Moreover, the identification of small molecules acting on neurogenesis is particularly attractive because they can serve as tools to investigate the mechanisms of neurogenesis.

1.4.1 Small molecules promoting neurogenesis

Several solid lines of evidence show that drugs and drug-like molecules can stimulate NSC-mediated neurogenesis. In **Figure 23** some examples are reported.

All-*trans* retinoic acid (ATRA, **58**) is one of the first molecules known to induce neurogenesis *in vitro*,¹⁸⁴ thus is widely used as reference compound in the search for proneurogenic small molecules.

Antidepressants currently on the market from multiple mechanistic classes, including fluoxetine **59**, imipramine **60**, have been shown to induce neurogenesis *in vitro* and *in vivo*.^{185,186} Even if the association between neurogenesis and antidepressant action remains controversial, they might exert some or all of their effects by promoting neurogenesis.¹⁸⁷

Increased hippocampal neurogenesis was also observed *in vivo* in rat treated with dehydroepiandrosterone (DHEA, **61**),¹⁸⁸ pregnenolone¹⁸⁹ or allopregnanolone **62**.¹⁹⁰

Triazinone molecule **63** showed to enhance neurogenesis in the hippocampus through a multi-target approach of β -secretase and GSK-3 β inhibition.¹⁹¹

Recently an orally active neurogenic small molecule, NSI-189 (**64**), entered in a clinical trial as anti-depressant drug¹⁹² and is progressing Phase 2 efficacy trial (ClinicalTrials.gov, 2016, Identifier: NCT02695472) for treatment of major depression.

In another study, NSI-189 showed to enhance cell proliferation and neurogenesis in a rat model of ischemic stroke.¹⁹³ Until now, the mechanism of action mediating the neurogenic effects of NSI-189 remain elusive.

Other examples of drug-like molecules promoting neurogenesis have been described.^{153,154}

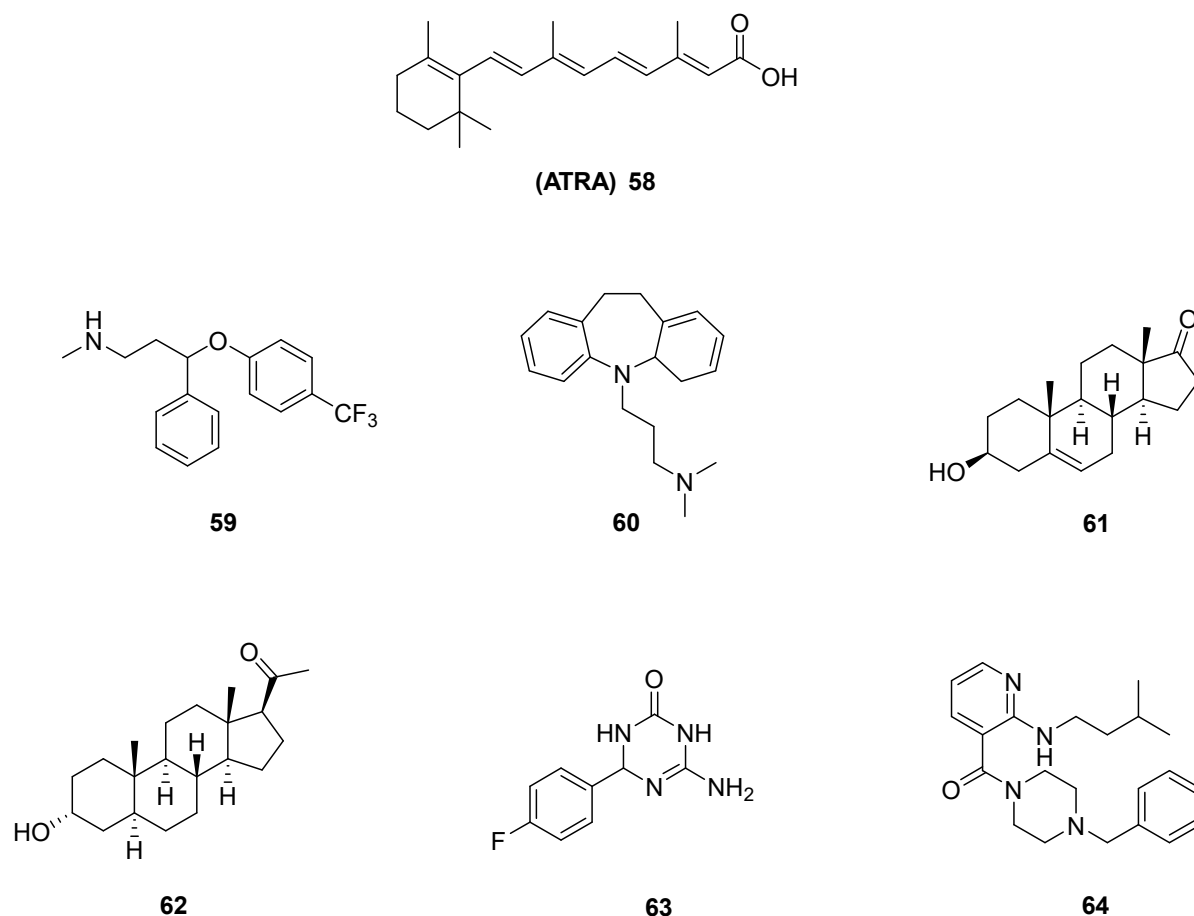


Figure 23. ATRA (**58**) and examples of recently discovered proneurogenic small molecules **59-64**.

2. Aim of the work

In this context, one of the goals of Professor Angela Russell's Group is to find proneurogenic compounds and to understand the mechanism through which they stimulate neurogenesis.

For this purpose, through a collaboration with the group of Professor Francis Szele, they have developed screening models able to identify new small molecules promoting neurogenesis *in vitro* and *in vivo*.

In a first screening, 1500 compounds (Mix of GSK-3 β inhibitors and structurally diverse drug-like molecules) were tested *in vitro* on murine-derived NSCs to assess the effect on neurogenesis via immunohistochemistry (**Figure 24**). The percentage of neurons against the total number of nuclei was calculated. (See Appendix B)

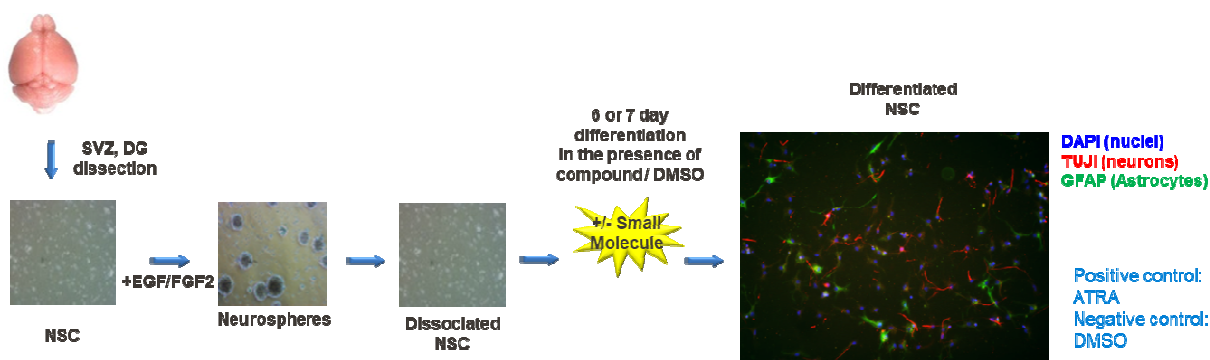


Figure 24. Initial screening carried out by Dr. Julie Davies (DPAG, University of Oxford).

From the initial screening, a number of compounds resulted active (*hit identification*), thus following a common drug discovery approach (**Figure 25**), they were resynthesized and retested in *in vitro* assays to confirm biological activity, according to the hit validation process. Some of the validated hit are progressing the *hit to lead optimisation*, to improve pharmacokinetic profile and to explore structure-activity relationships (SAR). (**Figure 25**)

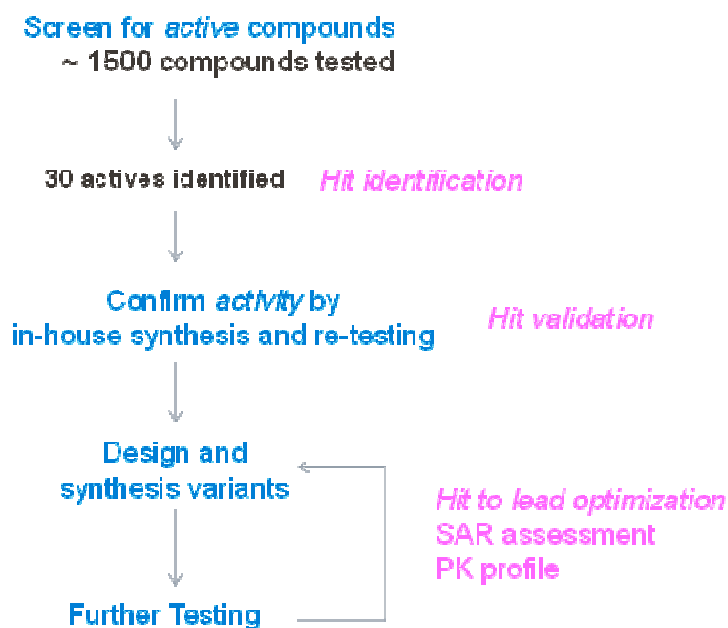


Figure 25. Drug discovery process in the search for proneurogenic compounds.

Among the first validated hits, OX02672 (**65**) (**Figure 26a**) (The structure of OX02672 can not be disclosed yet. Indeed, the work is still in progress and it is going to be submitted for patenting) showed a good dose-dependent increase in neurogenesis in both the DG-derived NSCs and SVZ-derived NSCs (**Figure 26b**). Pharmacokinetics (PK) studies and *in vivo* efficacy studies (wild type mice) were also performed. From preliminary data, compound OX02672 (**65**) showed a significant increase of neurogenesis *in vivo* in the DG. (**Figure 26c**).

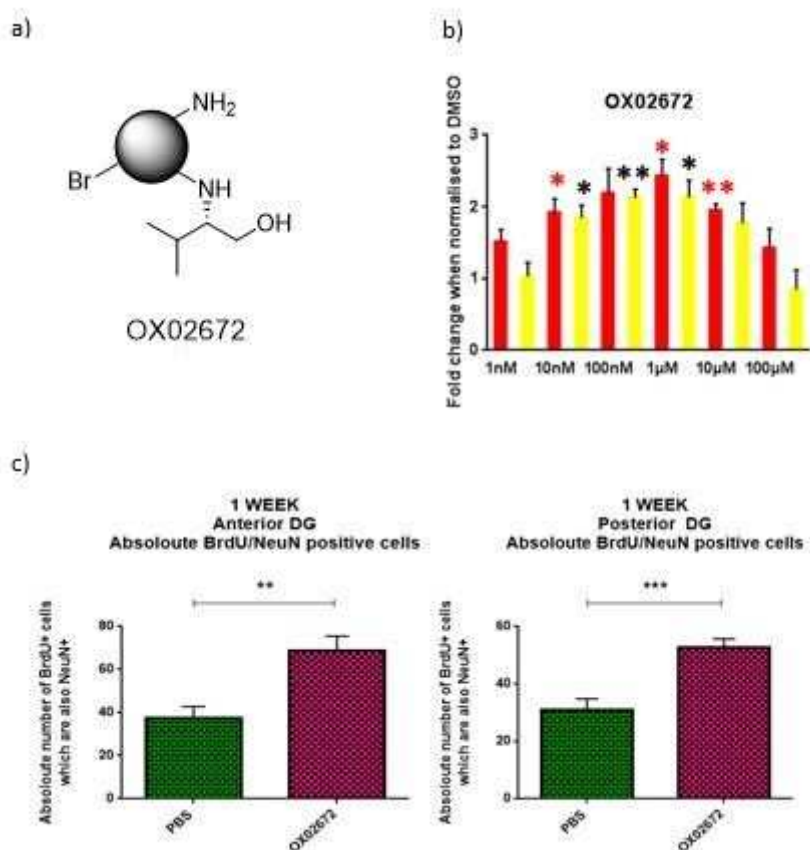


Figure 26. a) OX02672 (**65**) Masked structure. b) Dose dependent increases in neurogenesis from NSC's isolated from DG and SVZ. (Asterisks indicate significance when compared to DMSO. *P< 0.05. **P< 0.01). c) Quantification of BrdU/NeuN positive cells in the DG. Tests were carried out by Dr Julie Davies (DPAG, University of Oxford). For more details, see Appendix B.

While this compound requires further optimisation to be considered as a lead compound, its good activity *in vitro* and *in vivo* made it a useful tool compound for chemical biology investigations.

Since its proneurogenic activity was discovered from a NSC-based phenotypic assay, OX02672 acts through, as yet, unknown mechanism. Therefore, it represents a useful tool to investigate pathways involved in neurogenesis and NSC specification.

2.1 Development of OX02672 as fluorescent and affinity probe for chemical proteomics

On these premises, my work aims to use a chemical biology approach to develop OX02672 into affinity and fluorescent probe to be used in chemical proteomics to assess its molecular interactions and localization in NSCs.

Chemical proteomics uses chemically synthesized molecular probes usually coupled with high-resolution detection methods such as mass spectroscopy (MS) for the study of small molecule–protein interactions.¹⁹⁴ The Activity-Based Protein Profiling (ABPP) approach in particular has been successfully used for target identification of drugs and other bioactive small molecules.^{195–197} Chemical probes for ABPP (activity-based probes, ABP) are generally composed of a reactive group (the bioactive compound) for binding or modifying the target proteins and a reporter tag for the identification and purification of binding proteins. (**Figure 27a**)

There are two types of reporter: (i) fluorophores, such as rhodamine, for visualization by in-gel fluorescence coupled with SDS-PAGE to visualize binding proteins; (ii) affinity tags, such as biotin, for both western blot analysis and avidin enrichment prior to mass-spectrometry (MS)-based identification.¹⁹⁸

Classical ABPP methods (**Figure 27b**) present some limitations: the conjugation with the tag can significantly alter the structure of the original bioactive small molecule; most ABP have limited cell permeability due to their bulky reporter tag; ABPP experiments are conducted almost exclusively with cell and tissue homogenates.

It would be an ideal strategy one that can faithfully recapitulate protein-small molecule interactions *in situ* (e.g. in living cells).^{199,200}

Among *in situ* methods for cell-based proteome profiling of small molecules, “click chemistry ABPP” (**Figure 27c**) is based on “clickable” chemical probes: the original bioactive compound is modified through the introduction of a chemically ‘tractable’ tag; the tag must minimally disrupt protein–ligand interaction *in situ*, and provide a handle for subsequent *in vitro* protein enrichment and other proteomic applications. A terminal alkyne is a tag-of-choice because it is small and can be easily conjugated with high efficiency with azide-containing reporters through a click chemistry reaction, such as the copper-catalyzed azide–alkyne 1,3-dipolar cycloaddition (CuAAC).^{201–204}

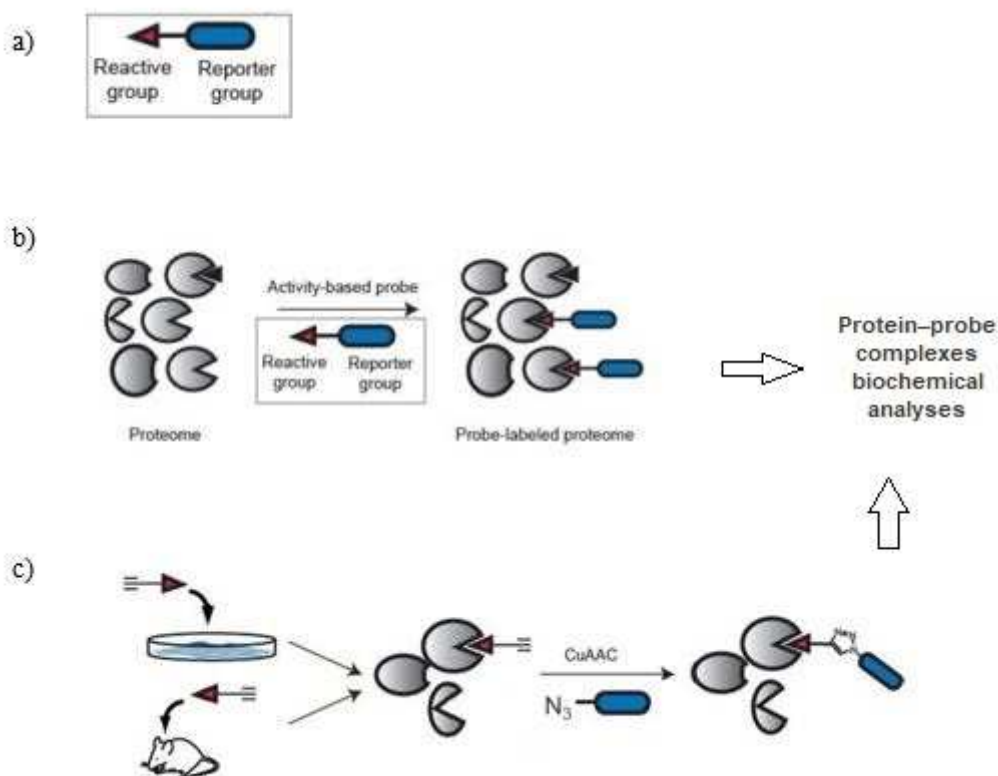


Figure 27. a) Activity based probe general structure (ABP); b) Classical ABPP; c) Click chemistry ABPP. (Adapted from Martell *et al.*²⁰¹)

Alkyne-tagged probes (**Figure 27c**) can be considered “in-cell small molecule clickable probes”: they first interact with the protein target(s) in cells or *in vivo*, then the bioorthogonal reaction CuAAC can be performed in living cells or *ex vivo*, allowing the *in situ* attachment of the reporter. Ghosh and Jones reviewed the use of small molecule imaging probes that rely on a click handle to which a fluorescent dye can be appended intracellularly.²⁰⁵

2.2 Chemistry

Following the click ABPP approach, cell permeable OX02672 probes containing a terminal alkyne tag have been designed. Then, CuAAC of some of the synthesized probes was performed, with simple azide and with a fluorescent dye, to prove the good reactivity of the new probes in the click reaction.

While the synthetic transformations can be discussed, the structures of the new derivatives can not be disclosed yet. Indeed, the work is still in progress and it is going to be submitted for patenting.

The first thing to consider in the design of a probe is the SAR assessment: thus, in order to identify where a tag could be appended while retaining the activity, a number of analogues of **65** modifying the 1, 2 and 3 positions were synthesized and submitted to biological evaluation by some member of the group.

In particular, the present work focused on the synthesis of some analogues (**66-68**) of **65** to expand SAR on the position 1, and mostly on the synthesis of the alkyne-tagged analogues **69-74** for probes development, modifying all the three positions, since the SAR of **65** were not yet determined. (**Figure 28**)

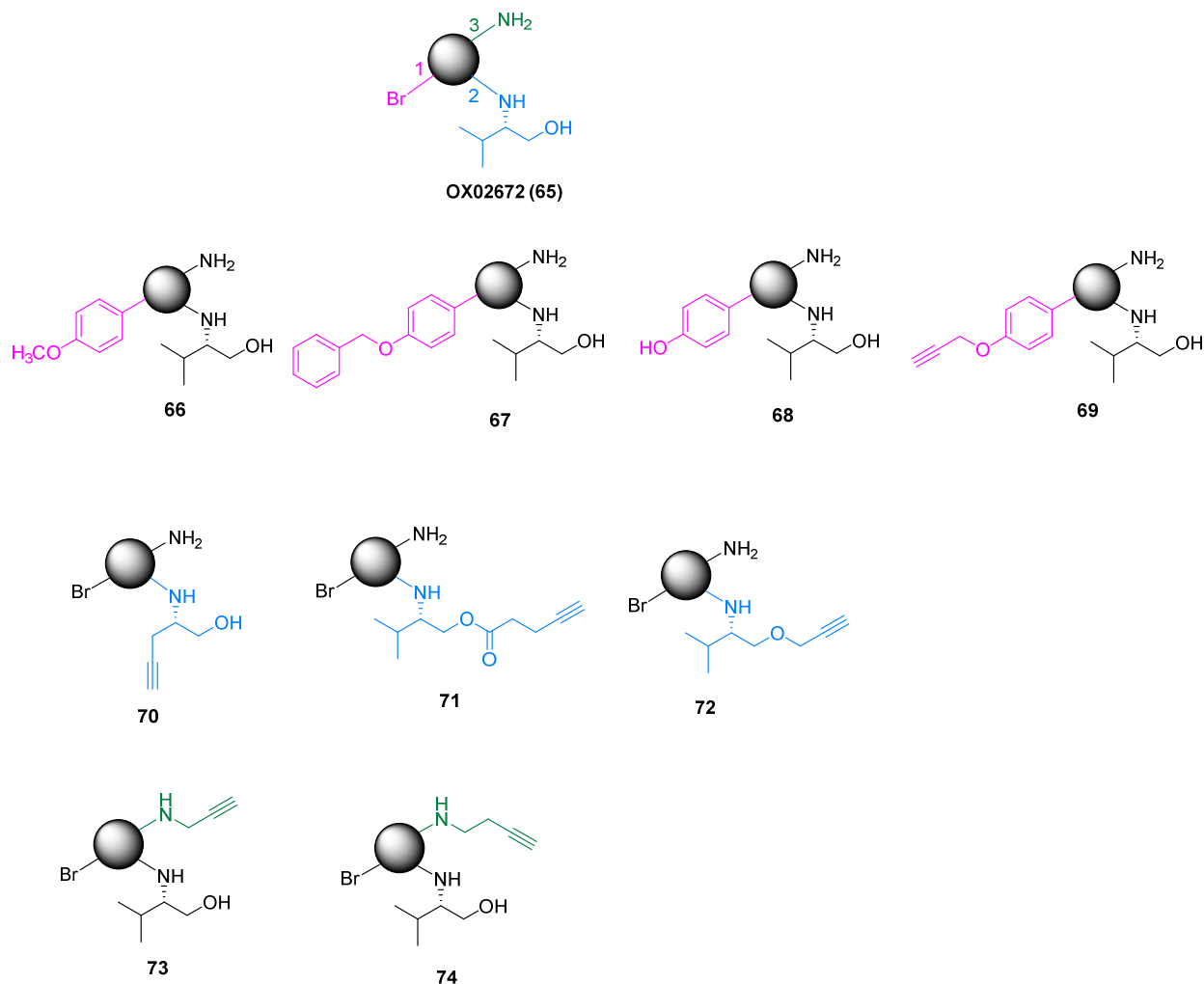
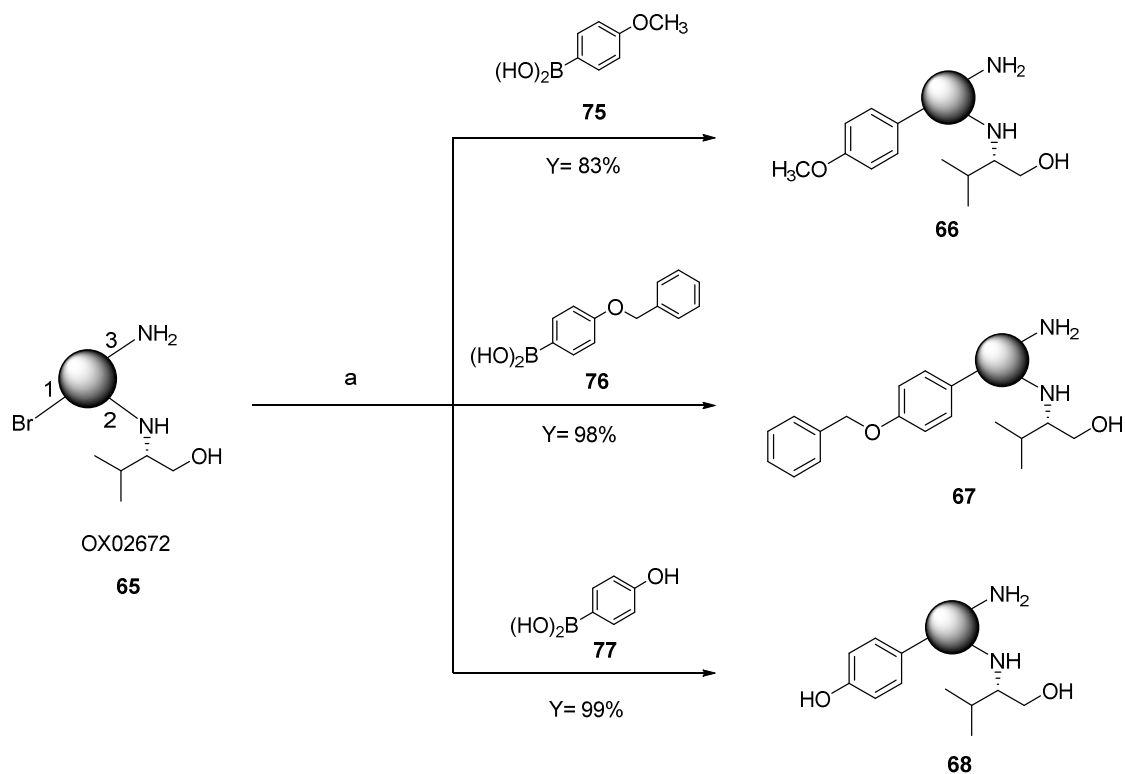


Figure 28. New analogues **66-68** for SAR studies and alkyne tagged derivatives **69-74** for probes development.

The synthesis of analogues **66-68** is shown in **Scheme 12**. Suzuki coupling was performed on compound **65** with three different boronic acids **75-77** to obtain methoxyphenyl- **66**, benzyloxyphenyl- **67** and phenol- **68** derivatives, respectively, with very good yields.

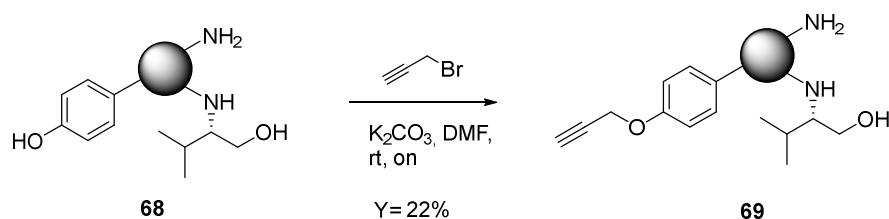
Scheme 12. Synthesis of derivatives **66-68**



Reagents and conditions: a) K_2CO_3 , $Pd(dppf)_2Cl_2$, Toluene/EtOH 2:1, 90 °C, 24 h.

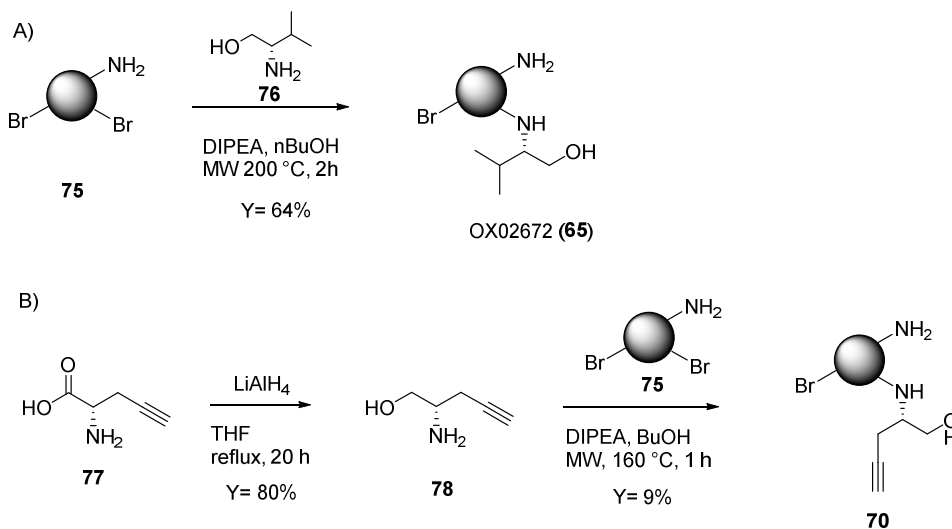
Then, derivative **68** through alkylation with propargyl bromide, using K_2CO_3 as base, gave the alkyne derivative **69** as shown in **Scheme 13**.

Scheme 13. Synthesis alkyne derivative **69**



Compound **70** (**Scheme 14B**) was obtained through microwave-assisted regioselective nucleophilic substitution starting from the dibromoderivative **75** and the synthesized amine **78**, in analogy to the synthesis of the parent compound **65**, showed in **Scheme 14A**. The amino alcohol **78** was obtained from the commercially available chiral amino acid **77** through reduction of the acid function with LiAlH_4 .

Scheme 14. A) synthesis of OX02672 (**65**) and **(B)** Synthesis of derivative **70**

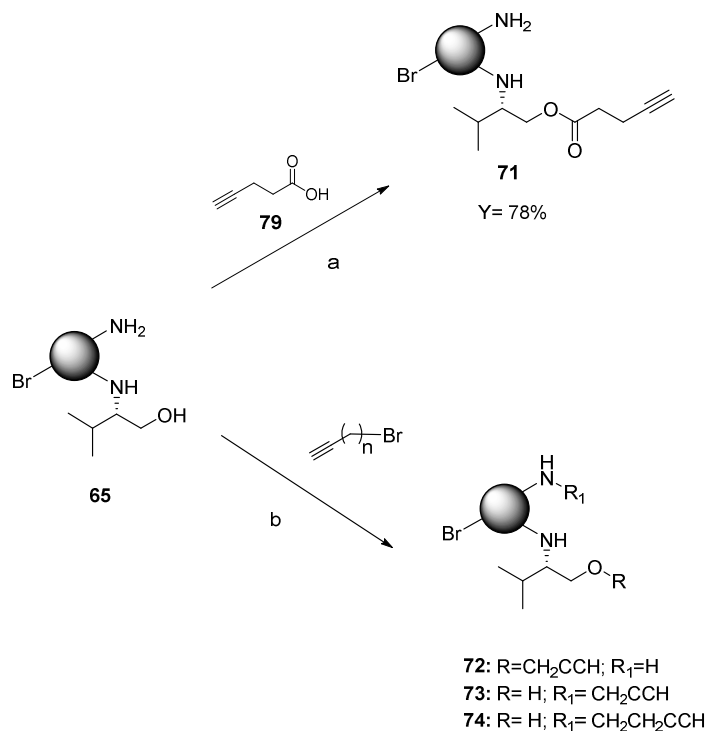


Synthesis of derivatives **71-74** is shown in **Scheme 15**. Through coupling reaction of **65** with commercial acid **79** in presence of EDC and DMAP, ester derivative **71** was obtained in very good yield.

To obtain the alkylated derivative **72-74**, alkylation reactions were performed with propargyl bromide and 4-bromo-1-butyne, KOH as base and DMF as solvent, varying the reaction condition as described in **Table 3**.

In presence of 1.5 eq of propargyl bromide and 1 eq of base at 35 °C, the alkylation of **65** occurred on the alcohol group in position 2 to give compound **72** (entry 1). Increasing the equivalent amounts of propargyl bromide and base, and the temperature, a mixture of alkylated derivatives **72** and **73** (derivative alkylated on the amine in position 3) was obtained (entry 2). Alkylation with 4-bromo-1-butyne occurred with excess of reagents at higher temperature to give **74**, the derivative alkylated on the amine in position 3 (entry 3).

Scheme 15. Synthesis alkyne analogues **71-74**



Reagents and conditions: a) EDC, DMAP, THF, rt, 12 h; b) KOH, DMF, see table 1 for conditions.

Table 3. Alkylation reaction conditions to obtain compounds **72-74**

entry	n	Bromide eq	KOH eq	T	t	Product (Y)
1	1	1.5	1	35 °C	12h	72 (13%)
2	1	3	3	60 °C	24h	72 (10%) + 73 (10%)
3	2	3	3	110 °C	20h	74 (10%)

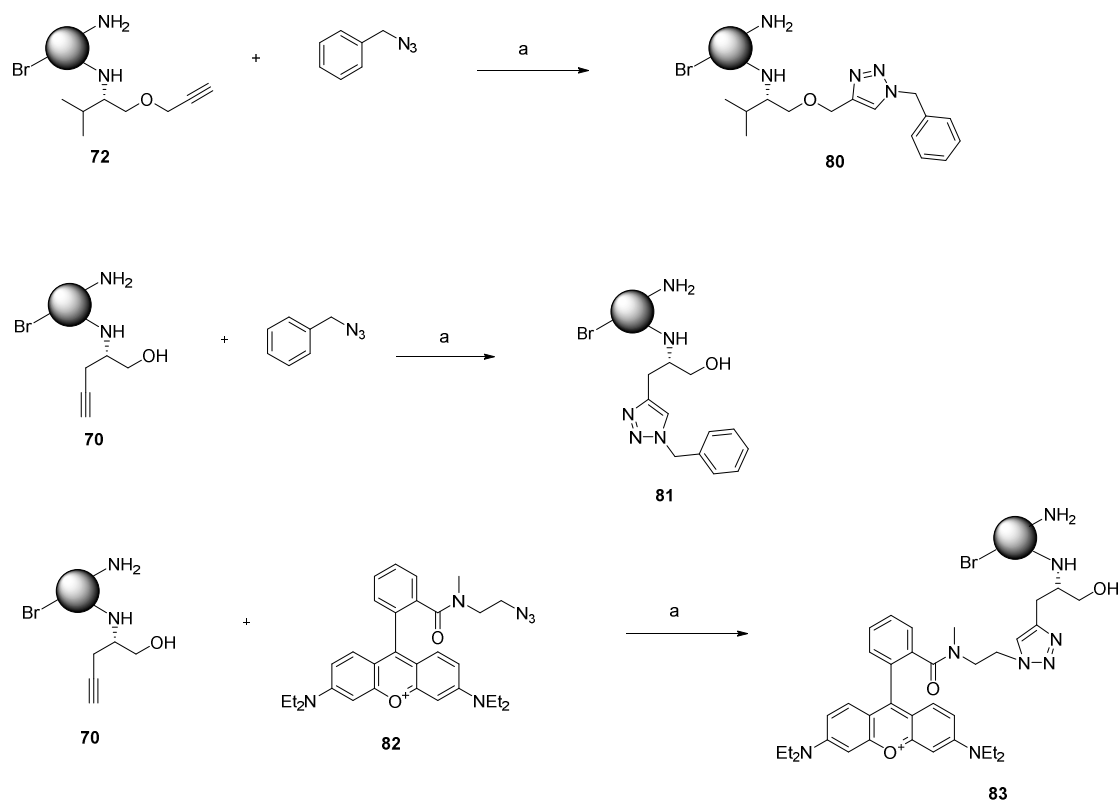
All the new derivatives were characterised with ¹H-NMR, ¹³C-NMR, IR spectroscopy and HRMS spectrometry; COSY, HSQC, HMBC and NOESY experiments were also performed when needed.

All the new derivatives were submitted to the biological evaluation to assess their proneurogenic activity, in order to gain information on the SAR of **65** and to decide which alkyne derivatives can progress in the probe development.

Finally, click reaction on some alkyne-probes was performed with simple azide and with a fluorescent dye (**Scheme 16**) to check if the compounds have a good reactivity in the CuAAC.

Not knowing yet which derivative maintains the bioactivity of the parent compound, we chose derivatives **72** and **70** to perform CuAAC with the commercial benzyl azide (1 eq) to assess the reaction conditions, obtaining the triazoles derivatives **80** and **81**. Then, the derivative **70** was chosen as the structurally closest analogue to the parent compound to perform the click reaction with the rhodamine azide derivative **82** obtaining the potentially useful fluorescent probe **83**, which was characterised by $^1\text{H-NMR}$, $^{13}\text{C-NMR}$ and HRMS.

Scheme 16. Click chemistry reaction



Reagents and conditions: a) CuSO₄ (0.2 eq), Na ascorbate (0.4 eq), H₂O / tBuOH 1:1, rt, 1-2 h.

3. Conclusions

In my six-month placement carried out under the supervision of Professor Angela Russell at Department of Chemistry (University of Oxford) my work aimed, through a chemical biology approach, on the development of small molecules as affinity and fluorescent probes to detect new pathways involved in neurogenesis and Neural Stem Cell (NSC) fate.

A series of different substituted and alkyne-tagged derivatives of the recently discovered proneurogenic compound OX02672 (**65**) have been synthesized and submitted for the biological evaluation.

Some of the alkyne-tagged analogs were «clicked» with a simple azide and a rhodamine-azide-derivative through click chemistry, proving this strategy can be useful for the further development of **65** into fluorescent probe.

Moreover, the alkyne-tagged derivatives which will show to maintain the bioactivity of the parent compound could be developed as diverse fluorescent probes (using different fluorophores) and also as affinity probes by bioconjugation with a biotin-azide-derivative in the click reaction. Then they can be used in chemical proteomics and other target identification *in situ* methods.

These studies may serve to assess the localization in NSCs and their progeny and to identify the target protein(s). This in turn may help to understand the mechanism of action of this proneurogenic compound and to gain a better knowledge of the signaling pathways that control adult neurogenesis, finally supporting the development of drugs that stimulate *de novo* neurogenesis for the treatment of central nervous system diseases.

Part III

DESIGN AND SYNTHESIS OF TACRINE-RESVERATROL FUSED HYBRIDS AS MULTI-TARGET-DIRECTED LIGANDS AGAINST ALZHEIMER'S DISEASE

1.Introduction

1.1 Project overview

This last section describes a side project carried out in collaboration with the groups of Professor Maria Laura Bolognesi and Professor Jan Korabecný of Prague University, aimed to the identification of a new series of multi-target-directed ligands (MTDLs) against Alzheimer's disease (AD).²⁰⁶

1.2 Multi-target drug discovery in Alzheimer disease

One of the most followed approaches in the central nervous system (CNS) therapeutic area is multi-target drug discovery, especially in the search for new drugs against AD.²⁰⁷ This is because multi-target-directed ligands (MTDLs) could more adequately address the complexity of this pathological condition, since they have the potential to promote a number of goals including (i) an inherently higher adequateness to confront the complex AD pathogenesis; (ii) a larger therapeutic window; and (iii) a simplified therapeutic regimen.²⁰⁸

Several promising anti-AD MTDLs have been reported,^{209,210} however, no one has progressed to clinical development.²¹¹ Thus, there is still a need for novel MTDLs potential useful as anti-AD drug candidates.

Molecular hybridization has been the most widely applied design strategy towards new MTDLs for AD.²¹² In these context, acetylcholinesterase (AChE) inhibitor tacrine, (**84**, **Figure 29**) has been used as starting scaffold to obtain molecular hybrids with improved biological profiles,²¹³ particularly its derivatives, the more potent 6-chlorotacrine **85**²¹⁴ and the less hepatotoxic 7-methoxytacrine **86**.²¹⁵

A wide set of tacrine-based hybrids reported in the literature incorporate a fragment derived or inspired by a natural product.²¹⁶ Indeed, natural products have intrinsic multi-target profile, being evolutionarily selected and biologically pre-validated, therefore they are considered suitable starting points for the development of MTDLs against

AD.²¹⁷ Among the natural products with therapeutic potential in the field of neurodegenerative diseases, resveratrol (**87**, **Figure 29**), a polyphenol mainly found in grapes and red wine, has attracted great attention for its beneficial effects due to its antioxidant and anti-inflammatory properties.²¹⁸ Notably, a recent clinical trial aimed to evaluate the impact of resveratrol treatment in patients with mild to moderate AD.²¹⁹

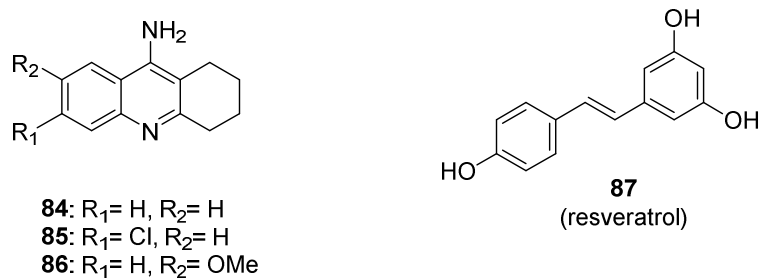


Figure 29. Tacrine **84**, tacrin derivatives **85-86** and resveratrol **87** structures.

2. Aim of the work

On these basis, with the aim to develop a new series of anti-AD MTDLs, the anticholinesterase properties of **84-86** were combined with the antioxidant, immunomodulatory and neuroprotective framework of resveratrol **87**, through the design of *fused* hybrids **88-95** (**Figure 30**). We reasoned that this structural hybridization might have positive effects in terms of neuroinflammation and safety. From toxicity point of view, resveratrol is known to be safe in humans²¹⁹ and, importantly, it has demonstrated beneficial effects in animal models of hepatic insult.²²⁰ In addition, the notion that resveratrol **87** might directly halt amyloid aggregation²²¹ potentially expands the therapeutic profile of the new hybrids derivatives.

Among the molecular hybridization approaches, we choose the *fusing* strategy because in principle, a *fused* hybrid should possess improved drug-like features (such as decreased size and complexity) compared to a *linked* one.²²² This aspect is of crucial importance in the design of hybrids directed to the CNS, where more stringent physiochemical properties are requested, particularly the hybrid must to permeate blood-brain-barrier to exert its effect.²²³

Toward the goal of a maximal structural overlap, we turned our attention to the 4'-amino derivative of resveratrol **96**, which has been reported to exert anti-aggregating, antioxidant and neuroprotective effects in AD cellular models.²²⁴ This allowed us to fuse the two structures through the common amino group (i.e. the 9-NH₂ of **84-86** and the 4'-NH₂ of **96**) (**Figure 30**).

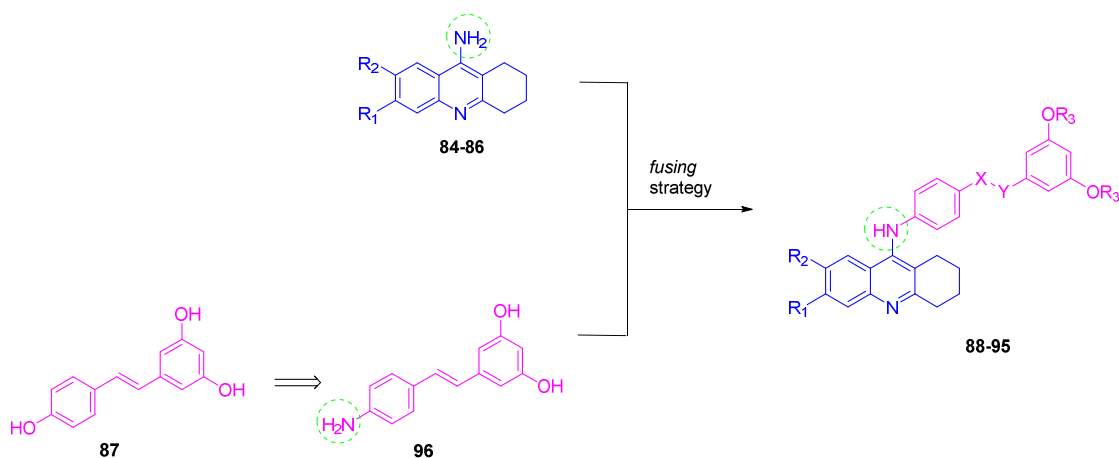
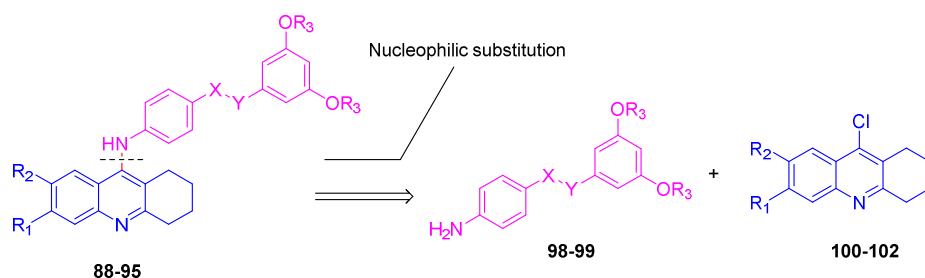


Figure 30. Design strategy to tacrin-resveratrol fused hybrids. (For structures see **Scheme 18**).

A large number of anti-AD tacrine-based^{212,213,225–227} and resveratrol-based^{228–230} hybrids have been reported. Notably, tacrine-resveratrol *linked* hybrids (featuring an alkoxy linker) have been patented as useful agents against neurodegenerative diseases,²³¹ but, to the best of our knowledge, there is no example of *fused* tacrine-resveratrol hybrids, that is the aim of the present project.

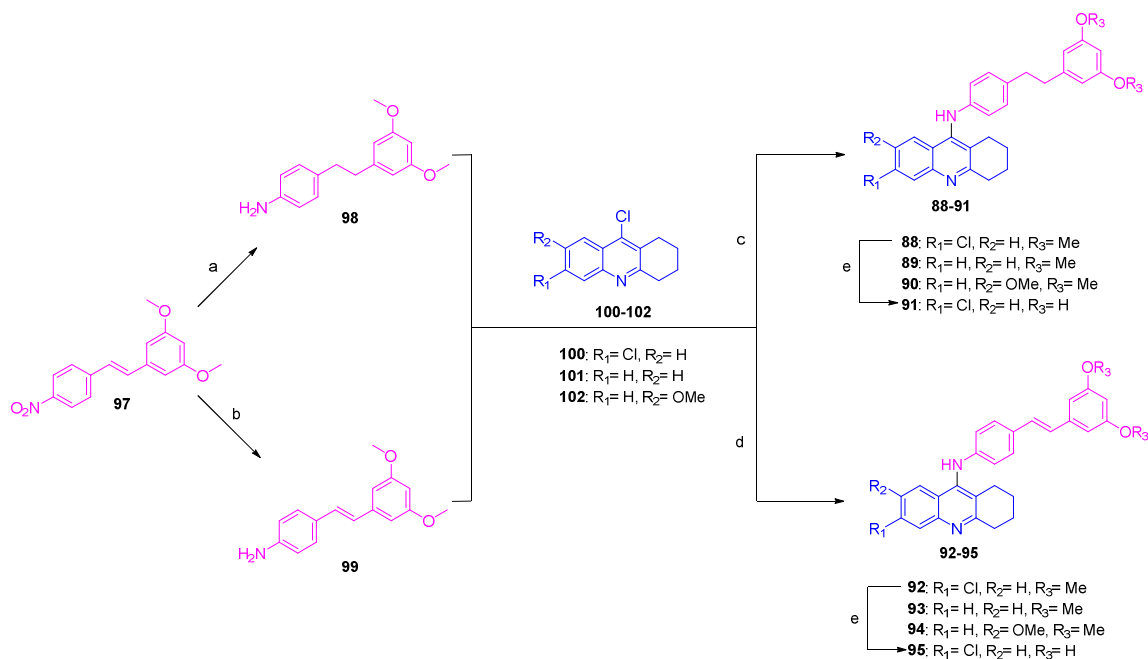
Retrosynthetic analysis suggested us to exploit a nucleophilic substitution between resveratrol amino derivatives (**98-99**) and 9-chlorotacrine derivatives (**100-102**) to obtain final tacrine-resveratrol fused hybrids **88-95** (**Scheme 18**).

Scheme 17. General retrosynthetic strategy. (For structures see **Scheme 18**).



Synthesis of hybrid compounds **88-95** is describe in **Scheme 22**. The key step consisted of a coupling between the amino-stilbene **99** or its corresponding dihydro derivative **98** and the appropriate 9-chlorotacrines **100-102**. The reaction, carried out in the presence of phenol under microwave irradiation and solvent free conditions, afforded the desired hybrid methoxylated compounds **88-90** and **92-94** in moderate to good yields (32-52%). The dihydroxy derivatives **91** and **95** were obtained, in 93% and 31% yield respectively, by demethylation of the corresponding dimethoxy hybrids **88** and **92** with boron tribromide at -78 °C.

Scheme 18. Synthesis of tacrine-resveratrol hybrids **88-95**



a) full H₂ mode, 10% Pd/C, EtOAc, r.t., 1 bar, flow rate 1.0 mL/min; b) EtOAc, SnCl₂ · 2H₂O, reflux, 1 h; c) phenol, MW, 150W, 120 °C, 120 min; d) phenol, MW, 150W, 120 °C, 60 min e) anhydrous DCM, BBr₃, -78 °C to rt, 20h.

Amino derivatives **98-99** were prepared starting from the common intermediate trans-nitro-stilbene derivative **97** as previously reported.^{232,233} Amino-stilbene **99**^{232,233} was obtained by selective reduction of the nitro group with Tin (II) chloride, whereas the corresponding dihydro derivative **98**²³⁴ was obtained by catalytic hydrogenation in continuous-flow reactor that allowed simultaneous reductions of the nitro group and the ethylene bridge. The 9-chlorotacrine derivatives **100-102** has been synthesized as previously described.^{235,236}

3. Biological evaluation and discussion of results

Biological evaluation of newly synthesized hybrids compounds was carried out by groups of Professors Manuela Bartolini, Barbara Monti (UniBO), and the group of Professor Jan Korabecny of Charles University in Prague. The biological experiment protocols and the in-depth analysis of biological results have been reported,²⁰⁶ thus only some relevant aspects are described in this paragraph.

To evaluate the potential interest as MTDLs against Alzheimer disease, they were first tested for cholinesterase inhibition and derivatives **88**, **89**, **91** and **95** showed significant inhibitory activity with IC₅₀ values from 0.8 to 14.2 μM (**Table 4**). The majority of the active compounds is part of the subset in which the stilbene double bond is reduced (**88**, **89** and **91**). Particularly, **88** is the most potent inhibitor of the series, displaying an IC₅₀ of 0.8 μM, which is comparable to that of reference drug tacrine **84** (IC₅₀ = 0.5 μM).²⁰⁶ Compound **95** is the only resulted active among the hybrids featuring the double bond of the stilbene moiety (**92-95**) with an IC₅₀ value of 8.8 μM. However, it should be noted that **95**, together with **88** and **91**, bears a 6-chlorotacrine fragment, confirming the essential role of this fragment in AChE recognition.

Since the potential of tacrin-based hybrids to act as inhibitors of amyloid aggregation has been widely recognised,^{213,225} as well as the antiaggregating properties of resveratrol,²²¹ **88-95** were tested for their ability to inhibit Aβ self-aggregation.²⁰⁶ Interestingly, the most active compounds result **91** and **95**, which showed slightly improved Aβ aggregation inhibitory profile compared to resveratrol **87** (**Table 4**).

Table 4. Inhibition of human AChE and Aβ Self-Aggregation of derivatives **88-95** and reference compounds **84-87**.

Compound	IC ₅₀ ± SEM (μM) for Human AChE	IC ₅₀ ± SEM (μM) for Human BChE	Aβ ₄₂ self-aggregation % Inhibition [I] = 50 μM
88	0.8 ± 0.05	n.a.	17.6 ± 1.6
89	14.2 ± 2.9	n.a.	n.d.
90	n.a.	n.a.	n.d.

91	1.3 ± 0.1	n.a.	37.3 ± 4.1
92	n.a.	n.a.	21.6 ± 4.9
93	n.a.	n.a.	n.d.
94	n.a.	n.a.	n.d.
95	8.8 ± 0.4	n.a.	31.2 ± 9.0
84	0.5 ± 0.1 ^a	0.023 ± 3 ^a	<5
85	0.007 ± 0.02 ^a	0.85 ± 30.6 ^a	<5
86	10.5 ± 2 ^a	21 ± 3000 ^a	n.d.
87	n.a. ^b	n.a. ^b	30.0 ± 8.7

n.a.- not active, no enzyme inhibition at compound's concentration of 10 μM.

n.d. - not determined.

^a Data taken from Nepovimova, E. et al.²²⁷

^b No inhibition observed in tested concentration up to 100 μM.

Compounds were then evaluated for neurotoxic effects on primary neurons (**Figure 31**)²⁰⁶ and compound **95** showed no clear neurotoxicity, thus it was further investigated and tested in a cell model of AD neuroinflammation, where it showed anti-inflammatory and immune-modulatory properties (data not shown).²⁰⁶

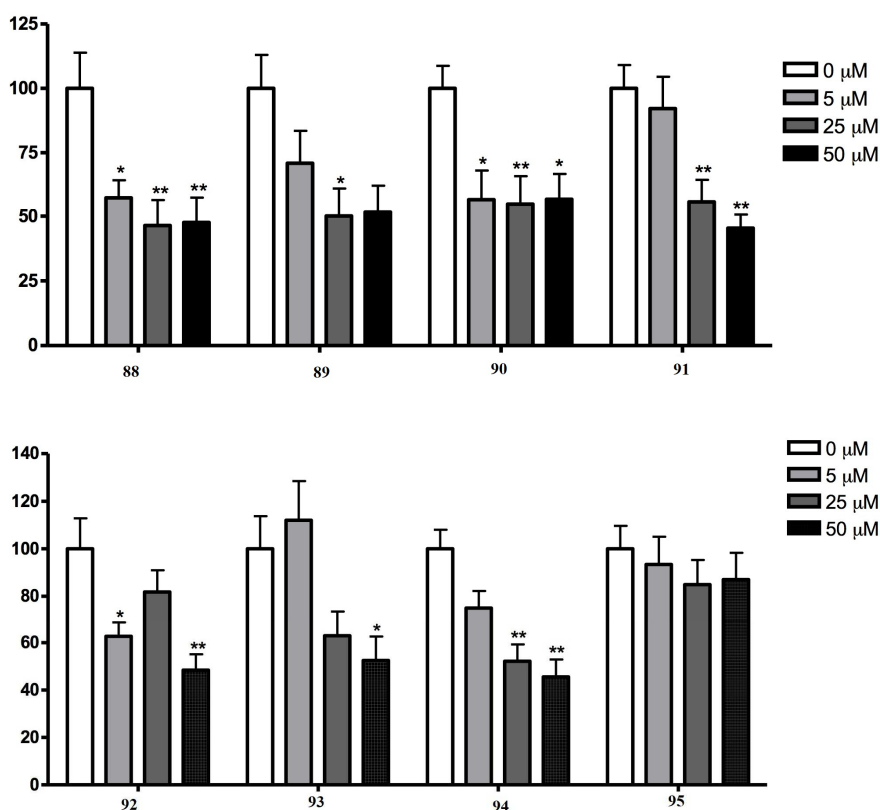


Figure 31. Neurotoxicity of **88-95** on primary rat cerebellar granule neurons (CGNs) after 24 h treatment. Results are expressed as percentage of controls and are the mean \pm SE of four different experiments run at least in quadruplicate.²⁰⁶

Compounds were then evaluated for the antioxidant activity and hepatotoxicity (data not shown). Only compound **88** showed reasonable antioxidant activity, albeit lower than that of resveratrol.²⁰⁶

The assessment of hepatotoxicity would be of critical importance for evaluating the drug-likeness of the newly synthesized hybrids, since the serious hepatotoxicity of **84** limited its clinical use.²²⁵ We hypothesized a lower hepatotoxicity for the hybrids compounds on the basis of the hepatoprotective properties of resveratrol **87**,²³⁷ but contrary to our expectations all the compounds displayed significant hepatotoxic effects.²⁰⁶

Importantly, preliminary evaluation through a BBB (blood-brain barrier) predictor server indicated high permeation properties for this series of compounds.²⁰⁶

4. Conclusions

The side project (Part III) was based on the rational design and synthesis of a new series of multi-target-directed ligands (MTDLs) against Alzheimer's disease (AD). A new series of *fused* tacrin-resveratrol hybrids that showed interesting multi-target profile against target proteins involved in AD pathogenesis has been identified. The most interesting compounds (**88**, **91**, **92** and **95**) inhibited human acetylcholinesterase at micromolar concentrations and effectively modulated A β self-aggregation in vitro (**91** and **95**). In addition, **95** showed anti-inflammatory and immuno-modulatory properties in AD cell models. However, a general hepatotoxicity is evident for all the derivatives, probably due to the presence of tacrin fragment. In this regard, when dealing with a drug discovery project one must be aware that since is not possible to *a priori* establish if a new hybrid (that is a new chemotype) can be toxic or not, toxicity issues should be addressed early in the discovery phase.

5. Experimental section

General methods

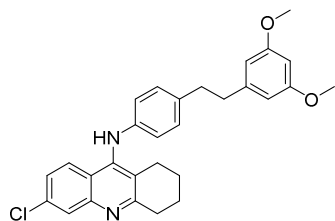
Reaction progress was monitored by TLC on pre-coated silica gel plates (Kieselgel 60 F254, Merck) and visualized by UV254 light. Flash column chromatography was performed on silica gel (particle size 40-63 μM , Merck). If required, solvents were distilled prior to use. All reagents were obtained from commercial sources and used without further purification. When stated, reactions were carried out under an inert atmosphere. Reactions involving microwave irradiation were performed using a microwave synthesis system (CEM Discover® SP, 2.45 GHz, maximum power 300 W), equipped with infrared temperature measurement. Catalytic hydrogenation was performed on H-Cube® Continuous-flow Hydrogenation Reactor (H-Cube, ThalesNano Nanotechnology, Budapest, Hungary). Compounds were named relying on the naming algorithm developed by CambridgeSoft Corporation and used in Chem-BioDraw Ultra 12.0. Unless state otherwise, $^1\text{H-NMR}$ and $^{13}\text{C-NMR}$ spectra were recorded on Varian Gemini at 400 MHz and 100 MHz respectively. Chemical shifts (δ) are reported relative to TMS as internal standard. Low resolution mass spectra ESI-MS were recorded on a Waters ZQ 4000 apparatus.

Experimental procedures

General procedure for coupling reactions (88-90 and 92-94)

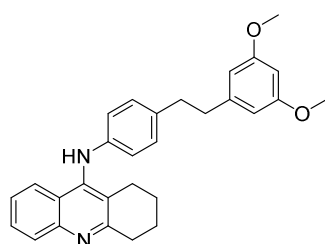
Tacrine derivatives **100-102** (1 equiv), the appropriate amine **98-99** (1-1.5 equiv) and phenol (4-9 equiv) were charged in a pressure tight microwave tube containing a stirring bar. The reaction mixture was submitted to microwave irradiation at 120 °C with an irradiation power of 150W for 1h. The mixture was dissolved in DCM and washed with sodium hydroxide 10%, brine and water, dried over sodium sulfate and evaporated. Crude product was purified by flash chromatography (petroleum ether/EtOAc, elution gradient 90:10 to 80:20).

6-chloro-N-(4-(3,5-dimethoxyphenethyl)phenyl)-1,2,3,4-tetrahydroacridin-9-amine (88)



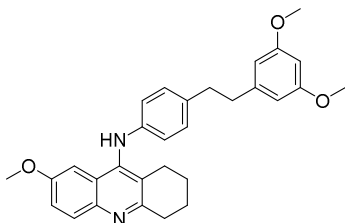
Coupling of compound **98** (0.270 g, 1.05 mmol) and **100** (0.264 g, 1.05 mmol) with phenol (0.889 g, 9 equiv) was performed according to the general procedure described above. Brown solid, 0.260 g, 0.55 mmol, 52% yield. ^1H NMR (CDCl_3 , 400 MHz) δ : 1.84-1.88 (m, 2H), 1.91-1.95 (m, 2H), 2.7 (t, J = 6.2 Hz, 2H), 2.82 (s, 4H), 3.11 (t, J = 6.6 Hz, 2H), 3.75 (s, 6H), 5.93 (br, 1H, -NH-), 6.29-6.32 (m, 3H, aromatic), 6.63 (d, J = 8.0 Hz, 2H, aromatic), 7.01 (d, J = 8.0 Hz, 2H, aromatic), 7.21 (dd, J = 2.0 Hz, 8.8 Hz, 1H, aromatic), 7.64 (d, J = 8.8 Hz, 1H, aromatic), 7.95 (d, J = 1.6 Hz, 1H, aromatic), ^{13}C NMR (CDCl_3 , 100 MHz) δ : 22.8, 22.9, 25.3, 34.2, 37.0, 38.4, 55.4, 98.0, 106.7, 106.8, 115.4, 117.5, 121.0, 122.5, 125.1, 125.7, 127.8, 129.36, 129.44, 134.5, 134.9, 142.4, 144.0, 144.3, 148.0, 160.9, 161.2; MS (ESI^+): m/z : 473 [$\text{M} + \text{H}$] $^+$.

N-(4-(3,5-dimethoxyphenethyl)phenyl)-1,2,3,4-tetrahydroacridin-9-amine (89)



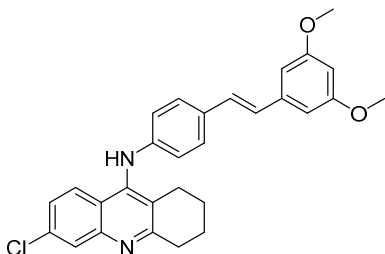
Coupling of compound **98** (0.170 g, 0.66 mmol) and **101** (0.144 g, 0.66 mmol) with phenol (0.560 g, 9 equiv) was performed according to the general procedure described above. Yellow solid, 0.15 g, 0.34 mmol, 52% yield. ^1H NMR (CDCl_3 , 400 MHz) δ : 1.85-1.88 (m, 2H), 1.93-1.99 (m, 2H), 2.73 (t, J =6.2Hz, 2H), 2.83 (s, 4H); 3.15 (t, J = 6.4 Hz, 2H), 3.77 (s, 6H), 5.82 (br, 1H, -NH-), 6.31-6.34 (m, 3H, aromatic), 6.64 (d, J = 8.4 Hz, 2H, aromatic), 7.02 (d, J = 8.0 Hz, 2H, aromatic), 7.32 (t, J = 7.6 Hz, 1H, aromatic), 7.59 (t, J = 7.6 Hz, 1H, aromatic), 7.76 (d, J = 8.4 Hz, 1H, aromatic), 7.98 (d, J = 8 Hz, 1H, aromatic), ^{13}C NMR (CDCl_3 , 100 MHz) δ : 22.6, 23.0, 25.5, 34.3, 37.0, 38.5, 55.4, 98.0, 106.7, 117.1, 122.9, 123.0, 123.3, 124.9, 128.7, 129.0, 129.3, 134.3, 142.7, 143.6, 144.4, 147.6, 160.0, 160.9; MS (ESI^+): m/z : 439 [$\text{M} + \text{H}$] $^+$.

N-(4-(3,5-dimethoxyphenethyl)phenyl)phenyl)-7-methoxy-1,2,3,4-tetrahydroacridin-9-amine (90)



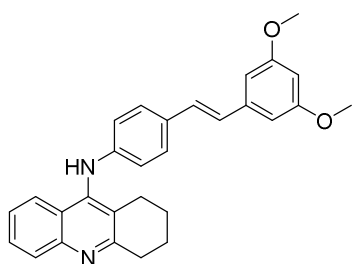
Coupling of compound **98** (0.100 g, 0.39 mmol) and **102** (0.096 g, 0.39 mmol) with phenol (0.328 g, 9 equiv) was performed according to the general procedure described above. Brown solid, 0.096 g, 0.13 mmol, 33% yield. ^1H NMR (CDCl_3 , 400 MHz) δ : 1.84-1.88 (m, 2H), 1.92-1.96 (m, 2H), 2.74 (t, $J=6.4$ Hz, 2H), 2.83 (s, 4H), 3.11 (t, $J=6.4$ Hz, 2H), 3.66 (s, 3H), 3.77 (s, 6H), 5.70 (br, 1H, -NH-), 6.30-6.34 (m, 3H, aromatic), 6.63 (d, $J=8.4$ Hz, 2H, aromatic), 6.98 (d, $J=2.8$ Hz, 1H, aromatic), 7.03 (d, $J=8.0$ Hz, 2H, aromatic), 7.24 (m, 1H, aromatic), 8.89 (d, $J=9.2$ Hz, 1H, aromatic). ^{13}C NMR (CDCl_3 , 100 MHz) δ : 22.9, 23.1, 25.5, 33.9, 37.0, 38.5, 55.38, 55.44, 98.0, 101.8, 106.7, 117.0, 121.3, 123.4, 123.8, 129.3, 130.4, 134.1, 142.6, 143.6, 144.3, 156.8, 157.2, 160.9; MS (ESI^+): m/z : 469 [$\text{M} + \text{H}$] $^+$.

N-(4-(3,5-dimethoxyphenethyl)phenyl)phenyl)-6-methoxy-1,2,3,4-tetrahydroacridin-9-amine (92)



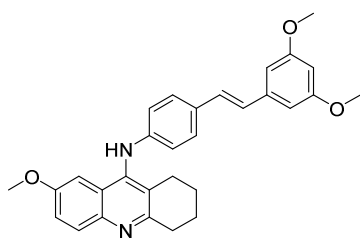
Coupling of compound **99** (0.170 g, 0.66 mmol) and **100** (0.168 g, 0.66 mmol) with phenol (0.248 g, 4 equiv) was performed according to the general procedure described above. Yellow solid, 0.140 g, 0.29 mmol, 45% yield. ^1H NMR (CDCl_3 , 400 MHz) δ : 1.86-1.90 (m, 2H), 1.94-1.98 (m, 2H), 2.75 (t, $J=6.2$ Hz, 2H), 3.14 (t, $J=6.4$ Hz, 2H), 3.83 (s, 6H), 5.87 (br, 1H, -NH-), 6.38 (t, $J=2$ Hz, 1H, aromatic), 6.64-6.69 (m, 4H, aromatic), 6.89 (d, $J=16$ Hz, 1H), 7.01 (d, $J=16.4$ Hz, 1H), 7.25-7.28 (m, 3H, aromatic), 7.37 (d, $J=8.0$ Hz, 2H, aromatic), 7.70 (d, $J=8.8$ Hz, 1H, aromatic), 7.99 (d, $J=2.0$ Hz, 1H, aromatic). ^{13}C NMR (CDCl_3 , 100 MHz) δ : 22.7, 22.8, 25.4, 34.2, 55.5, 99.8, 104.6, 117.0, 121.5, 123.8, 125.0, 126.1, 126.8, 127.9, 128.7, 130.4, 134.8, 139.8, 143.4, 144.0, 148.1, 161.15, 161.22; MS (ESI^+): m/z : 471 [$\text{M} + \text{H}$] $^+$.

(E)-N-(4-(3,5-dimethoxystyryl)phenyl)-1,2,3,4-tetrahydroacridin-9-amine (93)



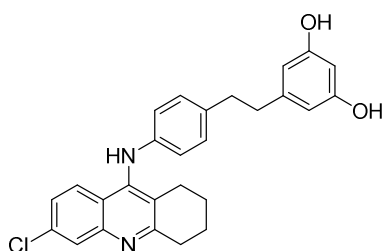
Coupling of compound **99** (0.176 g, 0.69 mmol) and **101** (0.100 g, 0.46 mmol) with phenol (0.390 g, 9 equiv) was performed according to the general procedure described above. Orange solid, 0.093 g, 0.21 mmol, 46% yield. ^1H NMR (CDCl_3 , 400 MHz) δ : 1.86-1.90 (m, 2H), 1.95-1.99 (m, 2H), 2.76 (t, $J = 6.2$ Hz, 2H), 3.17 (t, $J = 6.6$ Hz, 2H), 3.82 (s, 6H), 5.93 (br, 1H, -NH-), 6.37 (s, 1H, aromatic), 6.63-6.70 (m, 4H, aromatic), 6.89 (d, $J = 16.4$ Hz, 1H), 7.01 (d, $J = 16$ Hz, 1H), 7.33-7.38 (m, 3H, aromatic), 7.61 (t, $J = 7.6$ Hz, 1H, aromatic), 7.79 (d, $J = 8.8$ Hz, 1H, aromatic), 8.02 (d, $J = 8.0$ Hz, 1H, aromatic). ^{13}C NMR (CDCl_3 , 100 MHz) δ : 22.8, 23.0, 25.6, 31.0, 34.1, 55.5, 99.8, 104.5, 110.2, 116.8, 123.2, 125.3, 126.5, 127.8, 128.9, 129.0, 130.1, 139.9, 144.3, 144.5, 160.2, 161.2; MS (ESI $^+$): m/z : 437 [M + H] $^+$.

(E)-N-(4-(3,5-dimethoxystyryl)phenyl)-7-methoxy-1,2,3,4-tetrahydroacridin-9-amine (94)



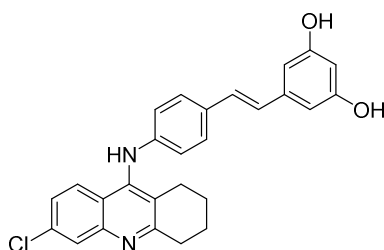
Coupling of compound **99** (0.268 g, 0.69 mmol) and **102** (0.174 g, 1.05 mmol) with phenol (0.590 g, 9 equiv) was performed according to the general procedure described above. Brown solid, 0.106 g, 0.23 mmol, 32% yield. ^1H NMR (CDCl_3 , 400 MHz) δ : 1.85 (m, 2H), 1.83-1.87 (m, 2H), 1.91-1.95 (m, 2H), 2.75 (t, $J = 6.2$ Hz, 2H), 3.11 (t, $J = 6.6$ Hz, 2H), 3.68 (s, 3H), 3.80 (s, 6H), 5.77 (br, 1H, -NH-), 6.35 (t, $J = 2.2$ Hz, 1H, aromatic), 6.62-6.65 (m, 4H, aromatic), 6.86 (d, $J = 16.4$ Hz, 1H), 6.98 (d, $J = 2.8$ Hz, 1H, aromatic), 6.99 (d, $J = 16.4$ Hz, 1H), 7.24-7.27 (m, 1H, aromatic), 7.34 (d, $J = 8.4$ Hz, 2H, aromatic), 7.89 (d, $J = 9.6$ Hz, 1H, aromatic). ^{13}C NMR (CDCl_3 , 100 MHz) δ : 15.4, 22.9, 23.0, 25.5, 33.8, 55.50, 55.53, 66.0, 99.8, 101.7, 104.5, 106.9, 116.6, 121.5, 124.1, 126.3, 127.8, 128.9, 129.7, 130.25, 130.32, 139.9, 144.3, 157.1, 161.2; MS (ESI $^+$): m/z : 467 [M + H] $^+$.

5-(4-(6-chloro-1,2,3,4-tetrahydroacridin-9-ylamino)phenethyl)benzene-1,3-diol (91)



Compound **88** (0.500 g, 1.06 mmol) was dissolved in anhydrous DCM (12 mL). The mixture was cooled to -78 °C and a 1M DCM solution of BBr₃ (4.2 mL, 4.2 mmol, 4 eq) was added dropwise under N₂ atmosphere. The reaction mixture was stirred at the same temperature for 0.5 h and then at rt for 20h. Ice and then aqueous NaOH 10% were added and the mixture was extracted with DCM (1x10 mL) to remove impurities. The alkaline aqueous phase was acidified with HCl 6N, and a yellow precipitate was formed. The precipitate was filtered and washed with water and diethyl ether and then purified by flash chromatography (DCM/MeOH 98:2). Yellow solid, 0.440 g, 0.98 mmol, 93% yield. ¹H NMR (CD₃OD, 400 MHz) δ 1.81-1.82 (m, 2H), 1.90-1.92 (m, 2H), 2.62-2.70 (m, 4H), 2.74-2.78 (m, 2H), 3.02-3.05 (m, 2H), 6.05-6.09 (m, 3H, aromatic), 6.63-6.64 (d, 2H, aromatic), 6.97-6.99 (d, 2H, aromatic), 7.25-7.27 (d, 1H, aromatic), δ: 7.78-7.81 (m, 2H, aromatic). ¹³C NMR (CD₃OD, 100 MHz): δ: 23.5, 26.5, 33.4, 38.1, 39.2, 101.2, 108.1, 120.4, 121.1, 122.0, 125.3, 126.4, 127.3, 130.4, 136.6, 137.3, 142.8, 145.3, 146.7, 148.9, 159.3, 160.6; MS (ESI⁺): m/z: 445 [M + H]⁺.

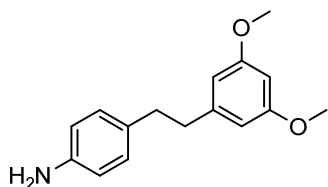
(E)-5-(4-((6-chloro-1,2,3,4-tetrahydroacridin-9-yl)amino)styryl)benzene-1,3-diol (95)



Compound **92** (0.400 g, 0.85 mmol) was dissolved in anhydrous DCM (12 mL). The mixture was cooled to -78 °C and a 1M DCM solution of BBr₃ (3.39 mL, 3.39 mmol, 4 eq) was added dropwise under N₂ atmosphere. The reaction mixture was stirred at the same temperature for 0.5 h and then at RT for 20 h. Aqueous NaOH 10% was added and mixture was extracted with EtOAc (3 x 20 mL). Combined organic phases were dried over sodium sulfate and evaporated. Crude product was purified by flash chromatography (petroleum ether/EtOAc 50:50). Yellow solid, 0.090 g, 0.20 mmol, 31% yield. ¹H NMR (CD₃OD, 400 MHz) δ: 1.80-1.84 (m, 2H), 1.93-1.96 (m, 2H), 2.71 (t, J= 6.4 Hz, 2H), 3.07 (t, J= 6.4 Hz, 2H), 6.14 (t, J= 2.0 Hz, 1H, aromatic), 6.42 (d, J= 2.0 Hz, 2H, aromatic), 6.67 (d, J= 8.4 Hz, 2H, aromatic), 6.81 (d, J= 16.4 Hz, 1H), 6.94 (d, J= 16.4 Hz, 1H), 7.29-7.35 (m, 3H, aromatic), 7.84-7.86 (m,

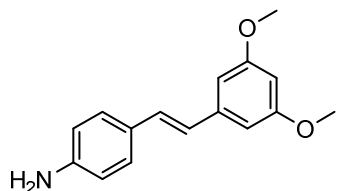
2H, aromatic). ^{13}C NMR (CD_3OD , 100 MHz) δ : 23.6, 26.7, 34.5, 102.8, 105.9, 118.1, 122.9, 125.1, 126.6, 126.9, 127.1, 127.5, 128.5, 129.2, 131.4, 135.5, 141.2, 145.6, 146.4, 148.5, 159.7, 162.6; MS (ESI $^+$): m/z : 443 $[\text{M} + \text{H}]^+$.

4-(3,5-dimethoxyphenethyl)aniline (**98**)



A solution of (E)-1,3-dimethoxy-5-(4-nitrostyryl)benzene **97** (0.2 g, 0.70 mmol) in EtOAc (20 mL) was reduced on an H-Cube® flow hydrogenator using a Palladium catalyst cartridge 10% Pd/C, with the following conditions: full H_2 mode, $T = \text{r.t.}$; $P(\text{H}_2) = 1$ bar; flow rate: 1.0 mL/min. Volatile components were evaporated in vacuum to give the crude 4-(3,5-dimethoxyphenethyl)aniline as brown oil. **98** was used in the coupling step without further purification. 0.17 g, 0.65 mmol, 93% yield. ^1H NMR (CDCl_3 , 400 MHz) δ 2.81 (s, 4H), 3.77 (s, 6H), 6.31 (t, $J = 2.4$ Hz, 1H, aromatic), 6.35 (d, $J = 2.4$ Hz, 2H, aromatic), 6.63 (d, $J = 8.0$ Hz, 2H, aromatic), 6.99 (d, $J = 8$ Hz, 2H, aromatic).

(E)-4-(3,5-dimethoxystyryl)aniline (**99**)



(E)-1,3-dimethoxy-5-(4-nitrostyryl)benzene **97** (0.2 g, 0.70 mmol) was dissolved in EtOAc (30 mL). 6 equivalents of Tin (II) chloride dehydrate (0.95 g, 4.20 mmol) were added and mixture was refluxed for 7h. Than other 2 equivalents (0.32 g, 1.42 mmol) were added and the mixture was refluxed for other 5h. Saturated aqueous sodium bicarbonate was added to achieve alkalinity. Precipitate was formed. The mixture was filtered and the filtrate was extracted with EtOAc (3 x 10mL), than evaporated to obtain the product as brown solid. The compound was used in coupling step without further purification. 0.17 g, 0.65 mmol, 93% yield. ^1H NMR (CDCl_3 , 400 MHz) δ : 3.83 (s, 6H), 6.36 (t, $J = 2.4$ Hz, 1H, aromatic), 6.64 (d, $J = 2.4$ Hz, 2H, aromatic), 6.68 (dd, $J = 2.0$ Hz, 6.4 Hz, 2H, aromatic), 6.85 (d, $J = 16.4$ Hz, 1H, aromatic), 7.00 (d, $J = 16.4$, 1H, aromatic), 7.33 (dd, $J = 2.0$ Hz, 6.8 Hz, 2H, aromatic).

CONCLUDING REMARKS

The totality of my PhD research has been directed to chemical manipulation of synthetic building blocks in order to obtain biologically active molecules, useful as tools both for drug discovery and chemical biology.

The main project (Part I) of my PhD program focused on the synthesis of structural analogs of the LDH-A inhibitor galloflavin (GF). Since the poor chemical manipulability of GF did not allow an easy access to synthesis of analogs, a structural simplification was performed which led to the identification of a natural dibenzopyranone, urolithin M6 (UM6).

An efficient and versatile synthetic procedure to obtain UM6 has been developed and preliminary biological test showed it reproduced GF's behaviour, making it a new *hit* suitable for our investigations. The synthetic route developed for UM6 has been exploited for the synthesis of a small library of UM6 structural analogs bearing the same dibenzopyranone scaffold or phenanthrene and biphenyl scaffolds, proving to be a convenient strategy in term of high yields, short reaction times and versatility. Furthermore, a small number of dibenzopyranone and dibenzopyrane derivatives were obtained through some of the previously reported procedures for urolithins synthesis. Biological evaluation of the new derivatives allowed a SAR assessment for this class of compounds. UM6 and the new active compounds are currently under further investigations to a deeper knowledge of their glycolytic inhibitor activity. These studies, in parallel with docking studies, could allow a further optimization of the active compounds toward more potent inhibitors.

Part II, related to the research activity carried out during the six-month placement under the supervision of Professor Angela Russell at Department of Chemistry (University of Oxford), focused on the development of small molecules useful as chemical tools to investigate pathways involved in neurogenesis and neural stem cell (NSC) fate.

A series of derivatives including alkyne-tagged analogs of the recently discovered proneurogenic compound OX02672 have been synthesized for subsequent development into fluorescent and affinity probes by "click" conjugation with azide-containing reporters. Some of the alkyne-tagged analogs were therefore conjugated with a simple

azide and a rhodamine-azide-derivative through click chemistry, proving this strategy can be useful for the development of OX02672 into fluorescent probes. With the same approach, alkyne-tagged derivatives could be developed also as affinity probes by conjugation with biotin-azide-derivative in the click reaction. These probes can be used in chemical proteomics and other chemical biology methods to assess the localization in NSCs and to identify the target protein(s). This in turn may help to understand the mechanism of action of OX02672 and to gain a better knowledge of the signaling pathways that control adult neurogenesis.

Finally, a side project (Part III) was carried out in collaboration with the group of Professor Maria Laura Bolognesi. It involved the rational design and synthesis of a new series of multi-target-directed ligands (MTDLs) against Alzheimer's disease (AD). By using a *fusing* strategy, a new series of tacrin-resveratrol hybrids have been designed and synthesized. New derivatives showed interesting multi-target profile against target proteins involved in AD pathogenesis and low toxicity on primary neurons. However, a general hepatotoxicity was evident for all the compounds, probably due to the presence of tacrin fragment. In this regard, is important to keep in mind that toxicity issues should be addressed very early in a drug discovery project. Our findings added new layers of information to multi-target drug discovery and may be useful for approaches aimed to the development of hybrid compounds.

Appendix A

Experiments performed by Professor Giuseppina Di Stefano's group

Enzymatic assays on purified human LDH-A

Purified LDH-A (from human liver) was obtained from Lee Biosolutions (St Louis, Missouri, USA). 20 mM stock solutions of compound was prepared in DMSO. It was added in scalar amounts (0 – 200 μ M final concentrations) to a reaction mix containing 100 mM phosphate buffer pH 7.5, 0.015 U LDH / ml, 1 mM pyruvate and 150 μ M NADH. For all the determinations (including those without the compounds), DMSO in the reaction mix was always kept to 0.6%. The enzymatic activity was measured by monitoring NADH oxidation for a period of 3 min. To avoid interference of the compounds with the UV reading of NADH oxidation, we adopted the procedure reported by Moran⁷, which measured LDH activity by recording the decrease of NADH fluorescence. The assay was performed in 96-well white body plates, using a Fluoroskan Ascent FL reader (Labsystems). The concentration of compounds causing 50% inhibition of LDH activity (IC_{50}) was calculated from the second order polynomial regression of the experimental data, using the Prism 5 GraphPad software.

Cell culture conditions

Raji cells were grown as a suspension culture in RPMI 1640 containing 10% FBS, 100 U/ml penicillin/streptomycin, 4 mM glutamine and were maintained at a concentration of $1-2 \times 10^5$ viable cells/ml. All media and supplements were from Sigma. In all experiments, inhibitors were added to the culture media in the presence of 0.6% DMSO. The same amount of DMSO was always added to the control, untreated cultures.

Effects of the inhibitors on lactate production

5×10^5 cells in 1 mL of culture medium were seeded in each well of a 6-well Nunclon plate. Scalar amounts of inhibitor (0-200 μ M, tested in duplicate) were then added to the cultures. Lactate was measured in 3 untreated wells at the start of experiment (baseline value) and 3 h after incubation at 37°C. In each well, we simultaneously measured released in medium and intracellular lactate: at the end of incubation 100 μ l of 100% trichloroacetic acid (TCA) solution was added; the cell lysate was collected and the well was washed with 1 mL 10% TCA. After centrifugation, lactate in the supernatant was

measured according to the method of Barker and Summerson.⁸ The amount of metabolite formed during the 3 h incubation with or without the inhibitor was calculated by subtracting the baseline value. The dose of compound causing 50% inhibition of lactate production (IC₅₀) was calculated from the second order polynomial regression of experimental data, using the Prism 5 GraphPad software.

Effects of the inhibitors on cell growth or viability

To study the effect of the inhibitor on cell proliferation, 1×10^5 cells were seeded in 24-multiwell plates and treated for 24 h at 37°C with scalar doses of inhibitors (0-200 μ M, tested in duplicate). After incubation, cells were counted under a light microscope using a Neubauer chamber and their viability was determined by Trypan blue exclusion. The cell growth was calculated from the difference between the number of viable cells counted at 24 h and that at the beginning of experiment. Data were plotted as cell growth vs dose of compound. The dose causing 50% inhibition of cell growth (cell growth IC₅₀) was calculated by applying the second order polynomial regression to the experimental data.

Appendix B

Experiments performed by Dr. Julie Davies (Oxford University)

Cell culture and *in vitro* compound screening procedures

DCX-GFP mice with CD1 background strain were sacrificed at 3-5 days old. NSCs from the DG and SVZ, and astrocytes from the cerebral cortex were dissected and grown in polyheme coated plates to prevent adherence with neural basal A media (Gibco), 1% pen/strep, 1% glutamax and 2% B27 supplement (all Sigma). The NSCs were also grown in the presence of EGF and FGF to encourage cell expansion. NSCs were incubated until secondary or tertiary neurospheres, at 37 °C and 5% CO₂ in a humidified incubator.

384 well plates were treated with poly-ornithine to encourage cell adhesion, left at rt overnight and the poly-ornithine extracted from the plate. Plates were then treated with laminin for 1 h at 37 °C and the laminin then extracted. The suspended neurospheres were removed from the polyheme coated plates, centrifuged at 1200 rpm for 5 min to form a pellet of cells and the supernatant media removed before being triturated to promote dissociation. The neurospheres were then treated with Accutase® to dissociate the cells and form a single cell suspension, and then centrifuged again. The suspension was made up in a known volume of media and the cell total counted using a Motics AE2000 microscope. Cells were seeded onto the coated 384 plates at 2000 cells/well in 10µL/well and incubated for 1 h. Compounds were dissolved in DMSO at a concentration of 10 mM, serially diluted and 40 µL of a given concentration was added to the well to give a final compound concentration of 100, 10, 1, 0.1, 0.01 and 0.001 µM. Experiments were repeated in both technical and biological triplicate. Plates were then incubated for 6 days. Immunocytochemistry was then performed by staining cells with GFAP, TUJ1, MAP2 antibodies and DAPI nuclear stain. 5 images of the stained cells were taken per well using a Perkin Elmer Operetta microscope and x20 objective, and the number DAPI+/TUJ1+ cells were counted. The percentage of neurons against the total number of DAPI stained cells was calculated.

The number of neurons in a compound-treated well was compared to that in the normalised, negative control of DMSO and the fold change calculated. All-trans retinoic acid (ATRA) known to induce neurogenesis *in vitro* (1) was used as the positive control. ATRA gave a dose dependent increase in the proportion of neurons up to ~2.5-

fold when compared to the DMSO control. At higher concentrations this effect decreased, attributed to increased toxicity.

- (1) Maden, M. Retinoic acid in the development, regeneration and maintenance of the nervous system. *Nat. Rev. Neurosci.* 8, 755-765 (2007)

In Vivo experiments with OX02672

Quantification BrdU/NeuN in the anterior and posterior dentate gyrus (1 week treatment)

- 3 breeding pairs (♂ Transgenics and ♀ wild types)
- 8 other J20s
- 25mg/kg via oral gavage TID for 7 days with BrdU in the drinking water
- 14 day resting period and then perfused
- BrdU (Proliferating cells), NeuN (Mature neurons) and DAPI (Nuclear dye)
- Hippocampal staining

Abbreviations and acronyms

ABP: Activity-based probe

ABPP: Activity-based protein profiling

AKT: Protein kinase B

COSY: Correlation spectroscopy

CuAAC: Copper(I)-catalyzed azide-alkyne cycloaddition

DCM: Dichloromethane

DCC: N,N'-Dicyclohexylcarbodiimide

DIBAL: Diisobutylaluminum hydride

DCE: 1,2-Dichloroethane

DCM: Dichloromethane

DG: Dentate gyrus

DIPEA: N,N-Diisopropylethylamine

DMA: N,N-Dimethylacetamide

DMAP: Dimethylaminopyridine

DME: 1,2-Dimethoxyethane

DMF: N,N-dimethylformamide

DMSO: Dimethyl sulfoxide

EA: Ellagic acid

ECAT: Endogenous cell activation therapy

EDC: N-(3-Dimethylaminopropyl)-N'-ethylcarbodiimide

GA: Gallic acid

GF: Galloflavin

GSK-3 β : Glycogen synthase kinase 3 beta

HIF: Hypoxia-inducible factor

HMBC: Heteronuclear multiple-bond correlation spectroscopy

HPLC: High performance liquid chromatography

HRMS: High-resolution mass spectrometry

HSQC: Heteronuclear single quantum coherence spectroscopy

HTS: High-throughput screening

IR: Infrared

LDH-A: Lactate dehydrogenase isoform A (tetramer)

LiHMDS: Lithium bis(trimethylsilyl)amide

mTOR: Mammalian target of rapamycin
NAD⁺: Nicotinamide adenine dinucleotide (oxidized form)
NADH: Nicotinamide adenine dinucleotide (reduced form)
NBS: N-bromosuccinimide
NSC: Neural stem cell
NPC: Neural progenitor cell
NIS: N-Iodosuccinimide
NMR: Nuclear magnetic resonance
NOESY: Nuclear Overhauser effect spectroscopy
PCC: Pyridinium chlorochromate
PDH: Pyruvate dehydrogenase
PDK: Pyruvate dehydrogenase kinase
PI3K: phosphatidylinositol 3-kinase
PG: Protecting group
SAR: Structure-activity relationship
SDS-PAGE: Sodium dodecyl sulphate - polyacrylamide gel electrophoresis
SGZ: Subgranular zone
SVZ: Subventricular zone
S-Phos: 2-Dicyclohexylphosphino-2',6'-dimethoxybiphenyl
THF: Tetrahydrofuran
TLC: Thin layer chromatography
UM6: Urolithin M6
UM7: Urolithin M7
Uro-A: Urolithin A
Uro-B: Urolithin B
Uro-D: Urolithin D
Uro-E: Urolithin E
VS: Virtual screening

References

1. Hanahan, D. & Weinberg, R. A. Hallmarks of cancer: The next generation. *Cell* **144**, 646–674 (2011).
2. Phan, L. M., Yeung, S.-C. J. & Lee, M.-H. Cancer metabolic reprogramming: importance, main features, and potentials for precise targeted anti-cancer therapies. *Cancer Biol. Med.* **11**, 1–19 (2014).
3. Warburg, O. The metabolism of tumors in the body. *J. Gen. Physiol.* **8**, 519–530 (1927).
4. Levine, A. & Puzio-Cuter, A. The control of the metabolic switch in cancers by oncogenes and tumor suppressor genes. *Science* **330**, 1340–1344 (2010).
5. DeBerardinis, R. J., Lum, J. & Hatzivassiliou, G. et al. The biology of cancer: metabolic reprogramming fuels cell growth and proliferation. *Cell Metab.* **7**, 11–20 (2008).
6. Buchakjian, M. & Kornbluth, S. The engine driving the ship: metabolic steering of cell proliferation and death. *Nat. Rev. Mol. Cell Biol.* **11**, 715–727 (2010).
7. Martinez-Outschoorn, U. E., Peiris-Pagés, M., Pestell, R. G., Sotgia, F., Lisanti, M. P. Cancer metabolism: a therapeutic perspective. *Nat Rev. Clin. Oncol* **14**, 11–31 (2017).
8. Vander Heiden, M. G. Targeting cancer metabolism: a therapeutic window opens. *Nat. Rev. Drug Discov.* **10**, 671–684 (2011).
9. Kim, J. W. & Dang, C. V. Cancer’s molecular sweet tooth and the warburg effect. *Cancer Research* **66**, 8927–8930 (2006).
10. Vander Heiden, M. G., Cantley, L. C. & Thompson, C. B. Understanding the Warburg effect: the metabolic requirements of cellproliferation. *Science* **324**, 1029–1033 (2009).
11. Cairns, R. A., Harris, I. S. & Mak, T. W. Regulation of cancer cell metabolism. *Nature Reviews Cancer* **11**, 85–95 (2011).
12. Granchi, C. & Minutolo, F. Anticancer Agents That Counteract Tumor Glycolysis. *ChemMedChem* **7**, 1318–1350 (2012).
13. Warburg, O. On the origin of cancer cells. *Science* **123**, 309–314 (1956).
14. Warburg, O. On respiratory impairment in cancer cells. *Science* **124**, 269–270 (1956).
15. DeBerardinis, R. J., Sayed, N., Ditsworth, D. & Thompson, C. B. Brick by brick: metabolism and tumor cell growth. *Current Opinion in Genetics and Development* **18**, 54–61 (2008).
16. Lunt, S. & Vander Heiden, M. Aerobic glycolysis: meeting the metabolic requirements of cell proliferation. *Annu. Rev. Cell Dev. Biol.* **27**, 441–464 (2011).
17. Kondoh, H. et al. A high glycolytic flux supports the proliferative potential of murine embryonic stem cells. *Antioxid. Redox Signal.* **9**, 293–299 (2007).
18. Kroemer, G. & Pouyssegur, J. Tumor cell metabolism: cancer’s Achilles’ heel. *Cancer Cell* **13**, 472–482 (2008).

19. Yeung, S. J., Pan, J. & Lee, M. H. Roles of p53, MYC and HIF-1 in regulating glycolysis - The seventh hallmark of cancer. *Cellular and Molecular Life Sciences* **65**, 3981–3999 (2008).
20. Hsu, P. P. & Sabatini, D. M. Cancer cell metabolism: Warburg and beyond. *Cell* **134**, 703–707 (2008).
21. Jones, R. G. & Thompson, C. B. Tumor suppressors and cell metabolism: A recipe for cancer growth. *Genes and Development* **23**, 537–548 (2009).
22. Gillies, R. J., Robey, I. & Gatenby, R. A. Causes and Consequences of Increased Glucose Metabolism of Cancers. *J. Nucl. Med.* **49**, 24S–42S (2008).
23. Bellance, N., Lestienne, P. & Rossignol, R. Mitochondria: from bioenergetics to the metabolic regulation of carcinogenesis. *Front. Biosci.* **14**, 4015–4034 (2009).
24. Hunt, T. *et al.* Aerobically derived lactate stimulates revascularization and tissue repair via redox mechanisms. *Antioxid. Redox Signal. Redox Signal.* **9**, 1115–1124 (2007).
25. Estrella, V. *et al.* Acidity generated by the tumor microenvironment drives local invasion. *Cancer Res.* **73**, 1524–1535 (2013).
26. Sonveaux, P. *et al.* Targeting lactate-fueled respiration selectively kills hypoxic tumor cells in mice. *J. Clin. Invest.* **118**, 3930–3942 (2008).
27. Zheng, J. Energy metabolism of cancer: Glycolysis versus oxidative phosphorylation (review). *Oncology Letters* **4**, 1151–1157 (2012).
28. Koppenol, W. H., Bounds, P. L. & Dang, C. V. Otto Warburg's contributions to current concepts of cancer metabolism. *Nat. Rev. Cancer* **11**, 325–337 (2011).
29. Jang, M., Kim, S. S. & Lee, J. Cancer cell metabolism: implications for therapeutic targets. *Exp. Mol. Med.* **45**, e45, 1-8 (2013).
30. Pylayeva-Gupta, Y., Grabocka, E. & Bar-Sagi, D. RAS oncogenes: Weaving a tumorigenic web. *Nature Reviews Cancer* **11**, 761–774 (2011).
31. Denko, N. C. Hypoxia, HIF1 and glucose metabolism in the solid tumour. *Nature Reviews Cancer* **8**, 705–713 (2008).
32. Yecies, J. & Manning, B. mTOR links oncogenic signaling to tumor cell metabolism. *J.Mol. Med.* **89**, 221–228 (2011).
33. Semenza, G. L. HIF-1 : upstream and downstream of cancer metabolism. *Curr. Opin. Genet. Dev.* **20**, 51–56 (2011).
34. Dang, C. V, Kim, J. W., Gao, P. & Yustein, J. The interplay between MYC and HIF in cancer. *Nature Reviews Cancer* **8**, 51–56 (2008).
35. Bensaad, K. *et al.* TIGAR, a p53-Inducible Regulator of Glycolysis and Apoptosis. *Cell* **126**, 107–120 (2006).
36. Vousden, K. H. & Ryan, K. M. P53 and metabolism. *Nature Reviews Cancer* **9**, 691–700 (2009).

37. Hay, N. Reprogramming glucose metabolism in cancer: Can it be exploited for cancer therapy? *Nature Reviews Cancer* **16**, 635–649 (2016).
38. Ganapathy-Kanniappan, S. & Geschwind, J.-F. H. Tumor glycolysis as a target for cancer therapy: progress and prospects. *Mol. Cancer* **12**, 152 (2013).
39. Li, X., Gu, J. & Zhou, Q. Review of aerobic glycolysis and its key enzymes - new targets for lung cancer therapy. *Thorac. Cancer* **6**, 17–24 (2015).
40. Pelicano, H., Martin, D. S., Xu, R. H. & Huang, P. Glycolysis inhibition for anticancer treatment. *Oncogene* **25**, 4633–4646 (2006).
41. Granchi, C., Fancelli, D. & Minutolo, F. An update on therapeutic opportunities offered by cancer glycolytic metabolism. *Bioorganic Med. Chem. Lett.* **24**, 4915–4925 (2014).
42. Deep, G. & Agarwal, R. Targeting tumor microenvironment with silibinin: promise and potential for a translational cancer chemopreventive strategy. *Curr. Cancer Drug Targets* **13**, 486–99 (2013).
43. Ooi, A. T. & Gomperts, B. N. Molecular pathways: Targeting cellular energy metabolism in cancer via inhibition of SLC2A1 and LDHA. *Clin. Cancer Res.* **21**, 2440–2444 (2015).
44. Maschek, G. *et al.* 2-Deoxy-D-glucose Increases the Efficacy of Adriamycin and Paclitaxel in Human Osteosarcoma and Non-Small Cell Lung Cancers in Vivo. *Cancer Res.* **64**, 31–34 (2004).
45. Goldin, N. *et al.* Methyl jasmonate binds to and detaches mitochondria-bound hexokinase. *Oncogene* **27**, 4636–4643 (2008).
46. Dwarakanath, B. *et al.* Clinical studies for improving radiotherapy with 2-deoxy-D-glucose: Present status and future prospects. *J. Cancer Res. Ther.* **5**, 21-26 (2009).
47. Papaldo, P. *et al.* Addition of either lonidamine or granulocyte colony-stimulating factor does not improve survival in early breast cancer patients treated with high-dose epirubicin and cyclophosphamide. *J. Clin. Oncol.* **21**, 3462–3468 (2003).
48. Hamanaka, R. B. & Chandel, N. S. Targeting glucose metabolism for cancer therapy. *J. Exp. Med.* **209**, 211–215 (2012).
49. Clem, B. F. *et al.* Targeting 6-Phosphofructo-2-Kinase (PFKFB3) as a Therapeutic Strategy against Cancer. *Mol. Cancer Ther.* **12**, 1461–1470 (2013).
50. Galluzzi, L., Kepp, O., Heiden, M. G. Vander & Kroemer, G. Metabolic targets for cancer therapy. *Nature Reviews Drug Discovery* **12**, 829–846 (2013).
51. Vander Heiden, M. G. *et al.* Identification of small molecule inhibitors of pyruvate kinase M2. *Biochem. Pharmacol.* **79**, 1118–1124 (2010).
52. Rani, R. & Kumar, V. Recent Update on Human Lactate Dehydrogenase Enzyme 5 (hLDH5) Inhibitors: A Promising Approach for Cancer Chemotherapy. *J. Med. Chem.* **59**, 487–496 (2016).

53. Fiume, L. *et al.* Inhibition of lactate dehydrogenase activity as an approach to cancer therapy. *Future Med. Chem.* **6**, 429–445 (2014).
54. Madern, D. Molecular evolution within the L-malate and L-lactate dehydrogenase superfamily. *J. Mol. Evol.* **54**, 825–840 (2002).
55. Blanco, A. & Zinkham, W. H. Lactate Dehydrogenases in Human Testes. *Science* **139**, 601–2 (1963).
56. Read, J. A., Winter, V. J., Eszes, C. M., Sessions, R. B. & Brady, R. L. Structural basis for altered activity of M-and H-isozyme forms of human lactate dehydrogenase. *Proteins Struct. Funct. Bioinforma.* **43**, 175–185 (2001).
57. McClelland, M. L. *et al.* An integrated genomic screen identifies LDHB as an essential gene for triple-negative breast cancer. *Cancer Res.* **72**, 5812–5823 (2012).
58. Brown, N. J. *et al.* Lactate Dehydrogenase-B Is Silenced by Promoter Methylation in a High Frequency of Human Breast Cancers. *PLoS One* **8**, 4–11 (2013).
59. Dang, C. V., Le, A. & Gao, P. MYC-induced cancer cell energy metabolism and therapeutic opportunities. *Clin. Cancer Res.* **15**, 6479–83 (2009).
60. Koukourakis, M. I., Giatromanolaki, A., Simopoulos, C., Polychronidis, A. & Sivridis, E. Lactate dehydrogenase 5 (LDH5) relates to up-regulated hypoxia inducible factor pathway and metastasis in colorectal cancer. *Clin. Exp. Metastasis* **22**, 25–30 (2005).
61. Semenza, G. L. Oxygen-dependent regulation of mitochondrial respiration by hypoxia-inducible factor 1. *Biochem. J.* **405**, 1–9 (2007).
62. Fantin, V. R., St-Pierre, J. & Leder, P. Attenuation of LDH-A expression uncovers a link between glycolysis, mitochondrial physiology, and tumor maintenance. *Cancer Cell* **9**, 425–434 (2006).
63. Shim, H. *et al.* c-Myc transactivation of LDH-A: Implications for tumor metabolism and growth. *Proc. Natl. Acad. Sci.* **94**, 6658–6663 (1997).
64. Le, A. *et al.* Inhibition of lactate dehydrogenase A induces oxidative stress and inhibits tumor progression. *Proc. Natl. Acad. Sci.* **107**, 2037–2042 (2010).
65. Cui, J. *et al.* FOXM1 promotes the warburg effect and pancreatic cancer progression via transactivation of LDHA expression. *Clin. Cancer Res.* **20**, 2595–2606 (2014).
66. Goldman, R. D., Kaplan, N. O. & Hall, T. C. Lactic Dehydrogenase in Human Neoplastic Tissues. *Cancer Res.* **24**, 389–399 (1964).
67. Neri, D. & Supuran, C. T. Interfering with pH regulation in tumours as a therapeutic strategy. *Nature Reviews Drug Discovery* **10**, 767–777 (2011).
68. Rong, Y. *et al.* Lactate dehydrogenase A is overexpressed in pancreatic cancer and promotes the growth of pancreatic cancer cells. *Tumour Biol.* **34**, 1523–1530 (2013).
69. Yao, F., Zhao, T., Zhong, C., Zhu, J. & Zhao, H. LDHA is necessary for the tumorigenicity of esophageal squamous cell carcinoma. *Tumor Biol.* **34**, 25–31 (2013).

70. Langhammer, S., Najjar, M., Hess-Stumpp, H. & Thierauch, K. H. LDH-A influences hypoxia-inducible factor 1 α (HIF1 α) and is critical for growth of HT29 colon carcinoma cells in vivo. *Target. Oncol.* **6**, 155–162 (2011).
71. Wang, Z. Y. *et al.* LDH-A silencing suppresses breast cancer tumorigenicity through induction of oxidative stress mediated mitochondrial pathway apoptosis. *Breast Cancer Res. Treat.* **131**, 791–800 (2012).
72. Arseneault, R. *et al.* Attenuation of LDHA expression in cancer cells leads to redox-dependent alterations in cytoskeletal structure and cell migration. *Cancer Lett.* **338**, 255–266 (2013).
73. Zhang, Y. *et al.* Inhibition of LDH-A by lentivirus-mediated small interfering RNA suppresses intestinal-type gastric cancer tumorigenicity through the downregulation of Oct4. *Cancer Lett.* **321**, 45–54 (2012).
74. Miyajima, H., Takahashi, Y., Suzuki, M., Shimizu, T. & Kaneko, E. Molecular characterization of gene expression in human lactate dehydrogenase-A deficiency. *Neurology* **43**, 1414–1419 (1993).
75. Maekawa, M., Sudo, K., Kanno, T. & Li, S. S. L. Molecular characterization of genetic mutation in human lactate dehydrogenase-A (M) deficiency. *Biochem. Biophys. Res. Commun.* **168**, 677–682 (1990).
76. Tsujino, S., Shanske, S., Brownell, A. K., Haller, R. G. & DiMauro, S. Molecular genetic studies of muscle lactate dehydrogenase deficiency in white patients. *Ann. Neurol.* **36**, 661–665 (1994).
77. Maekawa, M., Sudo, K., Nagura, K., Li, S. S. L. & Kanno, T. Population screening of lactate dehydrogenase deficiencies in Fukuoka Prefecture in Japan and molecular characterization of three independent mutations in the lactate dehydrogenase-B(H) gene. *Hum. Genet.* **93**, 74–76 (1994).
78. Kanno, T. *et al.* Lactate dehydrogenase M-subunit deficiency: a new type of hereditary exertional myopathy. *Clin. Chim. Acta* **173**, 89–98 (1988).
79. Papaconstantinou, J. & Colowick, S. P. The role of glycolysis in the growth of tumor cells. I. Effects of oxamic acid on the metabolism of Ehrlich ascites tumor cells in vitro. *J. Biol. Chem.* **236**, 278–284 (1961).
80. Zhou, M. *et al.* Warburg effect in chemosensitivity: Targeting lactate dehydrogenase-A re-sensitizes Taxol-resistant cancer cells to Taxol. *Mol. Cancer* **9**, 33, 1-12 (2010).
81. Zhao, Y. *et al.* Overcoming trastuzumab resistance in breast cancer by targeting dysregulated glucose metabolism. *Cancer Res.* **71**, 4585–4597 (2011).
82. Granchi, C., Paterni, I., Rani, R. & Minutolo, F. Small-molecule inhibitors of human LDH5. *Future Med. Chem.* **5**, 1967–1991 (2013).
83. Rani, R. & Kumar, V. When will small molecule lactate dehydrogenase inhibitors realize

- their potential in the cancer clinic? *Future Med. Chem.* **9**, 1113–1115 (2017).
84. Granchi, C. *et al.* Discovery of N-hydroxyindole-based inhibitors of human lactate dehydrogenase isoform A (LDH-A) as starvation agents against cancer cells. *J. Med. Chem.* **54**, 1599–1612 (2011).
 85. Granchi, C. *et al.* Assessing the differential action on cancer cells of LDH-A inhibitors based on the N-hydroxyindole-2-carboxylate (NHI) and malonic (Mal) scaffolds. *Org. Biomol. Chem.* **11**, 6588–6596 (2013).
 86. Calvaresi, E. C. *et al.* Dual targeting of the warburg effect with a glucose-conjugated lactate dehydrogenase inhibitor. *ChemBioChem* **14**, 2263–2267 (2013).
 87. Maftouh, M. *et al.* Synergistic interaction of novel lactate dehydrogenase inhibitors with gemcitabine against pancreatic cancer cells in hypoxia. *Br. J. Cancer* **110**, 172–182 (2014).
 88. Ward, R. A. *et al.* Design and synthesis of novel lactate dehydrogenase a inhibitors by fragment-based lead generation. *J. Med. Chem.* **55**, 3285–3306 (2012).
 89. Kohlmann, A. *et al.* Fragment growing and linking lead to novel nanomolar lactate dehydrogenase inhibitors. *J. Med. Chem.* **56**, 1023–1040 (2013).
 90. Dragovich, P. S. *et al.* Identification of substituted 2-thio-6-oxo-1,6-dihydropyrimidines as inhibitors of human lactate dehydrogenase. *Bioorganic Med. Chem. Lett.* **23**, 3186–3194 (2013).
 91. Fauber, B. P. *et al.* Identification of 2-amino-5-aryl-pyrazines as inhibitors of human lactate dehydrogenase. *Bioorganic Med. Chem. Lett.* **23**, 5533–5539 (2013).
 92. Fauber, B. P. *et al.* Identification of 3,6-disubstituted dihydropyrones as inhibitors of human lactate dehydrogenase. *Bioorganic Med. Chem. Lett.* **24**, 5683–5687 (2014).
 93. Purkey, H. E. *et al.* Cell Active Hydroxylactam Inhibitors of Human Lactate Dehydrogenase with Oral Bioavailability in Mice. *ACS Med. Chem. Lett.* **7**, 896–901 (2016).
 94. Boudreau, A. *et al.* Metabolic plasticity underpins innate and acquired resistance to LDHA inhibition. *Nat. Chem. Biol.* **12**, 779–786 (2016).
 95. Baker, B. R. & Bramhall, R. R. Irreversible Enzyme Inhibitors. 189. Inhibition of Some Dehydrogenases by Derivatives of 4-Hydroxyquinoline-2- and -3-carboxylic Acids. *J. Med. Chem.* **15**, 230–233 (1972).
 96. Baker, B. R. & Bramhall, R. R. Irreversible Enzyme Inhibitors. 192. Hydrophobic Bonding to Some Dehydrogenases with 5-Substituted-4-hydroxyquinoline-3-carboxylic Acids. *J. Med. Chem.* **15**, 237–241 (1972).
 97. Billiard, J. *et al.* Quinoline 3-sulfonamides inhibit lactate dehydrogenase A and reverse aerobic glycolysis in cancer cells. *Cancer Metab.* **1**, 19, 1-17 (2013).
 98. Xie, H. *et al.* Targeting lactate dehydrogenase-A inhibits tumorigenesis and tumor

- progression in mouse models of lung cancer and impacts tumor-initiating cells. *Cell Metab.* **19**, 795–809 (2014).
99. Rai, G. *et al.* Discovery and Optimization of Potent, Cell-Active Pyrazole-Based Inhibitors of Lactate Dehydrogenase (LDH). *J. Med. Chem.* **60**, 22, 9184-9204 (2017). doi:10.1021/acs.jmedchem.7b00941
 100. Shelley, M. D. *et al.* Stereo-specific cytotoxic effects of gossypol enantiomers and gossypolone in tumour cell lines. *Cancer Lett.* **135**, 171–180 (1999).
 101. Vander Jagt, D. L., Deck, L. M. & Royer, R. E. Medicinal Chemistry Feature Molecule Gossypol: Prototype of Inhibitors Targeted to Dinucleotide Folds. *Curr. Med. Chem.* **7**, 479–498 (2000).
 102. Jaroszewski, J. W., Kaplan, O. & Cohen, J. S. Action of Gossypol and Rhodamine 123 on Wild Type and Multidrug-resistant MCF-7 Human Breast Cancer Cells: 31P Nuclear Magnetic Resonance and Toxicity Studies. *Cancer Res.* **50**, 6936–6943 (1990).
 103. Lee, C. Y. G., Moon, Y. S., Yuan, J. H. & Chen, A. F. Enzyme inactivation and inhibition by Gossypol. *Mol. Cell. Biochem.* **47**, 65–70 (1982).
 104. Dodou, K. Investigations on gossypol: past and present developments. *Expert Opin. Investig. Drugs* **14**, 1419–1434 (2005).
 105. Yu, Y. *et al.* Selective active site inhibitors of human lactate dehydrogenases A4, B4, and C4. *Biochem. Pharmacol.* **62**, 81–89 (2001).
 106. Deck, L. M. *et al.* Selective inhibitors of human lactate dehydrogenases and lactate dehydrogenase from the malarial parasite *Plasmodium falciparum*. *J Med Chem* **41**, 3879–3887 (1998).
 107. Mazzio, E. & Soliman, K. Inhibition of anaerobic glucose metabolism and corresponding natural composition as a non-toxic approach to cancer treatment. *PCT Int. Appl.* 45 pp. (2006).
 108. Wang, Z. *et al.* Bioactivity-Guided Identification and Cell Signaling Technology to Delineate the Lactate Dehydrogenase A Inhibition Effects of *Spatholobus suberectus* on Breast Cancer. *PLoS One* **8**, 2, 1-12 (2013).
 109. Manerba, M. *et al.* Galloflavin (CAS 568-80-9): A Novel Inhibitor of Lactate Dehydrogenase. *ChemMedChem* **7**, 311–317 (2012).
 110. Manerba, M. *et al.* Lactate dehydrogenase inhibitors sensitize lymphoma cells to cisplatin without enhancing the drug effects on immortalized normal lymphocytes. *Eur. J. Pharm. Sci.* **74**, 95–102 (2015).
 111. Wen, H., An, Y. J., Xu, W. J., Kang, K. W. & Park, S. Real-time monitoring of cancer cell metabolism and effects of an anticancer agent using 2d in-cell NMR spectroscopy. *Angew. Chemie - Int. Ed.* **54**, 5374–5377 (2015).
 112. Vettrai, Marina; Manerba, Marcella; Govoni, Marzia; Di Stefano, G. Galloflavin

- suppresses lactate dehydrogenase activity and causes MYC downregulation in Burkitt lymphoma cells through NAD/NADH-dependent inhibition of sirtuin-1. *Anticancer. Drugs* **24**, 862–870 (2013).
113. Fiume, L. *et al.* Galloflavin prevents the binding of lactate dehydrogenase A to single stranded DNA and inhibits RNA synthesis in cultured cells. *Biochem. Biophys. Res. Commun.* **430**, 466–469 (2013).
 114. Farabegoli, F. *et al.* Galloflavin, a new lactate dehydrogenase inhibitor, induces the death of human breast cancer cells with different glycolytic attitude by affecting distinct signaling pathways. *Eur. J. Pharm. Sci.* **47**, 729–738 (2012).
 115. Han, X. *et al.* Evaluation of the anti-tumor effects of lactate dehydrogenase inhibitor galloflavin in endometrial cancer cells. *J. Hematol. Oncol.* **8**, 2 (2015).
 116. Manerba, M. *et al.* Lactate dehydrogenase inhibitors can reverse inflammation induced changes in colon cancer cells. *Eur. J. Pharm. Sci.* **96**, 37–44 (2017).
 117. Manerba, M. *et al.* LDH inhibition impacts on heat shock response and induces senescence of hepatocellular carcinoma cells. *Eur. J. Pharm. Sci.* **105**, 91–98 (2017).
 118. Hawort R. D. Galloflavin. Part I. *J. Chem. Soc.* 1583 (1952).
 119. Garazd, Y. L. & Garazd, M. M. Natural dibenzo[b,d]pyran-6-ones: Structural diversity and biological activity. *Chem. Nat. Compd.* **52**, 1–18 (2016).
 120. Koch, K., Podlech, J., Pfeiffer, E. & Metzler, M. Total synthesis of alternariol. *J. Org. Chem.* **70**, 3275–3276 (2005).
 121. Garino, C. *et al.* New 2-bromomethyl-8-substituted-benzo[c]chromen-6-ones. Synthesis and biological properties. *Bioorganic Med. Chem. Lett.* **15**, 135–138 (2005).
 122. Sun, W. *et al.* 6H-Benzo[c]chromen-6-one derivatives as selective ER?? agonists. *Bioorganic Med. Chem. Lett.* **16**, 1468–1472 (2006).
 123. Espín, J. C., Larrosa, M., García-Conesa, M. & Tomás-Barberán, F. Biological significance of the gut microbial ellagic acid-derived metabolites urolithins. *Evidence-Based Complement. Altern. Med.* **2013**, 1–15 (2013).
 124. Garcia-Villalba, R., Beltran, D., Espin, J. C., Selma, M. V. & Tomas-Barberan, F. A. Time course production of urolithins from ellagic acid by human gut microbiota. *J. Agric. Food Chem.* **61**, 8797–8806 (2013).
 125. Dobroslawa, B., Kasimsetty, S. G., Khan, S. I. & Daneel, F. Urolithins, intestinal microbial metabolites of pomegranate ~ellagitannins, exhibit potent antioxidant activity in a cell-based assay. *J. Agric. Food Chem.* **57**, 10181–10186 (2009).
 126. Ishimoto, H. *et al.* In vivo anti-inflammatory and antioxidant properties of ellagitannin metabolite urolithin A. *Bioorganic Med. Chem. Lett.* **21**, 5901–5904 (2011).
 127. Giménez-Bastida, J. A. *et al.* Intestinal ellagitannin metabolites ameliorate cytokine-induced inflammation and associated molecular markers in human colon fibroblasts. in

- Journal of Agricultural and Food Chemistry* **60**, 8866–8876 (2012).
128. Giménez-Bastida, J. A. *et al.* Ellagitannin metabolites, urolithin A glucuronide and its aglycone urolithin A, ameliorate TNF- α -induced inflammation and associated molecular markers in human aortic endothelial cells. *Mol. Nutr. Food Res.* **56**, 784–796 (2012).
 129. Larrosa, M. *et al.* Anti-inflammatory properties of a pomegranate extract and its metabolite urolithin-A in a colitis rat model and the effect of colon inflammation on phenolic metabolism. *J. Nutr. Biochem.* **21**, 717–725 (2010).
 130. González-Sarrías, A., Espín, J.-C., Tomás-Barberán, F. a & García-Conesa, M.-T. Gene expression, cell cycle arrest and MAPK signalling regulation in Caco-2 cells exposed to ellagic acid and its metabolites, urolithins. *Mol. Nutr. Food Res.* **53**, 686–698 (2009).
 131. Kasimsetty, S. G. *et al.* Colon cancer chemopreventive activities of pomegranate ellagitannins and Urolithins. *J. Agric. Food Chem.* **58**, 2180–2187 (2010).
 132. González-Sarrías, A. *et al.* Phase-II metabolism limits the antiproliferative activity of urolithins in human colon cancer cells. *Eur. J. Nutr.* **53**, 853–864 (2014).
 133. Adams, L. S., Zhang, Y., Seeram, N. P., Heber, D. & Chen, S. Pomegranate Ellagitannin-Derived Compounds Exhibit Antiproliferative and Antiaromatase Activity in Breast Cancer Cells In vitro. *Cancer Prev. Res.* **3**, 108–113 (2010).
 134. Ito, H., Iguchi, A. & Hatano, T. Identification of urinary and intestinal bacterial metabolites of ellagitannin geraniin in rats. *J. Agric. Food Chem.* **56**, 393–400 (2008).
 135. Tomás-Barberán, F., García-Selma, M., Beltrán, R., De Gea Espín, J. & García-Villalba, R. Micro-organism that can convert ellagic acid and ellagitannins into urolithins and use of same. PTC Pat WO2014147280 (2014).
 136. Rupiani, S. *et al.* Synthesis of natural urolithin M6, a galloflavin mimetic, as a potential inhibitor of lactate dehydrogenase A. *Org. Biomol. Chem.* **14**, 10981–10987 (2016).
 137. Cozza, G. *et al.* Urolithin as a Converging Scaffold Linking Ellagic acid and Coumarin Analogues: Design of Potent Protein Kinase CK2 Inhibitors. *ChemMedChem* **6**, 2273–2286 (2011).
 138. Pottie, I. R., Nandaluru, P. R. & Bodwell, G. J. An inverse electron-demand diels-alder-based total synthesis of urolithin M7. *Synlett.* **15**, 2245–2247 (2011). doi:10.1055/s-0030-1261203
 139. Rinsch, C. L. *et al.* Enhancing autophagy or increasing longevity by administration of urolithins or precursors thereof. WO2014004902 A2 (2014).
 140. Gao, P. & Wei, Y. NIS-mediated oxidative lactonization of 2-arylbenzoic acids for the synthesis of dibenzopyranones under metal-free conditions. *Synth.* **46**, 343–347 (2014).
 141. Reddy, M. D., Blanton, A. N. & Watkins, E. B. Palladium-Catalyzed, N-(2-Aminophenyl)acetamide-Assisted Ortho-Arylation of Substituted Benzamides: Application to the Synthesis of Urolithins B, M6, and M7. *J. Org. Chem.* **82**, 5080–5095

- (2017).
142. Krzeszewski, M., Vakuliuk, O. & Gryko, D. T. Color-tunable fluorescent dyes based on benzo[c]coumarin. *European J. Org. Chem.* 5631–5644 (2013). doi:10.1002/ejoc.201300374
 143. Devlin, J. . 6H-Dibenzo[b,d]pyrans. I. Synthesis. *Can. J. Chem.* **53**, 343–349 (1975).
 144. Lederer, E. & Polonsky, J. Synthesis of 4,4'-dihydroxydibenzo- α -pyrone, pigment of the scent glands of the beaver (Castor fiber). *Bull. Soc. Chim. Fr.* 831–834 (1948).
 145. Hennings, D. D., Iwasa, S. & Rawal, V. H. Anion-accelerated palladium-catalyzed intramolecular coupling of phenols with aryl halides. *J. Org. Chem.* **62**, 2–3 (1997).
 146. McElroy, W. T. & DeShong, P. Synthesis of the CD-ring of the anticancer agent streptonigrin: studies of aryl-aryl coupling methodologies. *Tetrahedron* **62**, 6945–6954 (2006).
 147. Bredesen, D. E., Rao, R. V. & Mehlen, P. Cell death in the nervous system. *Nature* **443**, 796-802 (2006).
 148. Yacoubian, T. A. Neurodegenerative Disorders: Why Do We Need New Therapies? in *Drug Discovery Approaches for the Treatment of Neurodegenerative Disorders: Alzheimer's Disease* 1–16 (2017).
 149. Young, A. B. Four Decades of Neurodegenerative Disease Research: How Far We Have Come! *J. Neurosci.* **29**, 12722–12728 (2009).
 150. Mason, C. & Dunnill, P. A brief definition of regenerative medicine. *Regen. Med.* **3**, 1–5 (2008).
 151. Bajada, S., Mazakova, I., Ashton, B. A., Richardson, J. B. & Ashammakhi, N. Stem Cells in Regenerative Medicine. in *Topics in Tissue Engineering* **4**, 1–28 (2008).
 152. Culme-Seymour, E. J., Davie, N. L., Brindley, D. A., Edwards-Parton, S. & Mason, C. A decade of cell therapy clinical trials (2000-2010). *Regen. Med.* **7**, 455–462 (2012).
 153. Davies, S. G. *et al.* Stemistry: The Control of Stem Cells in Situ Using Chemistry. *Journal of Medicinal Chemistry* **58**, 2863–2894 (2015).
 154. Längle, D., Halver, J., Rathmer, B., Willems, E. & Schade, D. Small molecules targeting in vivo tissue regeneration. *ACS Chem. Biol.* **9**, 57–71 (2014).
 155. Li, W., Jiang, K., Wei, W., Shi, Y. & Ding, S. Chemical approaches to studying stem cell biology. *Cell Res.* **23**, 81–91 (2013).
 156. Lyssiotis, C. A. *et al.* Chemical control of stem cell fate and developmental potential. *Angew. Chemie - Int. Ed.* **50**, 200–242 (2011).
 157. Lairson, L. L., Lyssiotis, C. A., Zhu, S. & Schultz, P. G. Small Molecule-Based Approaches to Adult Stem Cell Therapies. *Annu. Rev. Pharmacol. Toxicol.* **53**, 107–125 (2013).
 158. Russell, A. J. Regenerative medicinal chemistry: The in situ control of stem cells. *ACS*

- Medicinal Chemistry Letters* **4**, 365–368 (2013).
159. Russell, S. G. D. and A. J. Chapter 4: Chemical Biology of Stem Cell Modulation. in *New Frontiers in Chemical Biology: Enabling Drug Discovery* 97–150 (2011).
 160. Gage, F. H. Neurogenesis In The Adult Brain: New Strategies for Central Nervous System Diseases. *J. Neurosci.* **22**, 612–613 (2002).
 161. Gage, F. H. Mammalian Neural Stem Cells. *Science* **287**, 1433–1438 (2000).
 162. Gross, C. G. Neurogenesis in the adult brain: death of a dogma. *Nat Rev Neurosci* **1**, 67–73 (2000).
 163. Ming, G. & Song, H. Review Adult Neurogenesis in the Mammalian Brain : Significant Answers and Significant Questions. *Neuron* **70**, 687–702 (2011).
 164. Lie, D. C., Song, H., Colamarino, S. A., Ming, G. & Gage, F. H. Neurogenesis In The Adult Brain: New Strategies for Central Nervous System Diseases. *Annu. Rev. Pharmacol. Toxicol.* **44**, 399–421 (2004).
 165. Altman, J. & Das, G. D. Autoradiographic and histological evidence of postnatal hippocampal neurogenesis in rats. *J. Comp. Neurol.* **124**, 319–335 (1965).
 166. Reynolds, B. A. & Weiss, S. Nervous System Generation of Neurons and Astrocytes from Isolated Cells of the Adult Mammalian Central Nervous System. **255**, 1707–1710 (2014).
 167. Kempermann, G. & Gage, F. . New nerve cells for the adult brain. *Sci. Am.* **280**, 48–53 (1999).
 168. Eriksson, P. S., Perfilieva, E. & Björk-Eriksson, T. Neurogenesis in the adult human hippocampus. *Nat. Med.* **4**, 1313–1317 (1998).
 169. Zhao, C., Deng, W. & Gage, F. H. Mechanisms and functional implications of adult neurogenesis. *Cell* **132**, 645–660 (2008).
 170. Faigle, R. & Song, H. Signaling mechanisms regulating adult neural stem cells and neurogenesis. *Biochim. Biophys. Acta (BBA)-General Subj.* **1830**, 2435–2448 (2013).
 171. Gonçalves, J. T., Schafer, S. T. & Gage, F. H. Adult Neurogenesis in the Hippocampus: From Stem Cells to Behavior. *Cell* **167**, 897–914 (2016).
 172. Göritz, C. & Frisén, J. Neural stem cells and neurogenesis in the adult. *Cell Stem Cell* **10**, 657–659 (2012).
 173. Taupin, P. & Gage, F. H. Adult neurogenesis and neural stem cells of the central nervous system in mammals. *J. Neurosci. Res.* **69**, 745–749 (2002).
 174. Bond, A. M., Ming, G. L. & Song, H. Adult Mammalian Neural Stem Cells and Neurogenesis: Five Decades Later. *Cell Stem Cell* **17**, 385–395 (2015).
 175. Song, H.; Stevens, C.F.; Gage, F. H. Astroglia induce neurogenesis from adult neural stem cells. *Nature* **417**, 39–44 (2002).
 176. Curtis, M. A., Connor, B. & Faull, R. Neurogenesis in the Diseased Adult Human Brain:

- New Therapeutic Strategies for Neurodegenerative Diseases. *Cell Cycle* **2**, 427–429 (2003).
177. Curtis, M. A., Low, V. F. & Faull, R. L. M. Neurogenesis and progenitor cells in the adult human brain: A comparison between hippocampal and subventricular progenitor proliferation. *Dev. Neurobiol.* **72**, 990–1005 (2012).
 178. Bonaguidi, M. A. *et al.* In vivo clonal analysis reveals self-renewing and multipotent adult neural stem cell characteristics. *Cell* **145**, 1142–1155 (2011).
 179. Calzolari, F. *et al.* Fast clonal expansion and limited neural stem cell self-renewal in the adult subependymal zone. *Nat. Neurosci.* **18**, 490–492 (2015).
 180. Ortega, F. *et al.* Oligodendroglial and neurogenic adult subependymal zone neural stem cells constitute distinct lineages and exhibit differential responsiveness to Wnt signalling. *Nat. Cell Biol.* **15**, 602–613 (2013).
 181. Kuipers, S. D. *et al.* Environmental control of adult neurogenesis: from hippocampal homeostasis to behavior and disease. *Neural Plasticity* **2014**, 1–3 (2014).
 182. Winner, B. & Winkler, J. Adult neurogenesis in neurodegenerative diseases. *Cold Spring Harb. Perspect. Biol.* **7**, a021287 (2015).
 183. Casarosa, S., Bozzi, Y. & Conti, L. Neural stem cells: ready for therapeutic applications? *Mol. Cell. Ther.* **2**, 31 (2014).
 184. Maden, M. Retinoic acid in the development, regeneration and maintenance of the nervous system. *Nat. Rev. Neurosci.* **8**, 755–765 (2007).
 185. Malberg, J. E., Eisch, J., Nestler, E. J. & Duman, R. S. Chronic antidepressant treatment increases neurogenesis in adult rat hippocampus. *J. Neurosci.* **20**, 9104–9110 (2000).
 186. Malberg, J. E. & Blendy, J. A. Antidepressant action: To the nucleus and beyond. *Trends Pharmacol. Sci.* **26**, 631–638 (2005).
 187. Taupin, P. Neurogenesis and the effect of antidepressants. *Drug Target Insights* **1**, 13–17 (2006).
 188. Karishma, K. K. & Herbert, J. Dehydroepiandrosterone (DHEA) stimulates neurogenesis in the hippocampus of the rat, promotes survival of newly formed neurons and prevents corticosterone-induced suppression. *Eur. J. Neurosci.* **16**, 445–453 (2002).
 189. Mayo, W. *et al.* Pregnenolone sulfate enhances neurogenesis and PSA-NCAM in young and aged hippocampus. *Neurobiol. Aging* **26**, 103–114 (2005).
 190. Irwin, R. W., Wang, J. M., Chen, S. & Brinton, R. D. Neuroregenerative mechanisms of allopregnanolone in Alzheimer's disease. *Front. Endocrinol. (Lausanne)*. **3**, 1–14 (2012).
 191. Prati, F. *et al.* Multitarget drug discovery for Alzheimer's disease: Triazinones as BACE-1 and GSK-3 β inhibitors. *Angew. Chemie - Int. Ed.* **54**, 1578–1582 (2015).

192. Fava, M. *et al.* A Phase 1B, randomized, double blind, placebo controlled, multiple-dose escalation study of NSI-189 phosphate, a neurogenic compound, in depressed patients. *Mol. Psychiatry* **21**, 1372–1380 (2016).
193. Tajiri, N. *et al.* NSI-189, a small molecule with neurogenic properties, exerts behavioral, and neurostructural benefits in stroke rats. *J. Cell. Physiol.* **232**, 2731–2740 (2017).
194. Rix, U. & Superti-furga, G. review Target profiling of small molecules by chemical proteomics. *Nat. Publ. Gr.* **5**, 616–624 (2009).
195. Li, J. *et al.* Target identification in small cell lung cancer via integrated phenotypic screening and activity-based protein profiling. *Mol. Cancer Ther.* **15**, 334–342 (2016).
196. Fonovic, M. & Bogoyo, M. Activity based probes as a tool for functional proteomic analysis of proteases. *Expert. Rev. Proteomics* **5**, 721–730 (2008).
197. Ziegler, S., Pries, V., Hedberg, C. & Waldmann, H. Target identification for small bioactive molecules: Finding the needle in the haystack. *Angew. Chemie - Int. Ed.* **52**, 2744–2792 (2013).
198. Speers, A. E. & Cravatt, B. F. Chemical Strategies for Activity-Based Proteomics. *ChemBioChem* **5**, 41–47 (2004).
199. Su, Y. *et al.* Target identification of biologically active small molecules via in situ methods. *Curr. Opin. Chem. Biol.* **17**, 768–775 (2013).
200. Wright, M. H. & Sieber, S. A. Chemical proteomics approaches for identifying the cellular targets of natural products. *Nat. Prod. Rep.* **33**, 681–708 (2016).
201. Martell, J. & Weerapana, E. Applications of copper-catalyzed click chemistry in activity-based protein profiling. *Molecules* **19**, 1378–1393 (2014).
202. Speers, A. E., Cravatt, B. F. & Jolla, L. Profiling Enzyme Activities In Vivo Using Click Chemistry Methods. *Chem Biol.* **11**, 535–546 (2004).
203. Rostovtsev, V. V., Green, L. G., Fokin, V. V. & Sharpless, K. B. A stepwise Huisgen cycloaddition process: Copper(I)-catalyzed regioselective ‘ligation’ of azides and terminal alkynes. *Angew. Chemie - Int. Ed.* **41**, 2596–2599 (2002).
204. Kolb, H. C. & Sharpless, K. B. The growing impact of click chemistry on drug discovery. *Drug Discov. Today* **8**, 1128–1137 (2003).
205. Ghosh, B. & Jones, L. H. Target validation using in-cell small molecule clickable imaging probes. *Medchemcomm* **5**, 247–254 (2014).
206. Jeřábek, J. *et al.* Tacrine-resveratrol fused hybrids as multi-target-directed ligands against Alzheimer’s disease. *Eur. J. Med. Chem.* **127**, 250–262 (2017).
207. Cavalli, A. *et al.* Multi-target-directed ligands to combat neurodegenerative diseases. *Journal of Medicinal Chemistry* **51**, 347–372 (2008).
208. Bolognesi, M. L. Polypharmacology in a single drug: multitarget drugs. *Curr. Med. Chem.* **20**, 1639–1645 (2013).

209. Estrada, M. *et al.* New cinnamic - N-benzylpiperidine and cinnamic - N,N-dibenzyl(N-methyl)amine hybrids as Alzheimer-directed multitarget drugs with antioxidant, cholinergic, neuroprotective and neurogenic properties. *Eur. J. Med. Chem.* **121**, 376–386 (2016).
210. Yahiaoui, S. *et al.* Design, synthesis, and pharmacological evaluation of multitarget-directed ligands with both serotonergic subtype 4 receptor (5-HT₄R) partial agonist and 5-HT₆R antagonist activities, as potential treatment of Alzheimer's disease. *Eur. J. Med. Chem.* **121**, 283–293 (2016).
211. Bolognesi, M. L. & Cavalli, A. Multitarget Drug Discovery and Polypharmacology. *ChemMedChem* **11**, 1190–1192 (2016). doi:10.1002/cmdc.201600161
212. Singh, M., Kaur, M., Chadha, N. & Silakari, O. Hybrids: a new paradigm to treat Alzheimer's disease. *Molecular Diversity* **20**, 271–297 (2016).
213. Minarini, A. *et al.* Multifunctional tacrine derivatives in Alzheimer's disease. *Curr. Top. Med. Chem.* **13**, 1771–86 (2013).
214. Camps, P. *et al.* New tacrine-huperzine A hybrids (huprines): Highly potent tight-binding acetylcholinesterase inhibitors of interest for the treatment of Alzheimer's Disease. *J. Med. Chem.* **43**, 4657–4666 (2000).
215. Soukup, O. *et al.* A resurrection of 7-MEOTA: a comparison with tacrine. *Curr. Alzheimer Res.* **10**, 893–906 (2013).
216. Decker, M. Hybrid molecules incorporating natural products: applications in cancer therapy, neurodegenerative disorders and beyond. *Curr. Med. Chem.* **18**, 1464–1475 (2011).
217. Ji, H. F. & Zhang, H. Y. Multipotent natural agents to combat Alzheimer's disease. Functional spectrum and structural features. *Acta Pharmacologica Sinica* **29**, 143–151 (2008).
218. Koeberle, A. & Werz, O. Multi-target approach for natural products in inflammation. *Drug Discovery Today* **19**, 1871–1882 (2015).
219. Turner, R. S. *et al.* A randomized, double-blind, placebo-controlled trial of resveratrol for Alzheimer disease. *Neurology* **85**, 1383–1391 (2015).
220. Bishayee, A., Darvesh, A. S., Politis, T. & McGory, R. Resveratrol and liver disease: from bench to bedside and community. *Liver Int.* **30**, 1103–1114 (2010).
221. Feng, Y. *et al.* Resveratrol inhibits beta-amyloid oligomeric cytotoxicity but does not prevent oligomer formation. *Neurotoxicology* **30**, 986–995 (2009).
222. Morphy, J. The challenges of multi-target lead optimization. *RSC Drug Discov. Ser.* **21**, 141–154 (2012).
223. Rankovic, Z. CNS Drug Design: Balancing Physicochemical Properties for Optimal Brain Exposure. *Journal of Medicinal Chemistry* **58**, 2584–2608 (2015).

224. Lu, C. *et al.* Design, synthesis, and evaluation of resveratrol derivatives as A β (1-42) aggregation inhibitors, antioxidants, and neuroprotective agents. *Bioorg. Med. Chem. Lett.* **22**, 7683–7687 (2012).
225. Romero, A., Cacabelos, R., Oset-Gasque, M. J., Samadi, A. & Marco-Contelles, J. Novel tacrine-related drugs as potential candidates for the treatment of Alzheimer's disease. *Bioorganic and Medicinal Chemistry Letters* **23**, 1916–1922 (2013).
226. Xie, S. S. *et al.* Multi-target tacrine-coumarin hybrids: Cholinesterase and monoamine oxidase B inhibition properties against Alzheimer's disease. *Eur. J. Med. Chem.* **95**, 153–165 (2015).
227. Nepovimova, E. *et al.* Multitarget drug design strategy: Quinone-tacrine hybrids designed to block amyloid- β aggregation and to exert anticholinesterase and antioxidant effects. *J. Med. Chem.* **57**, 8576–8589 (2014).
228. Lu, C. *et al.* Design, synthesis, and evaluation of multitarget-directed resveratrol derivatives for the treatment of Alzheimer's disease. *J. Med. Chem.* **56**, 5843–5859 (2013).
229. Mao, F. *et al.* New multi-target-directed small molecules against Alzheimer's disease: a combination of resveratrol and clioquinol. *Org. Biomol. Chem.* **12**, 5936–5944 (2014).
230. Giacomini, E., Rupiani, S., Guidotti, L., Recanatini, M. & Roberti, M. The Use of Stilbene Scaffold in Medicinal Chemistry and Multi-Target Drug Design. *Curr. Med. Chem.* **23**, 2439–2489 (2016).
231. Yong, D. *et al.* Diphenylvinyloxy alkylamine compound and preparation method as well as application thereof. CN 103073440 (2013).
232. Murty, M. S. R., Penthala, R., Polepalli, S. & Jain, N. Synthesis and biological evaluation of novel resveratrol-oxadiazole hybrid heterocycles as potential antiproliferative agents. *Med. Chem. Res.* **25**, 627–643 (2016).
233. Roberti, M. *et al.* Synthesis and biological evaluation of resveratrol and analogues as apoptosis-inducing agents. *J. Med. Chem.* **46**, 3546–3554 (2003).
234. Sun, B. *et al.* Design, synthesis, and biological evaluation of resveratrol analogues as aromatase and quinone reductase 2 inhibitors for chemoprevention of cancer. *Bioorganic Med. Chem.* **18**, 5352–5366 (2010).
235. Hu, M. K., Wu, L. J., Hsiao, G. & Yen, M. H. Homodimeric tacrine congeners as acetylcholinesterase inhibitors. *J. Med. Chem.* **45**, 2277–2282 (2002).
236. Spilovska, K. *et al.* 7-Methoxytacrine-adamantylamine heterodimers as cholinesterase inhibitors in Alzheimer's disease treatment--synthesis, biological evaluation and molecular modeling studies. *Molecules* **18**, 2397–418 (2013).
237. Chen, W.-M. *et al.* Hepatoprotective effect of resveratrol against ethanol-induced oxidative stress through induction of superoxide dismutase in vivo and in vitro. *Exp.*

Ther. Med. **11**, 1231–1238 (2016).

Acknowledgments

At the end of this three year journey I want to thank many people for making it possible and for supporting me both scientifically and personally.

I thank my supervisor, Prof. Marinella Roberti for her guidance, support and the precious advices she has provided throughout my PhD research studies.

I thank the group leaders at UniBo I had the pleasure to collaborate with, Prof. Maurizio Recanatini, Prof. Maria Laura Bolognesi, Prof. Giuseppina di Stefano and Prof. Laura Mercolini.

I thank the past and current members of our group I worked with during the past three years, Dr. Elisa Giacomini, Dr. Sebastiano Rupiani, Ludovica Piscicelli, Alessandra Agnoletti.

I thank the precious collaborators that contributed to make this thesis possible, Dr. Federico Falchi, Dr. Marcella Manerba, Dr. Uliassi Elisa, Dr. Michele Protti and Lorenza Di Ianni.

I thank Prof. Angela Russell and all the members of her group of talented scientists for their guidance during my placement at Oxford University. I thank Prof. Francis Szele and all his group I had the pleasure to collaborate with.

I thank Dr. Laia Jose Currere, Dr. Laura Mola Sola, Dr. Daniel Conole for their special support and friendship.

I thank all my friends and colleagues with whom I shared many beautiful and gratifying moments during these three years.

I thank my boyfriend Antonio, my parents Giuseppe and Gabriella and my brother Fabio for always being close and supporting me especially in difficult times.